INTERACTION OF AQUEOUS INORGANIC ORTHOPHOSPHATE

AND

PHOSPHATE ROCK

Thesis by

John Zoltek, Jr.

In Partial Fulfillment of the Requirements

For the Degree of

Doctor of Philosophy

California Institute of Technology

Pasadena, California

1973

(Submitted October 20, 1972)

ACKNOWLEDGEMENT

ABSTRACT

An experimental study was made of the interaction of phosphate rock and aqueous inorganic orthophosphate, calcium, and hydroxyl ions. A model of the reaction was developed by observing electron diffraction patterns in conjunction with concentration changes of chemical components. The model was applied in explaining the performance of batch suspensions of powdered phosphate rock and packed columns of granular phosphate rock. In both cases the reaction consisted initially of a rapid nucleation phase that occurred in a time period of minutes. In the batch system the calcium phosphate nuclei then ripened into larger micro-crystals of hydroxyapatite, which eventually became indistinguishable from the original phosphate rock surface. During column operation the high supersaturation ratio that existed after the rapid nucleation phase resulted in a layer of small nuclei that covered a slowly growing hydroxyapatite crystal.

The column steady-state rate constant was found to increase with increasing temperature, pH, and fluoride concentration, and to decrease with increasing concentrations of magnesium sulfate, ammonium chloride, and bicarbonate ion.

An engineering feasibility study indicated that, based on economic considerations, nucleation of apatite on phosphate rock ore has a potential use as a wastewater phosphate removal treatment process.

TABLE OF CONTENTS

LIST OF FIGURES

LIST OF TABLES

Chapter 1

Introduction

1-1   General background

Phosphorus, nitrogen, and carbon are the primary nutrients responsible for algal blooms in lakes and streams, with man-made wastes being the major sources of these nutrients. Nitrogen and carbon can be fixed by algae from atmospheric nitrogen and carbon dioxide gas and consequently are difficult to control. The best hope for ultimate control of eutrophication appears to be in effecting a substantial decrease in the phosphorus concentration in wastewater in conjunction with a program of general water pollution control.

The solution to the eutrophication problem encompasses many complex engineering and environmental decisions. In agricultural communities farm land runoff is usually the major source of nutrients to lakes and streams, while in urban areas wastewater contributes the largest proportions of nutrients (Eliassen and Tchobanoglous, 1969). Very little has been done to date to minimize the agricultural runoff contribution to eutrophication problems. An attempt has been made to reduce the concentration of phosphorus in wastewater by reducing the amount of phosphate "fillers" in detergents. In some instances communities have banned outright the use of detergents that contain more than a few percent phosphorus[1]. However the low phosphate cleaners

_____

(1) High phosphorus detergents contain approximately 30% P by weight (Weaver 1969, Kessick 1972).

usually have less cleaning effectiveness, and in many instances can be very dangerous if accidentially spilled into one's eye or swallowed by children. Estimates of the amount of phosphorus in wastewater directly attributable to detergents usually range around 50% of the total phosphorus present (Weaver 1969).

1-2   Phosphorus in the environment

The element phosphorus is widely distributed in nature but is never found in a free or uncombined state because of its great affinity for oxygen. Phosphate rock is the common term used for most commerical phosphorus ores. It does not have a definite molecular composition but contains phosphorus minerals generally in the apatite group. During 1972 approximately 4.5×10^6 short tons of phosphorus as P will be used domestically, with 76% going into fertilizers and 7% being used for soaps and detergents (Bureau of Mines, 1970). Approximately 16×10^6 short tons will be commercially mined domestically in 1972, with about one-half being returned to the environment as losses in washer and flotation operations.

Agricultural use of phosphorus is primarily in the form of fertilizer for growing crops for both human consumption and the raising of livestock. The livestock return almost all of the phosphorus to the soil, usually in the form of animal wastes which then are ultimately introduced into the hydrological cycle as runoff. A small amount of phosphorus also is introduced as pesticides. The only effective method of reducing pollution from agricultural use of

phosphorus is by proper and timely application of fertilizers so as to minimize runoff.

Domestic wastes have phosphorus concentrations that usually range from 0.1 to 0.3 mM (Eliassen and Tchobanoglous, 1969). Based on equilibrium calculations these high phosphorus concentrations should spontaneously produce solid apatite phases, particularly considering the large amount of nucleating surfaces contained on the colloidal and suspended matter in wastewater. Solids are not formed because the rate of nucleation and crystal growth of calcium phosphate is exceedingly slow. Unfortunately almost no information exists in the literature on any growth rate constants of the various solid calcium phosphates. It therefore is presently impossible to determine at what kinetic state a body of water may be with respect to soluble and solid phosphorus.

Control of phosphorus in domestic wastes is accomplished either by reducing the source, as in detergents, or by treatment of sewage to remove phosphorus. Spiegel and Forrest (1969) list fourteen systems for phosphorus removal, and all are modifications of ion exchange or chemical precipitation. Enhanced phosphorus removal (up to 90%) has also been observed in activated sludge secondary treatment systems (Menar and Jenkins 1970, Scalf et al 1969, and Wells 1969) but the mechanism of removal has yet to be satisfactorily explained.

More importantly the activated sludge plant operating criteria that produce the high removals have not yet been defined, and consistently good removals can not be reliably predicted.

1-3   Purpose of the present work

It was the purpose of this research to investigate the reaction between the soluble protonated orthophosphate ion and solid phosphate rock with two objectives in mind. The first was to explain the manner in which calcium phosphates nucleate and grow on solid phosphate rock. By developing chemical reactions and rate constants that explain the observed phenomena, a better understanding of the formation of solid calcium phosphates in nature will result. In this section of the research the techniques employed electron microscope diffraction studies in conjunction with chemical analysis on batch runs using powdered phosphate rock and synthetic phosphate feed.

The second objective was to develop a method of phosphate removal that could be evaluated for use as a full-scale treatment process. It was decided to limit the investigation to a column configuration using granular phosphate rock.

Two models are developed, one for the batch system and one for the column system, that qualitatively describe the phenomena occurring in each case.

Chapter 2

Soluble orthophosphate reactions with solid phases

In this chapter the theories of homogeneous and heterogeneous nucleation are briefly presented along with their relevance and limitations with respect to the work discussed herein. Also discussed is the semi-empirical equation that was used for analyzing both the batch runs and column runs. Finally a literature review of recent research pertaining to the growth of calcium phosphate solid phases is presented.

2-1   The solid-solution system

In a natural aquatic environment the protonated species of the orthophosphate ion is the most abundant form of phosphorus. The solid forms can vary widely in composition, but most are combinations of inorganic orthophosphate and calcium, magnesium, aluminum, or iron[1]. This study deals with the protonated species of inorganic orthophosphate and their reactions with calcium phosphate solids in the apatite form. For a more detailed treatment than presented below the reader is referred to Van Wazer (1958 & 1961), and a summary on phosphorus by the American Water Works Association Committee on the "Chemistry of Nitrogen and Phosphorus in Water" (1970).

---

(1) Palache et al (1951) found that of the 187 known natural phosphorus minerals that occur on the surface of the earth all are phosphates, with the majority being in the apatite form.

2-1-1   Phosphorus in solution

The most abundant forms of dissolved inorganic phosphorus exist as the protonated orthophosphates $H_xPO_4^{-(3-x)}$, protonated pyrophosphates $H_xP_2O_7^{-(4-x)}$, protonated trimetaphosphates $H_xP_3O_9^{-(3-x)}$, and protonated tripolyphosphates $H_xP_3O_{10}^{-(5-x)}$.

The condensed inorganic phosphates are found in all plants and animals, where they are synthesized enzymatically and constitute a part of the polyphosphate pool. A substantial portion of the condensed inorganic phosphates are man-made and are introduced into the natural environment as fillers for detergents. Weaver (1969) gives the form of these fillers as:

$$Na^+O^- - \overset{\overset{\displaystyle O}{\|}}{\underset{\underset{\displaystyle Na^+}{O^-}}{P}} - O - \overset{\overset{\displaystyle O}{\|}}{\underset{\underset{\displaystyle Na^+}{O^-}}{P}} - O - \overset{\overset{\displaystyle O}{\|}}{\underset{\underset{\displaystyle Na^+}{O^-}}{P}} - O^-Na^+$$
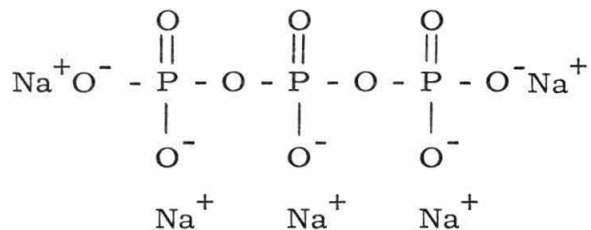
The decomposition of the detergent fillers produces condensed polyphosphates which then hydrolyze to orthophosphates. The hydrolysis can be represented by

$$P_3O_{10}^{-5} + H_2O = P_2O_7^{-4} + PO_4^{-3} + 2H^+ \qquad (2\text{-}1)$$

$$P_2O_7^{-4} + H_2O = 2PO_4^{-3} + 2H^+ \qquad (2\text{-}2)$$
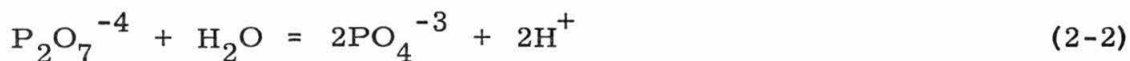
Heinke & Norman (1971) found that, in general, the rate of hydrolysis is increased as temperature is increased; is faster in the presence

of organic enzymes; and is directly proportional to the concentration
of condensed phosphates. They found the rate of hydrolysis of poly-
phosphates in an activated sludge tank to be 10,000 times faster than
that in natural domestic water. In secondary sewage effluents the
protonated orthophosphates represent 70 to 90 percent of the total
phosphorus present (AWWA, 1970).

Soluble cation complexes of phosphorus can at times significantly
affect the distribution of the soluble phosphorus form. For example
if $(Ca_T) = 1.0$ mM, $(PO_{4T}) = 0.01$ mM, and pH $= 7.0$, 20% of the phos-
phate is complexed as $CaHPO_4$(aq). Leckie (1969) calculated the solu-
bility of phosphorus in contact with HAP[1] considering both complexes
of calcium and orthophosphate and no complexes. Figure 2-1 shows
that in the pH range from 6 to 8, the range of interest in this research,
the complexation between calcium and orthophosphate has only a
minimal effect on the total soluble orthophosphate concentration.

Theoretically all polyphosphates in the natural environment will
eventually hydrolyze into orthophosphates, and accordingly almost
all phosphorus minerals contain the phosphorus in the orthophosphate
form. Consequently the interaction between the soluble orthophosphate
group and solids containing orthophosphates becomes an area of
significant importance in the natural environment.

2-1-2   Solid phases of phosphorus

The phosphorus-containing solids of primary interest are the
calcium phosphates, with the apatites being the most thermodynamically

[1] HAP is the abbreviation used for hydroxyapatite - a list of the
meaning of the abbreviations used is presented in the nomenclature.
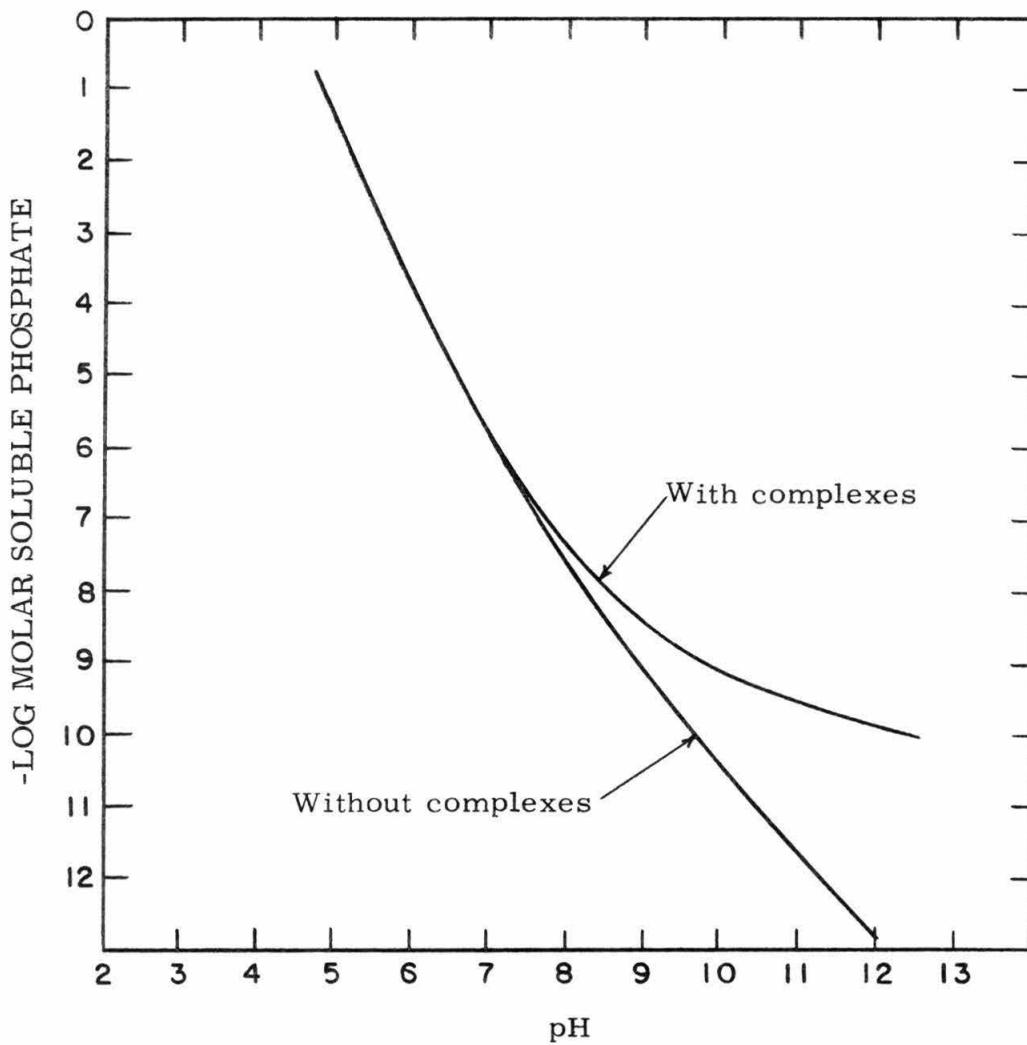
Figure 2-1. Comparison of calculated hydroxyapatite solu-
bility with and without calcium phosphate complexes. pK_s of
HAP_{5-3-1} = 56.9, (Ca_T) = 1.0 mM, Temperature = 25°C
(Leckie 1969).

stable form. There are many different isomorphic substitutions which are possible in the apatite structure and it would be difficult to write a general formula that would be applicable to all cases. However for illustrative purposes the apatite structure can be represented by the simple stoichiometric formula

$$M_{10}(RO_4)_6X_2$$

Neglecting oxidation states and charge McConnel (1938), Van Wazer (1958), and Leckie (1969) report the following possible atom substitutions:

1) M can be Ca, Na, K, Mn, Sr, Mg, C, Al, Fe, & H_3O.

2) R can be P, S, Si, As, V, C, Al, and the RO_4 group can be "replaced" by CO_3 to form carbonate apatites.

3) X can be F, Cl, O, OH, and H_2O.

Hydroxyapatite (HAP) has the formula

$$Ca_{10}(PO_4)_6(OH)_2$$

In fluoroapatite (FAP) the hydroxyl ions are replaced by fluoride ions to give

$$Ca_{10}(PO_4)_6F_2$$

The solid calcium phosphates that are not in the apatite form are

$CaHPO_4$ Dicalcium phosphate (DCP)

$CaHPO_4 \cdot 2H_2O$ Dicalcium phosphate dihydrate (DCPD)
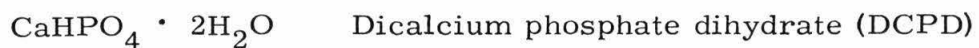
$Ca_3(PO_4)_2$ Tricalcium phosphate (TCP)

$Ca_4H(PO_4)_3$ Octacalcium phosphate (OCP)

The above listed phosphorus solids have been found to be the major intermediate phases forming apatites (Morena et al 1960, Eanes 1970, Eanes et al 1965). The reader is referred to Sillen and Martell (1964) and Leckie (1969) for a more detailed listing of the many other possible solid forms of phosphorus.

2-2 Formation of solids from dilute aqueous solutions

The growth of a solid from aqueous solution can proceed by one of two mechanisms; homogeneous nucleation or heterogeneous nucleation. Homogeneous nucleation is the case where no solids exist in the solution and growth occurs by the aggregation of molecules until a critical radius is exceeded, after which growth proceeds spontaneously.[1] Heterogeneous nucleation is the growth of material on an already existing surface. In both cases the nuclei will grow into larger micro-crystals by a process usually referred to as ripening or aging.

In the case of heterogeneous nucleation the substrate that initiated the nucleation may not necessarily have the same characteristics as the growing micro-nuclei. Crystal growth can be regarded as a special case of heterogeneous nucleation where the growing phase

---

(1) As an illustration, the critical radius of forming water droplets in air with $P/P_0 = 4$ is about 8Å, with the critical drop containing 90 molecules of water (Adamson, 1967).

has the same chemical and physical structure as the bulk solid.

2-2-1   Homogeneous nucleation

As one gradually increases the concentration of a solution so that the solubility product of a solid phase is exceeded, the solid phase is not formed until a certain supersaturation has been achieved. This phenomenon can be modeled by imagining the molecules making up the solid to cluster initially in small spherical shapes. One can think of these small clusters as having molecules with a high probability of escaping into the solution due to the sharp curvature of the surface. The tendency is for the clusters to remain small until some critical size is achieved, after which growth can proceed in a regular manner. The theoretical analysis of nucleation from solution is covered in detail by Nielsen (1964), and Walton (1967). Stumm and Morgan (1970) also present a summary of nucleation theory with reference to its effect on natural processes. Walton (1967) gives 3 steps in the formation of a solid phase by precipitation from solution. A cluster is first formed by the aggregation of molecules:

$$X + X = X_2 \qquad\qquad\qquad (2\text{-}3)$$

$$X_2 + X = X_3 \qquad\qquad\qquad (2\text{-}4)$$

$$X_{j-1} + X = X_j (\text{cluster}) \qquad\qquad\qquad (2\text{-}5)$$

$$X_j + X = X_{j+1} (\text{nucleation}) \qquad\qquad\qquad (2\text{-}6)$$

Material is subsequently deposited on the nuclei with resultant
crystal growth:

$$X_{j+1} + X = \text{crystal growth} \tag{2-7}$$

Finally larger crystals will be formed from fine crystallites by
ripening.

The standard free energy of formation of a nucleus consists of
work required to form a surface and of energy gained from making
bonds. For a spherical nucleus the first quantity is the mean free
surface energy (interfacial tension) times the surface area, $\bar{\gamma}4\pi r^2$,
where r is the radius of the spherical particle. The second quantity,
which is always negative, can be expressed as $jkT\ln S$, where k is
the Boltzman constant, T is the absolute temperature and S is the
supersaturation ratio.[1] j is the number of molecules in the nucleus
and can be expressed in terms of the molar volume v as $j = 4\pi r^3/3v$.
Hence the free energy of nucleus formation may be written as

$$\Delta G^o = -(4\pi r^3/3v)kT\ln S + 4\pi r^2\bar{\gamma} \tag{2-8}$$

The rate at which nuclei form is related to the free energy of
formation by

$$J = A' \exp(-\Delta G^*/kT) \tag{2-9}$$

---

(1) The general definition of supersaturation ratio is $S = (Q/K)^{1/n}$.
Q is the ion product, K is the equilibrium constant, and n is the
number of ions in the neutral molecule (n = 10 for HAP, etc.)

where   J = rate of nuclei formation in cm^3 per sec

A' = a factor related to the efficiency of collision of ions or molecules (approximately equal to 10^{25})

$\Delta G^* =$ activation energy = maximum value of ΔG^o

$\Delta G^* =$ can be calculated by substituting the equation for the radius of the critical nucleus

$$r_j = 2 \tilde{\gamma} v / kT \ln S \qquad (2\text{-}10)$$

into equation 2-8 to obtain

$$\Delta G^* = 16 \pi \tilde{\gamma}^3 v^2 / 3(kT \ln S)^2 \qquad (2\text{-}11)$$

Figure 2-2 shows a plot of J against supersaturation. The curve shows that a relatively small change in supersaturation has a marked change in the rate of nuclei formation.

2-2-2   Heterogeneous nucleation

There presently are two distinctly different models for heterogeneous nucleation. The first assumes that the nucleus resembles a small piece of the bulk phase. This model has been studied by Turnbull and Vonnegut (1952). It can be schematically represented as shown in Figure 2-3. The nucleus is distorted by the influence of the substrate affecting the interatomic forces and consequently modifying the energy relationships involved in bonding. The result is that the coherence of the interface can be marred by dislocations. Also the solid-solid interface modifies the surface energy requirements involved
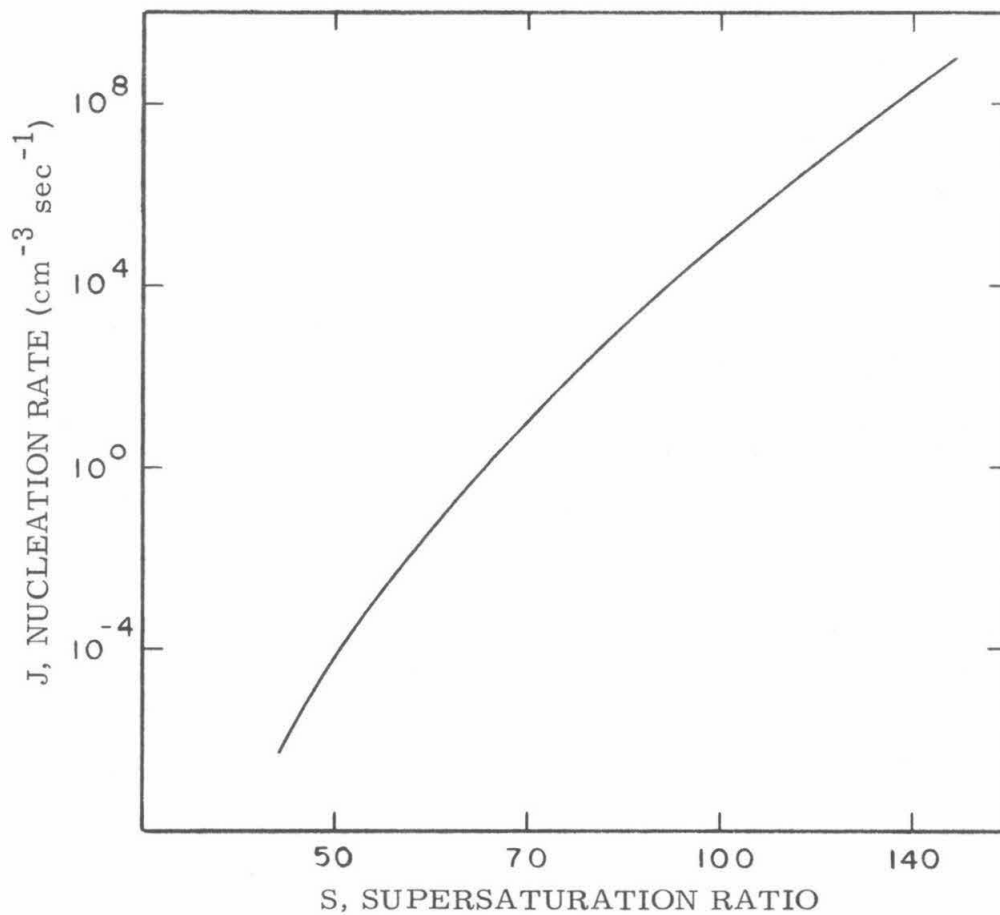
Figure 2-2. Double logarithmic plot of nucleation rate versus supersaturation. For this curve the following values were assumed: $\bar{\delta}$ = 100 ergs cm^{-2}; v = 3 x 10^{-23}cm^3 ; A' = 10^{30} cm^{-3} sec^{-1} (Stumm and Morgan 1970).
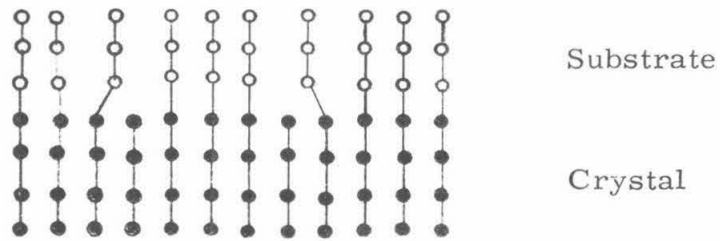
Figure 2-3. Schematic of the Turnbull and Vonnegut
model for heterogeneous nucleation.
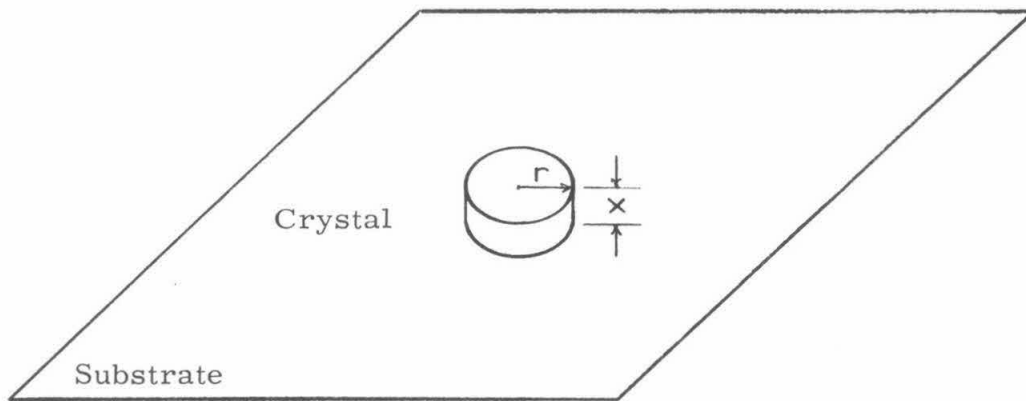
Figure 2-4. Geometrical assumption for crystal growth
used in the Turnbull and Vonnegut theory.

in creating a new surface. The free energy of formation can be written as

$$\Delta G^O = \Delta G^O\text{(bond formation)} + \Delta G^O\text{(surface formation)} \qquad (2\text{-}12)$$

Geometrically the growing surface can be represented by Figure 2-4 as a cylindrical nucleus growing on a planar substrate. Using this geometry Turnbull and Vonnegut (1952) represent the free energy equation by

$$\Delta G^O = \pi r^2 \times ((NkT/v)\ln S + c\phi^2) +$$
$$(2\pi r \times \gamma_e + \pi r^2 (\gamma_{CL} + \gamma_{CS} - \gamma_{SL})) \qquad (2\text{-}13)$$

where
r = radius of the cylinder

x = height of the cylinder

k = Boltzman constant

T = absolute temperature, ^OK

v = molar volume (cm^3/mole)

N = number of ions in the neutral molecule

S = supersaturation ratio

c = elastic molecules

ϕ = a measure of the misfit of the nucleus on the substrate

= $(a_o^{sub} - a_o^{nuc}) / a_o^{sub}$ where a_o is a lattice parameter of the substrate and nucleus

γ_e = cluster edge energy (energy per unit length required to expand the perimeter)

γ_{CL} = interfacial energy at the crystal-solution

γ_{CS} = interfacial energy at the crystal-substrate

γ_{CL} = interfacial energy at the substrate-solution

The $c\phi^2$ term in Equation 2-13 accounts for bond distortion due to lattice mismatch, with this energy change due to bond distortion going to zero when there is perfect match between the substrate and nucleus (ie. seed crystals of precipitating material). The critical supersaturation is then derived by maximizing Equation 2-13 and substituting into the Equation 2-9 to give the critical supersaturation as described by

$$N \ln S^* = (v/kT)c\phi^2 +$$
$$(2\gamma_e v \pi^{1/2}/kT)((\gamma_{CL} + \gamma_{CS} - \gamma_{SL})/kT\ln A')^{1/2} \qquad (2-14)$$

The second model, proposed by Upreti and Walton (1966), assumes a sequence of solute diffusion to the surface-solution interface, adsorption, surface diffusion or diffusion through a surface layer, and incorporation into a cluster. Without going into the complete derivation, which is given by Walton (1967), the rate of formation of nuclei is given by

$$J = (A''R^2 a v / (v')^2) \exp((2Q_{ads} - Q_D - \Delta G^*)/kT) \qquad (2-15)$$

with the expression for critical supersaturation given as

$$N \ln S^* = (4d^2 \gamma_e^2/m\sigma kT)/(2Q_{ads} - Q_D + BkT) \qquad (2-16)$$

where $\quad A'' = 4\,1^{*}Z'$

$\quad\quad\quad B = \ln(4\,A\,1^{*}\,(R/\nu')^{2}\,a\nu)$

$\quad\quad\quad 1^{*} = $ edge length of a square cluster

$\quad\quad\quad Z' = $ a two dimensional Zeldovich factor

$\quad\quad\quad \nu' = $ vibration frequency of adsorbed ions

$\quad\quad\quad \nu = $ frequency for jump diffusion $= kT/h$, where

$\quad\quad\quad\quad\quad h = $ Plank's constant

$\quad\quad\quad a = $ distance of separation between active sites

$\quad\quad\quad \sigma = $ the ratio of the interionic distance in an undistorted

$\quad\quad\quad\quad\quad$ cluster divided by the distorted distance

$\quad\quad\quad d = $ average ion diameter

$\quad\quad\quad R = $ the rate of arrival of ions at the surface

$\quad\quad\quad Q_{ads} = $ adsorption energy

$\quad\quad\quad Q_{D} = $ activation energy of surface diffusion

Although very few of the parameters in Equation 2-13 through 2-16 are actually known for conditions encountered in natural systems, the theoretical derivations do have the ability to predict qualitatively what conditions will help or hinder nucleation. From Equation 2-14 it can be concluded that solid impurities in solution will catalyze precipitation, with the better the lattice match the more effective the nucleating ability of the substrate. Equation 2-15 predicts that the rate of nucleation, J, will increase with the number of sites of high adsorption energy, will decrease with increasing surface diffusion energy, and will increase with a decrease in ΔG^{*}. From Equation 2-16 it can be concluded that the critical supersaturation will decrease

with an increase in temperature.

2-2-3 Crystal growth

The theories of growth kinetics may broadly be divided into two categories; those describing the rate-limiting process in terms of transport to the crystal surface, and others relating the rate control to processes occurring in the interface region. The former classification will be referred to as diffusion controlled, and the latter as interface controlled growth.

Diffusion controlled crystal growth can readily be analyzed by applying Fick's first law to a plane surface. A schematic of the particle surface in a constant volume batch system is represented in Figure 2-5 as a flat plane surface. In this developement C is the concentration in bulk solution and C_i is the concentration at the interface. Fick's first law states that

$$(1/A)dm/dt = D \, dC/dx \tag{2-17}$$

where m is the mass of the particles, A is the area, and D is the diffusion coefficient. But if the growth process is diffusion controlled the concentration at the interface can be replaced by the equilibrium concentration, C_e. Equation 2-17 can be approximated by

$$dm/dt \cong A(D/\delta)(C-C_e) \tag{2-18}$$

where δ is the "film thickness".

Since there is no mass flux into or out of the constant volume batch
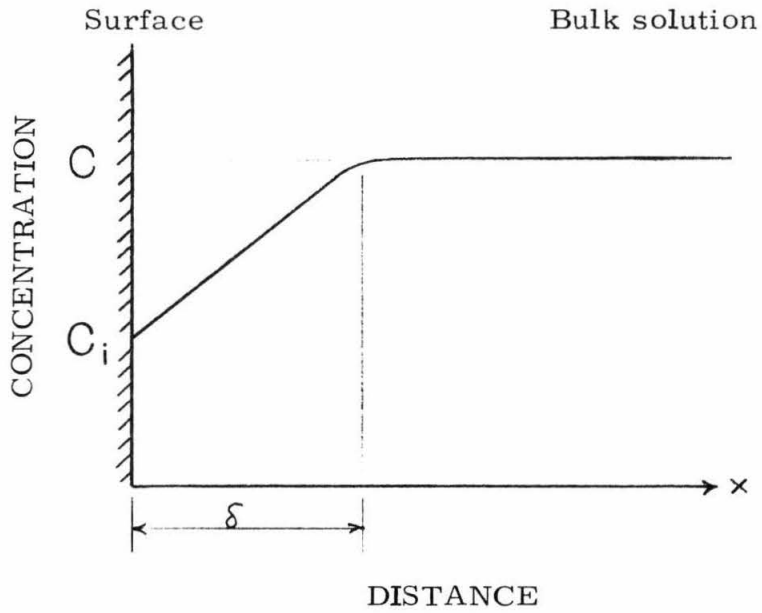
Figure 2-5. Schematic representation of diffusion from a bulk liquid phase to a flat surface.
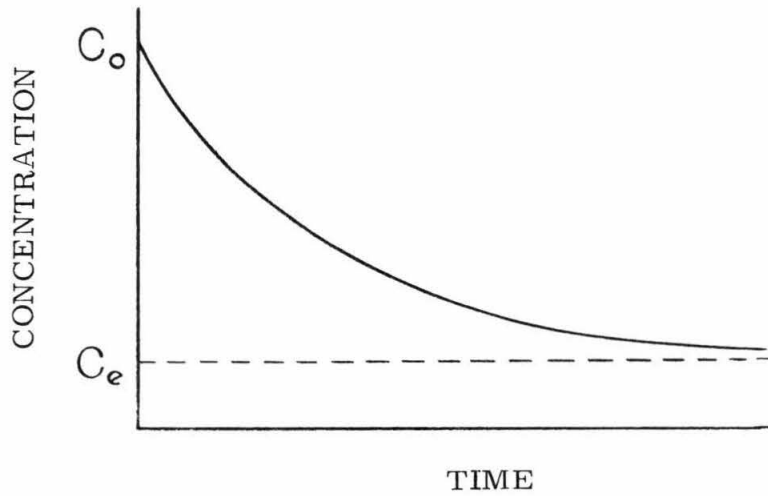
Figure 2-6. Sketch of concentration vs time in a batch system with crystal growth on seed material.

system the mass increase on the crystal surfaces can be related to the concentration change in solution by

$$dm/dt = -V \, dC/dt \qquad (2-19)$$

where V is the volume of the batch system. Substituting Equation 2-19 into 2-18 we get

$$dC/dt = -(A/V)(D/\delta)(C-C_e) \qquad (2-20)$$

or

$$dC/dt = -(k'A/V)(C-C_e) \qquad (2-21)$$

k' will vary with both the diffusion coefficient and the turbulence in the reaction vessel.

Interface controlled reactions are more difficult to analyze theoretically and to date no satisfactory approach has been developed. However many chemical reactions have been found to follow a rate law of the type

$$rate = k'' C^n \qquad (2-22)$$

where k'' is a velocity constant and n is the order of the reaction. It has been observed empirically (Walton 1963, Nielson 1964, Doremus 1958) that the growth rate of seed crystals from super-saturated solutions does follow a rate law similar to that of Equation 2-22, specifically

$$dC/dt = -(kA/V)(C-C_e)^n \qquad (2-23)$$

where k is a rate constant independent of turbulence. Stumm and Morgan (1970) report that n has been determined for silver chloride (n=2), silver chromate (n=3), magnesium oxalate (n=2), and potassium chloride (n=1). Note in the case of potassium chloride that even though n=1, the growth process was interface controlled, for k was found not to depend on turbulence. Equation 2-23 can be rewritten as

$$\log(-dC/dt) \;=\; \log(kA/V) \;+\; n\log(C-C_e) \tag{2-24}$$

As crystal growth proceeds the concentration of the lattice ions in solution must decrease. Consequently the experimental data plot of concentration vs. time will always have a negative slope as shown in Figure 2-6. The equilibrium concentration C_e is the asymptote of the curve. dC/dt is always a negative quantity, so that $-dC/dt$ is always a positive number enabling its logarithm to be computed as a real number. By using the notation that $px = -\log x$ Equation 2-24 can be written as

$$p(-dC/dt) \;=\; p(kA/V) \;+\; np(C-C_e) \tag{2-25}$$

Nancollas (1968) used such a plot in examining the crystallization of sulfates of barium, lead, and strontium onto seed crystals from relatively pure supersaturated solutions. He found that, after an initial growth surge of effective order n greater than two, the reactions followed the second order rate law where n=2 in Equation 2-23. His results are illustrated in Figure 2-7. In an attempt to explain the
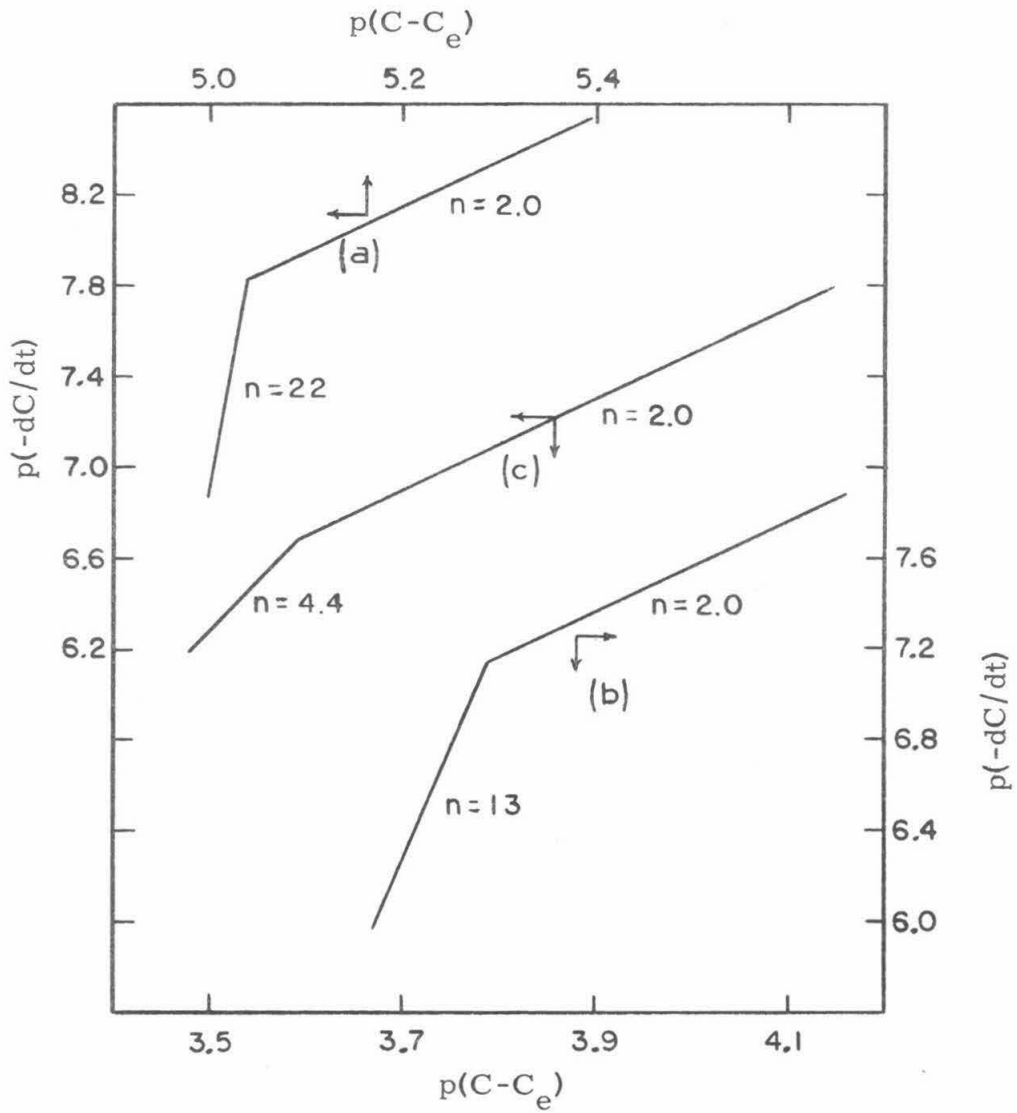
Figure 2-7. Plots of p(-dC/dt) against p(C-C$_e$) for the crystallization of barium sulfate (a), lead sulphate (b), and strontium sulfate (c) from their respective supersaturated solutions (Nancollas 1968).

initial growth surge, a number of experiments were made in which the seed crystals were modified before use as innoculants. Pre-growth of the crystals, aging in a solution containing an excess of lattice ion, or increase in the surface roughness had little effect upon the initial fast period . When the initial supersaturation was decreased or the innoculating seed concentration was increased, the surge period was completely removed, and second order growth began immediately. Factors other than surface geometry seemed to be responsible for the initial surge. Surface nucleation was the probable cause for the initial surge, for decreasing the supersaturation would have the effect of decreasing the rate of nucleation. Figure 2-2 shows that a small change in the supersaturation ratio has a very large effect on the rate of nuclei formation.

Ferguson et al (1971) found in studies where calcium phosphate was precipitated from a synthetic wastewater near pH 8 that the soluble phosphate concentration obeyed the empirical rate law

$$dC/dt = kC^{2.7} \qquad (2-26)$$

where the "order" of the reaction was 2.7. C_e for HAP at a pH of 8 is on the order of $10^{-7.5}$ M and was neglected in the rate law calculation. The rate constant k was found to be inversely proportional to the total bicarbonate concentration up to approximately 3.5 mM CO_{3T} and a pH range from 7 to 9. Magnesium in solution also inversely affected the rate constant, but not in direct proportion.

In this study Equation 2-25 was used for plotting the results

obtained from the batch studies and k was calculated for each of the different runs. The values of k and n were found to vary during each batch run, but in the final stages of each reaction n was approximately equal to 2. The value of n=2 was used for analyzing the column data at steady-state conditions, and the computed values of k approximated those observed in the batch runs that were run under similar conditions. Once k for the column runs was determined it was possible to compute prototype retention times and column sizes for any desired degree of removal.

2-3   Results of recent studies and their relation to this research

In most of the recent work on the precipitation of calcium phosphate solids, x-ray powder diffraction analysis was used as the method for identifying the material formed, as well as indicating its degree of crystallinity. The method can be schematically sketched as shown in Figure 2-8. A widely used method of analysis is to put the powdered sample on a specimen holder and to measure the intensity of the reflected x-rays by a rotating x-ray counter. The plot of intensity against the angle 2 Θ is representative of the particular crystals being observed. Well-defined crystals exhibit patterns such as sketched in Figure 2-9a, and liquids or truly amorphous solids exhibit patterns with diffuse peaks (Figure 2-9b).

The size of the crystallite also has an effect on the sharpness of the peaks, with the smaller the micro-crystal the broader the observed peak. Mathematically this relationship is described by the
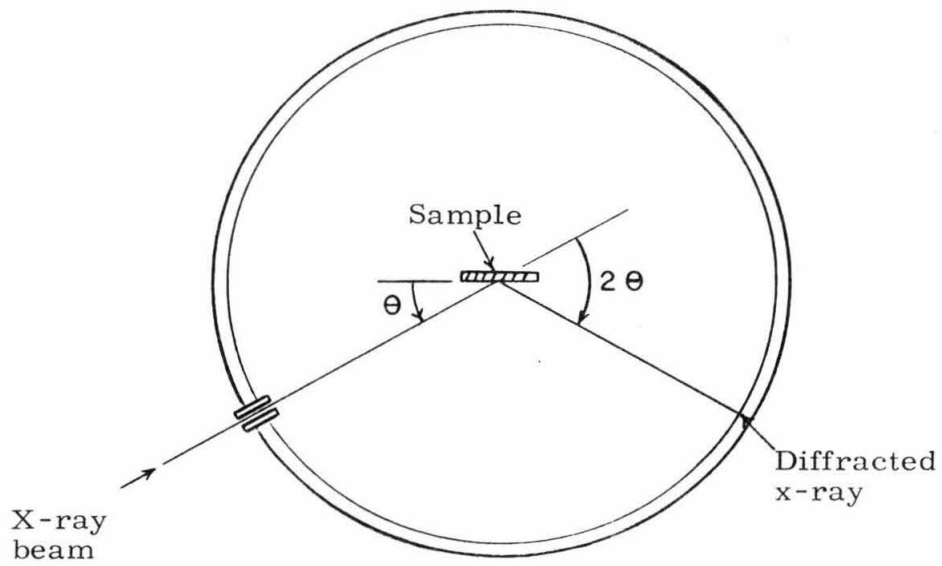
Figure 2-8. Schematic of powder x-ray diffraction analysis technique.
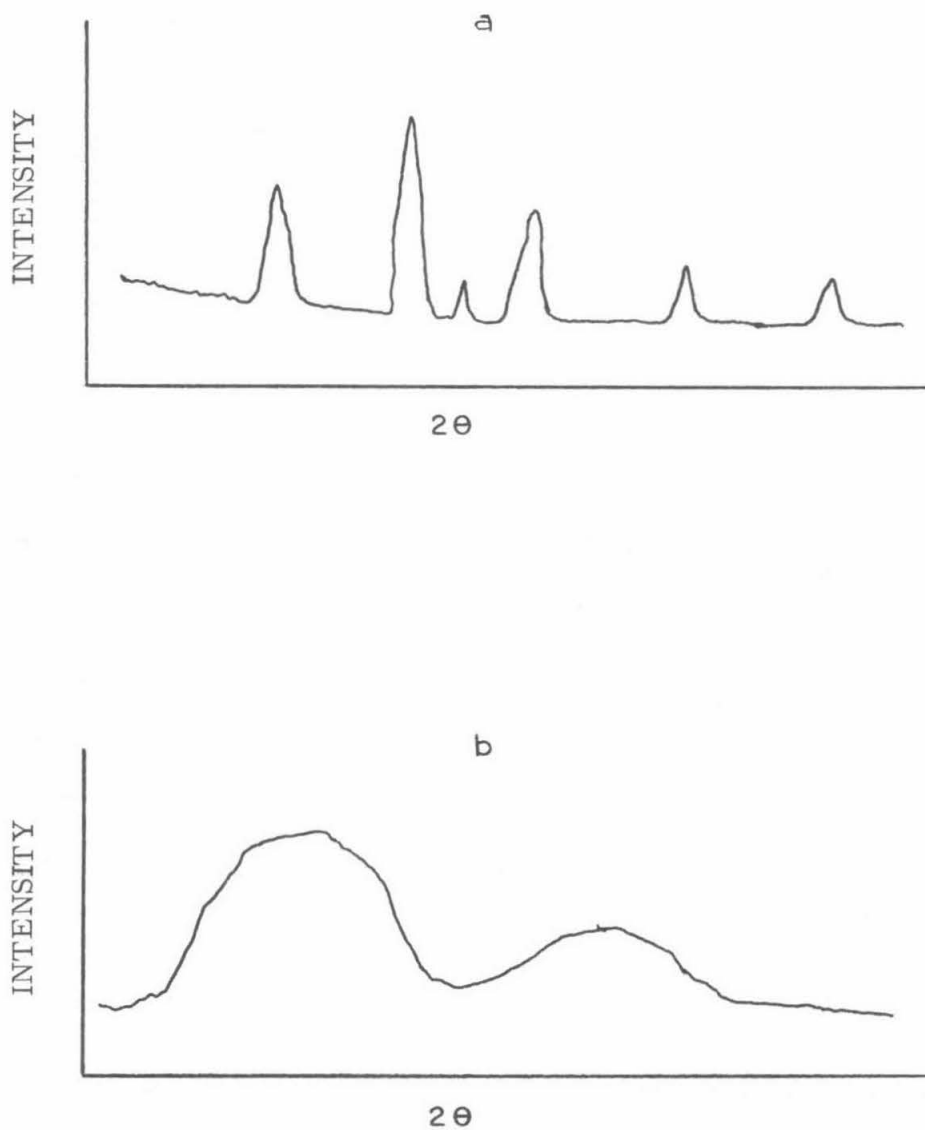
Figure 2-9. Sketches of the type of x-ray powder diffraction patterns for crystalline material (a), and amorphous material (b).

Scherrer formula[1]

$$d = 0.9 \lambda / (B \cos \Theta) \qquad (2\text{-}27)$$

where   d = grain size

         λ = x-ray wavelength

         B = 1/2 width of peak in radians

         Θ = Bragg angle of peak

For HAP[2] crystals of 100 $\overset{o}{A}$ size the half width of the peak is 0.8^{o}.

For 10 $\overset{o}{A}$ crystals the half width is 8.0^{o}, a relatively broad peak

which is on the order of what would be observed with amorphous

materials. In actual analysis there also are other factors that

tend to broaden the peaks. Among the more important ones are the

degree of vacuum in the diffractometer, the fact that the incident

x-rays can never be wholly parallel or monochromatic, and inherent

crystal imperfections.

In practice it is found that when crystal grains are smaller than

25 $\overset{o}{A}$ considerable care must be taken when trying to differentiate

between a truly amorphous substance and micro-crystals. Unfortu-

nately in most of the literature concerning dilute aqueous solutions that

has been reviewed to date, the crystal size is seldom referred to

when differentiating between an amorphous or a crystalline solid.

The most recent work on differentiating amorphous and crystalline

phases[3] seems to indicate that in actuality ionic solids like calcium

---

(1) A detailed analysis of x-ray diffraction can be found in Cullitz (1956).
(2) Assuming $2\Theta = 31^{o}$ and $\lambda = 1.5$ A.
(3) Private conversation with Dr. Pol E. Duwez, Prof. of Materials
Science, Caltech.

phosphates never really are amorphous. When they appear amorphous on x-ray diffractograms, they in reality are very small micro-crystals, perhaps even a fraction of a unit cell, that are randomly packed. The micro-crystals themselves can be any of the calcium phosphates that are in a state of supersaturation with respect to the solution.

Amorphous as used in this research will refer to a solid that may be either a truly non-determinate amorphous compound, or may actually be a conglomeration of very small crystallites. The more definite term of micro-crystal will be used to indicate very small crystals approximately 100 $\overset{o}{A}$ or less, regardless if they are formed by homogeneous nucleation from solution or by nucleation and crystal growth on catalyzing surfaces.

2-3-1   Intermediate phases during the formation of hydroxy-apatite

In precipitating calcium phosphates under controlled conditions many researchers find various intermediate forms precursory to the final HAP. Walton et al (1967) found an amorphous metastable material with a Ca/P ratio of 1.5 intermediate to the formation of HAP, which was assumed to be $Ca_3(PO_4)_2$. Clark (1955) studied the solubility of HAP by developing an experiment described by the schematic reaction

$$Ca(OH_2) + H_3PO_4 + N_2(g) \underset{90°C}{\overset{120 \text{ hr.}}{=}} HAP(s) \qquad (2-28)$$
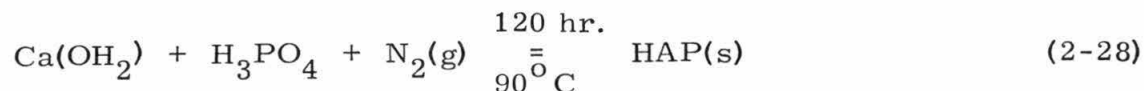
It is interesting to note that a high temperature and an extended period of time was necessary to produce crystalline HAP. In all cases the

crystallinity was verified by x-ray powder analysis. It was found that at a pH range of 5 to 9 the pK_{sp} of HAP was 115.40 ± 1.16.

Rootare et al (1962) and Deitz et al (1964) postulated the formation of a surface complex on the HAP crystal with the corresponding chemical equilibria:

$$Ca_{10}(PO_4)_6(OH)_2 + 6H_2O = 4Ca_2HPO_4(OH)_2 + 2Ca^{+2}$$
$$+ 2HPO_4^{-2} \qquad (2-29)$$

$$Ca_2HPO_4(OH)_2 = 2Ca^{+2} + HPO_4^{-2} + 2OH^- \qquad (2-30)$$
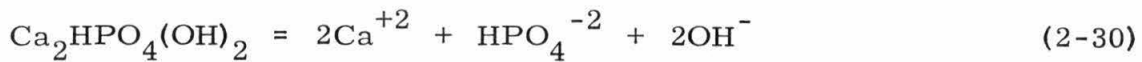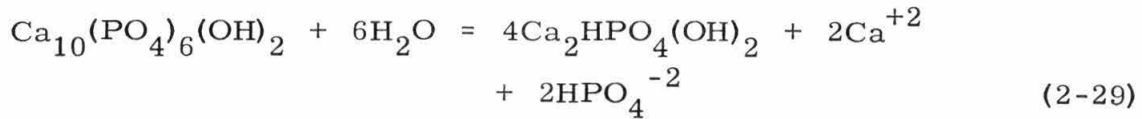
Dissolution of the surface complex could also follow the reaction

$$Ca_2HPO_4(OH)_2 + 2CO_2 = 2Ca^{+2} + HPO_4^{-2} + 2HCO_3^- \qquad (2-31)$$
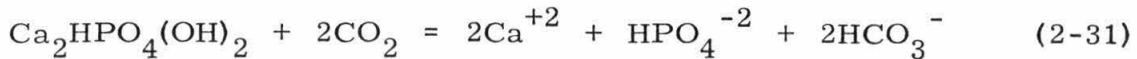
The equilibrium constant for HAP varied with the crystal weight to solvent ratio (m/V), but the equilibrium constant for the surface complex remained relatively constant at a $pK_{sp} = 27.28$ over a wide m/V ratio.

Moreno et al (1960) found in leaching studies with dicalcium phosphate dihydrate that the surface phases varied between OCP and DCPD. Leaching columns of DCPD crystals, they found DCPD present on the crystal at pH<6.38, and OCP present on the crystal at pH>6.38, but at no time (as determined by x-ray analysis) was HAP present.

Eanes and Posner (1968) and Eanes (1970) found that at a pH of approximately 9.5, amorphous calcium phosphates nucleated from a supersaturated solution and consisted of:

1) Calcium deficient HAP of the general formula

$$Ca_{(10-x)}H_x(PO_4)_6(OH)_{(2-x)}$$

2) Lamellar intergrowths of DCPD and/or OCP with HAP of the form:

$$CaHPO_4 \cdot 2H_2O : HAP_{5-3-1}$$

$$Ca_4H(PO_4)_3 \cdot 2.5H_2O : HAP_{5-3-1}$$
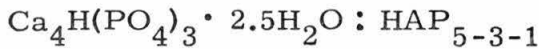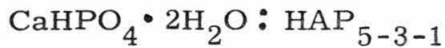
3) Hydrated TCP of the form

$$Ca_3(PO_4)_3 \cdot xH_2O$$
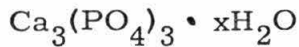
The water in the amorphous precipitate maintained its molecular identity, and upon heating to $600^{\circ}C$ in the presence of water vapor the precipitate converted rapidly into HAP. When the water vapor was minimized upon heating to $600^{\circ}C$, α TCP and β TCP were found instead of HAP. Eanes et al (1965) had earlier postulated that the interfacial surfaces of the emerging crystalline phase act as sites for heterogeneous nucleation and thereby accelerate the rate of conversion from the amorphous phase to the crystalline phase. The non-crystalline calcium phosphates remained stable if kept dry, so apparently water molecules are necessary for the formation of the crystal phase. However in light of the limitations of the x-ray powder diffraction technique used in his study it is possible that the actual process observed was not one where a non-determinate form of calcium phosphate transformed into a crystalline form, but rather simply a

phenomenon where micro-crystals ripened into larger, observable crystals.

Eanes et al (1965) found that the presence of magnesium ions retarded the formation of HAP from the amorphous calcium phosphates. When the Mg/Ca ratio was 1/4, the time of crystallization into HAP increased from 6 hrs. to 30 hrs. at 25°C. When the Mg/Ca ratio was 1/25, the time of crystallization into HAP increased from 2 hrs. to 6 hrs. at 30°C. The conversion into HAP was prolonged to a slight extent even when the magnesium was added after the calcium phosphate precipitate was formed. Ferguson (1969), studying a system of high total solids and low dissolved oxygen (as in anaerobic digestors), found that magnesium retarded the precipitation of phosphates at a pH less than 9 but enhanced precipitation at a pH greater than 9. Srivastava and Agrawal (1967) found that magnesium enhanced the dissolution of phosphates from a suspension of DCP.

Eanes and Posner (1968) found that strontium formed an intermediate phase, $Sr_3(PO_4)_2 \cdot 4H_2O$, before converting autocatalytically into $Sr_{10}(PO_4)_6(OH)_2$. However barium precipitated and crystallized immediately into $Ba_{10}(PO_4)_6(OH)_2$. Simpson (1968a) found that potassium-bearing apatites formed at low temperatures were variable in composition and contained excess volatiles. In experiments with low temperature FHAP formation Simpson (1968b) found that fluoride not only displaces the hydroxyl ion in HAP, but also has a significant effect on the crystal size. In work with Durango FAP Simpson (1969b) leached fluoride ions out of the FAP and concluded that the fluoride forms an amorphous surface coating that has a F^- concentration

less than the starting solid. FAP that had a fluoride concentration of 3.8% by weight and was precipitated in seawater was found to be metastable. Simpson (1969b) postulated that the precipitated FAP was in reality a fluor-carbonate apatite of marine phosphorite. He also found that low temperature sodium HAP would uptake fluoride from a solution as low as 10^{-4} M NaF by the reaction

$$1.25Ca_8Na_2(PO_4)_6(H_2O)_2 + 2F^- =$$
$$Ca_{10}(PO_4)_6F_2 + 2.5Na^+ + 1.5PO_4^{-3} + 2H_2O \quad (2-32)$$
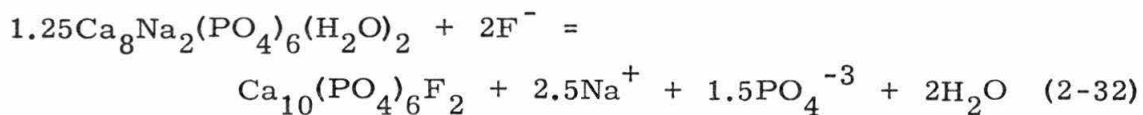
Simpson (1969a) succeeded in manufacturing an oxygen rich apatite containing 2% excess oxygen by doubly heating TCP to $1100^{\circ}C$ and then boiling it in a 30% H_2O_2 solution for 12 hours. The excess oxygen was retained up to $580^{\circ}C$ indicating that it was not water but was incorporated into the crystal lattice. Fisher and McConnel (1969) manufactured an aluminum-rich apatite by heating morinite to $600^{\circ}C$. They found that the aluminum substituted into both the calcium and phosphorus positions in the crystal lattice. Olsen et al (1960) found that HAP crystals adsorbed sulfate ions whereas DCPD did not. Any material adsorbed on the surface of a crystal would effect the surface chemistry of the crystal and would thereby influence the rate of crystallization. Olsen's work would indicate that perhaps the DCPD effectively forms a barrier for the crystallizing HAP and actually increases the purity of the final apatite formed. Illig (1960) found that glassy phosphate, $(NaPO_3)_6$, was effective in inhibiting iron and manganese precipitation in water distribution mains by forming an iron-phosphate complex. A 2/1 weight ratio of glassy phosphate to total iron and maganese in solution was found to be sufficient in inhibiting precipitation in actual case histories.

Old water systems with precipitated iron-manganese required higher concentration of glassy phosphate with periodic flushing to remove the accumulated scale.

Dietz et al (1942) found phosphorite deposits on the sea floor off Southern California and concluded that the nodules[1] were formed by direct precipitation. Although the seawater was saturated with respect to TCP the material actually precipitated was a mixture of compounds having the apatite structure. Kramer (1964) calculated that seawater was supersaturated with respect to HAP and FAP, but only by 1-2%.

2-3-2 Intermediate phases during the formation of carbonate-apatites

When the ion product of a solution of calcium and carbonate ions exceeds the solubility product of solid calcium carbonate, there is a driving force tending to precipitate that solid phase from solution. Homogeneous nucleation will occur only if the critical supersaturation is exceeded by a certain degree. However the presence of apatite crystals introduces a nucleating surface which induces heterogeneous nucleation even at relatively low supersaturation values. Leckie (1969) found that in most aqueous systems where HAP and calcium carbonate were both in a state of supersaturation, the calcium carbonate would precipitate first and present a catalyzing surface for the nucleation and crystal growth of HAP. In order to minimize this co-precipitation effect, all synthetic feed experiments in this research were designed so

(1) Average diameter of the nodules was about 5 cm., but some irregularly shaped samples were as large as 60 x 50 x 20 cm.

that the solubility product of calcium carbonate was not exceeded. In this manner the analysis of the data was simplified because only the rate equation for the formation of HAP need be considered. However in many secondary treated effluents the chemical composition favors precipitation of calcium carbonate,and this effect must be considered. The results of Ferguson et al (1971) indicate that the type of rate equation used in this research (Equation 2-23) is valid for systems where calcium carbonate is slightly supersaturated. The solid formed is a combination of calcium carbonate and HAP and is called carbonate-apatite (CHAP, CFAP, etc.). The secondary effluent used in this study had a calcium carbonate supersaturation ratio of 1.20.

Evidence that the carbonate was contained in the apatite structure was first presented by McConnel (1938). Neuman and Neuman (1953) concluded that the carbonate ion could be adsorbed on the crystal surfaces. From thermodynamic considerations calcite and aragonite should phosphatize into an apatite in the presence of ortho-phosphate groups,but the reaction rate is unknown. Leckie (1969) could not induce crystallization of apatite in natural water systems. Instead apatite grew on calcite crystals, probably in the form of a carbonate apatite. Simpson (1966a) found that even though a pure magnesium apatite is unknown substantial amounts of magnesium are found in some natural carbonate-apatites. Bachra et al (1963) found that under physiological conditions a CO_{3T}/P_T molar ratio less than 300 prevented the spontaneous precipitation of calcium carbonate. When apatite was precipitated in the presence of carbonate the crystallinity of the apatite was reduced. An amorphous calcium

carbonate apatite was obtained when the CO_{3T}/P_T ratio was greater
than 17. The precipitate gradually changed into a poorly crystallized
apatite as it was kept in contact with the solution for several days.
The amorphous precipitate had a Ca/P ratio that varied from 2.1 - 2.3,
while the crystalline precipitate had a Ca/P ratio that varied from
1.4 - 2.2. The larger the CO_{3T}/P_T ratio in the solution, the larger was the
Ca/P ratio in the precipitate. Bachra et al (1963) postulated that
20-27% of the calcium ions were bound to the carbonate. They also
found that the presence of magnesium enhances the formation of the
$Ca-CO_3-PO_4$ amorphous precipitate and retarded its crystallization
into an apatite. Trautz (1960) found that in CHAP the CO_3^{-2} will be
randomly distributed throughout the crystal structure. The force
field of the CO_3^{-2} groups is different from the surrounding PO_4^{-3}
groups and causes a distortion of the atomic planes and, at times, a
break in the coherence of the lattice. Ferguson (1969) concluded that
carbonate decreased the precipitation of phosphates by ion complex
formation with calcium, by competitive precipitation of calcium
carbonate, and by lattice substitution into the amorphous and crystal-
lized calcium phosphates. In his studies he also found that increased
temperature in the range of $20^{\circ}C$ to $45^{\circ}C$ generally decreased the
apparent solubility of phosphates. This is not in agreement with thermo-
dynamic predictions and he consequently concluded that the increased
temperature hastened the crystallization of a more insoluble solid.
Simpson (1964) found that the quantity of hydroxyl ions in CHAP was
usually insufficient to compensate for the charge difference resulting
from the substitution of carbonate for phosphate. Heating of the sample

between $300^{\circ}C$ and $700^{\circ}C$ expelled the carbonate, and as it was
expelled, the mean index of refraction approached that for pure HAP.
Such changes can only be accounted for if the CO_2 is contained in the
crystal structure. When the CHAP crystals were subjected to reduced
pressures, no effect was observed on the carbonate or the total weight
of the material. Only about one half of the total weight loss due to
heating could be accounted for by carbonate ions.

The question of an intermediate phase when considering phosphati-
zation of solid $CaCO_3$ seems to hinge upon OCP and DCPD. Clark (1955)
found DCPD as the intermediate phase with HAP as the stable
crystalline phase. In his experiments he found the relationship between
phosphate and time to vary with temperature as shown in Figure 2-10.
Cole et al (1953) found that soluble orthophosphate reacted with
$CaCO_3(s)$ by forming DCPD on the surface of the $CaCO_3(s)$.
Simpson (1967) ran experiments where 0.2 M Na_2HPO_4 was quiescently
contacted with 3.0 cm of solid fine-grained $CaCO_3$ crystals for 9
months in the absence of any gas. The pH changed from 7.5 to 9.16
during the time interval. Upon x-ray analysis he found the surface to
consist of pure HAP, the 5-mm depth to consist of HAP and calcite,
and the 15-mm depth to consist of only calcite. It was interesting that
no OCP was found at any level. In a shorter time experiment of 15
days, he found OCP at the surface and HAP at the 1.5 and 3.0-mm
levels. He concluded that OCP was the intermediate phase in the
formation of HAP on calcite. In light of Clark's (1955) short-term
experiment it appears that the chain of crystallization of apatite on
calcite may follow a DCPD→OCP→HAP route. Cole et al (1953) used
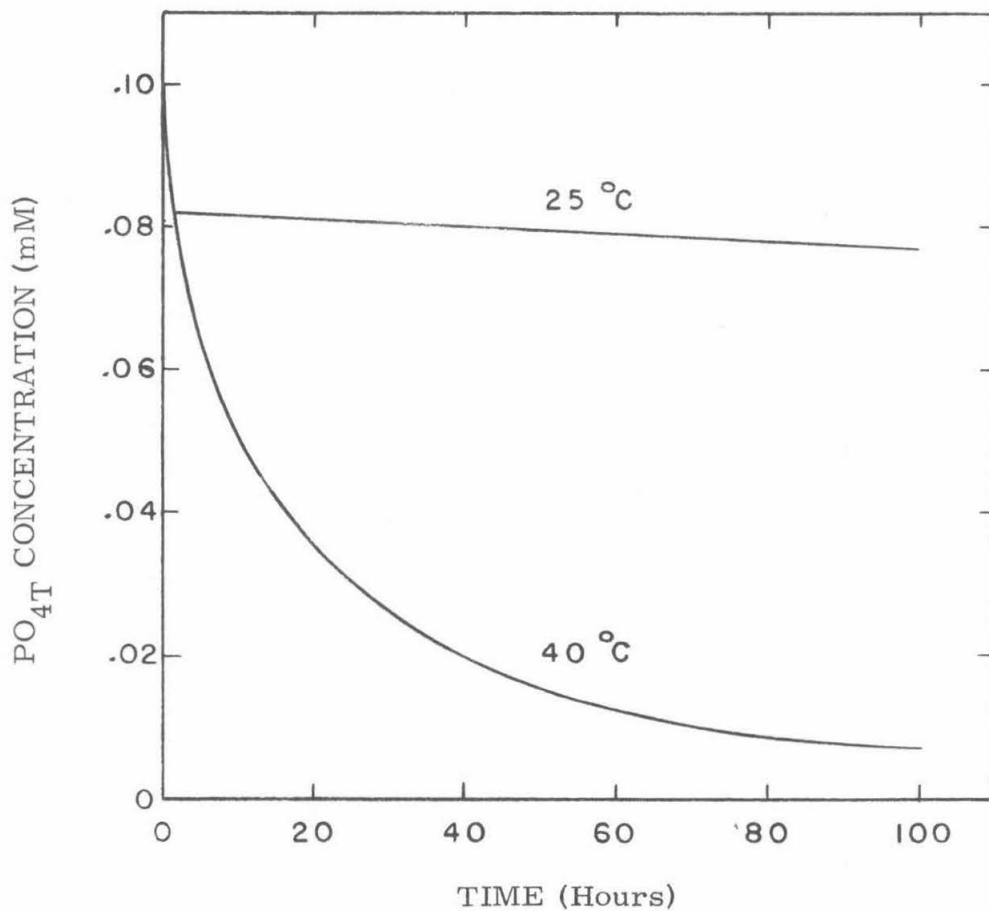
Figure 2-10. Time and temperature dependence of soluble phosphorus in a $CO_2(g)$ - $CaCO_3(s)$ - $KH_2PO_4(aq)$ system. P_{CO_2} = .0003 atm (Clark & Turner 1955).

P^{32} as a tracer to study phosphorus migration into calcite. In short term studies he found that adsorbed phosphorus was readily desorbed. But as the contact time between soluble P^{32} and $CaCO_3(s)$ was increased, the tagged phosphorus became less exchangeable with the new solution. Simpson (1966b) found in precipitation experiments with CO_2 partial pressures of 10% and 1% that OCP was formed at the expense of HAP. The addition of fluoride ions enabled a fluoroapatite to form over a wider pH range than previously possible.

2-4   Rationale of this research

Although the literature contains many references to the chemistry of phosphorus in the natural environment, the information is notably lacking in uniformity of results. The major difficulty seems to result from the application of the Ostwald-Gay Lussac Step Rule (Van Wazer, 1958), which states that the less thermodynamically stable, and hence the more soluble, form of polymorphous solid is generally the most readily precipitable. Consequently in the nucleation of calcium phosphates the more soluble forms are the ones that are nucleated first. The more soluble calcium phosphates then transform into apatites with the passage of time. It therefore becomes highly important to pinpoint the existing state during this transformation process in order to be able to analyze the phenomena that are occurring.

The theories of nucleation and crystal growth from dilute aqueous solutions are presently in a state of development only for pure systems. For all practical purposes the many parameters involved in the

equations become impossible to measure in the natural aquatic environment. The approach best justified at this time appears to be one of semi-empirically analyzing the phenomena, utilizing as many variables as possible that would make the resultant equations applicable to a wide variety of conditions.

Once the type of equation and corresponding rate constants are determined, it becomes possible to establish engineering criteria for a phosphorus removal process based on nucleation and crystal growth of calcium phosphate on phosphate rock.

Chapter 3

Experimental Apparatus and Procedures

The experiments performed were divided into two categories: batch systems and column systems. Chemical component concentrations were determined on aliquots of each batch run after the solid phosphate rock was removed by centrifugation or filtration. Concentrations were determined directly on the column effluent since no solids were ever observed in the column effluent samples. Electron diffraction analysis was performed on a batch run, and a brief explanation of the technique used is presented with the data in Chapter 5.

3-1   Feed solutions

3-1-1   Synthetic feed solutions

All synthetic feed solutions were made with distilled water and reagent grade chemicals. All glassware was washed, rinsed with hot tap water, rinsed with a cleaning solution of 50% 3N HCl and 50% ethanol, and then distilled water rinsed 5 times. Pipettes were tap water rinsed, soaked in a solution of 1M KOH in ethanol for 15 minutes, distilled water rinsed 3 times, and oven dried.

Anhydrous calcium chloride was dissolved in distilled water to make a stock solution. Aliquots of this stock were introduced into the feed solution as the source of Ca^{+2} ions. The HCO_3^- ion was furnished from powdered sodium bicarbonate that was weighed and introduced

directly into the feed solution. All material weighing was performed to the nearest milligram. A stock solution of PO_4^{-3} ions was made from anhydrous dibasic potassium phosphate stablized with chloroform. Aliquots of this stock were used as the source of phosphate ions. Powdered sodium fluoride was weighed out and introduced directly into the feed solutions as the source of F^- ions. Anhydrous powdered magnesium sulfate was weighed and used directly as the source of both Mg^{+2} and SO_4^{-2} ions. Granular ammonium chloride was weighed out and directly used as the source of NH_4^+ ions. When the borax buffer[1] system was used in some runs the procedure for making the buffer as given in the "Handbook of Physics and Chemistry 50th Edition" was followed. This procedure utilizes reagent grade 0.025 M $Na_2B_4O_7 \cdot 10H_2O$ and concentrated HCl as the buffering components. The approximate ionic strength of the borax buffered solutions[2] was 0.076 M.

The concentrations for the synthetic feed solutions used in this study are given in Table 3-1. The values listed under the bicarbonate-buffered systems indicate the ranges used in the batch runs. The values listed under the column systems represent the concentrations in the stock feed. To this feed various ions were added in order to determine their effect on column operation. The partial pressure of $CO_2(g)$ was also varied in order to study the effects of changing the alkalinity and pH on the column operation.

---

(1) Borax is the trade name for sodium tetra borate, $Na_2B_4O_7 \cdot 10H_2O$.
(2) As determined by extrapolated conductivity data.

Property	Concentrations		
	Batch systems (initial values)		Column Systems (stock feed)
	Borax buffered	Bicarbonate buffered	
Na^+ (mM)	-	0.9 – 1.3	0.65
K^+ (mM)	0.63	0.6 – 0.8	0.60
Ca^{+2} (mM)	2.00	1.0 – 2.0	1.0
Cl^- (mM)	33.1	2.0 – 4.0	2.0
HCO_3^- (mM)	-	0.70 – 0.94	0.65
PO_{4T} (mM)	0.315	0.30 – 0.40	0.30
Borax (mM Formal)	17.0	-	-
Conductivity (m mho/cm)	3.80	0.350	0.35
$CO_2(g)$ (atm)	-	3×10^{-4}	3×10^{-4}
pH	8.3	8.0	8.0

Table 3-1. Composition of the various synthetic feed solutions used in this study.

3-1-2   Secondary treated wastewater feed solution

The secondary effluent used for feed was collected from The Whittier Narrows Water Reclamation Plant, Los Angeles County, California. The plant utilized primary settling and activated sludge biological treatment.

Typical concentrations in the effluent are presented in Table 3-2, which represents the values determined from a 24-hour composite collected from 3 April 1972 to 4 April 1972[1]. The actual feed used in the column experiment was a grab sample collected in the afternoon of 20 March 1972 and consequently had constituent concentrations slightly different from the composite analysis. The concentrations in the grab sample that were measured by the author are presented in Table 3-3.

3-2   Solid phosphate rock

The phosphate rock used was supplied by International Minerals & Chemicals Corporation, Agricultural Chemicals Division, Bartow, Florida. The cleaned and sieved ore supplied was reported as $33.3 \pm 0.1\%$ phosphoric acid (dry basis P_2O_5). It should be noted that no special handling was given to the material supplied. It was one of the standard grade ores normally supplied to manufacturers of phosphate fertilizers. Tables 3-4 and 3-5 give an indication of various mineral constituents of the phosphate rock used. An x-ray powder

---

(1) Collected and analyzed by the County Sanitation Districts of Los Angeles County, Los Angeles, California.

Property	Concentration (mM)
pH	7.88
Suspended solids, mg/l	8.0
Dissolved solids, mg/l	600
Total solids, mg/l	608
Conductivity, m mhos/cm	1.07
Total hardness, mM	1.70
Total alkalinity, mM	2.60
Chloride, mM	3.04
Sulfate, mM	1.42
Phosphate, mM	0.295
Fluoride, mM	0.074
Nitrate, mM	0.057
Nitrite, mM	0.043
Ammonia, mM	1.28
Organic nitrogen, mM	0.17
Total chemical oxygen demand, mM O	2.62
Soluble chemical oxygen demand, mM O	2.38
Biochemical oxygen demand, 5 day, $20^{\circ}C$, mM O	0.38
Phenols, mM C_6H_5OH	$< 1.0 \times 10^{-4}$
Methelyne blue alkyl sulfonates, mg/l ABS	0.2
Hexane extractables, mg/l	0.4
Arsenic, mM	0.00
Boron, mM	0.078
Cadmium, mM	2.5×10^{-5}
Total chromium, mM	0.001
Copper, mM	0.001
Iron, mM	0.001
Manganese, mM	5.0×10^{-4}
Potassium, mM	0.33
Sodium, mM	5.91
Zinc, mM	0.002
Calcium, mM	1.05
Magnesium, mM	0.65
Lithium, mM	0.0029
Cyanide, mM	4.0×10^{-4}
Nickel, mM	0.0056
Selenium, mM	6.3×10^{-4}
Silver, mM	6.0×10^{-4}

Table 3-2. 24 hour composite of Whittier Narrows Water Reclamation Plant secondary effluent, April 3/4, 1972. Courtesy of County Sanitation Districts of Los Angeles County.

-46-

Property	Total concentration of all protonated and complexed species (mM)
Ca^{+2}	1.08
PO^{-3}	0.232
Total Alkalinity	5.35
HCO_3^-	5.16
F^-	0.051
	pH = 7.68
	Conductivity = 1.11 m mhos/cm

Table 3-3. Measured quantities for the Whittier Narrows Secondary Effluent that was used as column feed.

Constituent	% of total (by weight)
P_2O_5	35.5
CaO	48.8
MgO	0.04
Al_2O_3	0.9
Fe_2O_3	0.7
SiO_2	6.4
SO_3	2.4
F	4.0
Cl	0.01
CO_2	1.7
Organic Carbon	0.3
Na_2O	0.07
K_2O	0.09
H_2O	1.8

Table 3-4. Representative analysis of Florida land pebble phosphate rock (Van Wazer 1961).

Element	Concentration (ppm)
Arsenic as As_2O_5	5-30
Barium as BaO	trace
Beryllium as Be_2O_2	ca. 10^2
Boron as B_2O_3	20-100
Cadmium as CdO	ca. 10
Cesium as Cs_2O	ca. 10
Chromium as Cr_2O_3	1-130
Copper as CuO	5-30
Iodine as I	5-15
Lead as PbO	ca. 10
Lithium as Li_2O	ca. 10
Manganese as MnO	20-500
Mercury as HgO	ca. 10^2
Molybdenum as MoO_3	20-50
Nickel as NiO	20-50
Nitrogen as N	60-150
Rare earths as Re_2O_3	300-700
Rubidium as Rb_2O	ca. 10^2
Selenium as SeO_3	0-15
Silver as Ag_2O	ca. 10^2
Strontium as SrO	ca. 10^3
Tin as SnO_2	10-50
Titanium as TiO_2	300-700
Uranium as U_3O_8	100-200
Vanadium as V_2O_3	10-200
Zinc as ZnO	5
Zirconium as ZrO_2	ca. 10

Table 3-5. Trace impurities in Florida land pebble phosphate rock (Van Wazer, 1961).

diffraction analysis[1] of the ore supplied showed that it was a mixture of crystalline FAP and HAP.

It was obvious at the outset of this research that various types and grades of phosphate ores could have marked effects on the phosphorus removal ability of a system under study, whether it be a batch or a column type of system. It was decided to concentrate on studying the effects of controllable parameters such as surface area and solution concentrations rather than the properties of various types of phosphate rocks. However it should be recognized that before attempting any engineering design of a prototype phosphate removal process utilizing micro-crystallization on phosphate rock, a comprehensive study of the various grades and types of phosphate ores available will be an absolute necessity to insure use of the most effective mineral available.

International Minerals & Chemicals Corporation supplied 2 sizes of phosphate rock, one sample with 72% greater than 10 mesh, the other with 1.1% greater than 10 mesh. The larger size was milled and sieved through screens ranging from a 14 Tyler mesh to a 325 Tyler mesh.[2] The material passing through the 325 mesh was collected and used for all batch runs and had a BET surface area[3] of $13.5 m^2/g$. The material passing the 14 mesh but collected on the 32 mesh (1.168 mm x 0.495 mm) was used for some of the column runs, and is referred to as PR 14x32. It had a BET surface area of $8.8 m^2/g$.

_____

(1) X-ray diffraction was performed by Elizabeth Bingham, Geological and Planetory Sciences Division, California Institute of Technology, Pasadena, California.
(2) The 14 Tyler mesh screen has openings of 1.168 mm and the 325 Tyler mesh has openings of 0.043 mm.
(3) All BET analyses were run by Mr. William Cannon, Jet Propulsion Laboratory, Pasadena, California.

In order to vary the phosphate rock surface area the raw ore with only 1.1% greater than 10 mesh was also used in some column runs. It had a BET surface area of 12.3 m^2/g and a mean diameter of 0.24 mm. The absolute specific gravity of the phosphate rock was found to be 2.93 g/cm^3. The bulk specific weight of the phosphate rock was approximately equal to 1.77 g/cm^3 for the PR-10 sample, and 1.50 g/cm^3 for the PR 14x32 sample. The corresponding porosities were respectively 0.40 and 0.48.

3-3   Analytical equipment and techniques

3-3-1   Orthophosphate determination

Total orthophosphate was determined by using the stannous chloride without extraction technique described in the Thirteenth Edition of "Standard Methods for the Examination of Water and Waste-water", pp 530-532. A sample (or diluted sample) of 50 ml was reacted in a 50-ml stoppered graduated cylinder for 10 minutes, at which time the absorbance was measured at 700mμ in a "Lumetron Colorimeter, Model 402-E"[1]. Round lumetron glass vials of 1.1-cm inside diameter were used, giving a light path of approximately 1 cm.

3-3-2   pH measurement

pH was measured with a "Radiometer #25" expanded scale pH meter[2]. The electrodes were a Beckman #39301 glass electrode

(1) Photovolt Corp., New York 10, New York.
(2) Radiometer, Copenhagen, Denmark.

and a Beckman #39402 calomel reference electrode[1]. The samples
were equilibrated with the electrodes for 5.0 minutes by slight stirring
with a magnetic stirrer and stirring bar before the pH reading was
recorded. For standardizing the meter the electrodes were similarly
calibrated for 5.0 minutes in a "Beckman #3007 pH 7.00" buffer solution.
Rather than make an ionic strength correction to determine the hydrogen
ion concentration the proton activity as calculated from the measured
pH was used in all calculations. Therefore any equilibrium constants
containing proton or hydroxyl ion concentrations are reported as
mixed constants.

3-3-3 Alkalinity determination

Total alkalinity was measured by titration of each sample with
0.02 N HCl to a pH value of 4.5. The samples were first equilibrated
with the electrodes as described in section 3-3-2 in order to measure
the sample pH, after which the titration was accomplished in approxi-
mately 2 minutes. The value of the total alkalinity concentration in
the synthetic feed is given by

$$Total\ alkalinity) = (OH^-) - (H^+) + (HCO_3^-) + 2(CO_3^{-2})$$
$$+ (HPO_4^{-2}) + 2(PO_4^{-3}) \qquad (3-1)$$

In the pH range of 4.5 to 8.0, the total alkalinity can be approximated
to within 2% by

$$(Total\ alkalinity) = (HCO_3^-) + (PO_{4T}) \qquad (3-2)$$

[1] Beckman Instruments Inc., Fullerton, California.

The bicarbonate concentration can then be computed from measurements of the total alkalinity and total phosphate concentrations. For each sample a computer program was used to calculate the distribution of the carbonate and phosphate ion forms.

3-3-4   Calcium determination

Total calcium was determined by the EDTA titrimetric method as described on pp 84-86 of the Thirteenth Edition of "Standard Methods...". Eriochrome blue black R indicator was used in conjunction with 8N NaOH for the end point determination.

3-3-5   Fluoride determination

Total fluoride was determined by use of an Orion fluoride electrode model #94-09A. Total ionic strength adjustment buffer (TISAB) was used on a 1 to 1 dilution as described on pp 172-174 of the Thirteenth Edition of "Standard Methods...". A Corning #476012 sleeve type calomel electrode was used for a reference potential. Standards were always run at the start and end of each set of samples and 3 minute reading of standards and samples were recorded for fluoride calculation.

3-3-6   Conductivity determination

Conductivity was measured using a "Radiometer Conductivity Meter Type CDM 2e" in conjunction with a type CDC114-CT radiometer conductivity cell. Conductivities were routinely measured on all samples in order to give some indication of the ionic strength

fluctuation during each run.

3-3-7   Solids separation

On all of the batch runs solid phosphate rock slurry was separated
from the aqueous solution by centrifugation at approximately 2,000 G
for 30 minutes or by filtration through a 0.22 micron millipore filter.
Centrifugation was accomplished on an "International Centrifuge,
Universal Model UV"[1].

When the solid phase was to be examined for diffraction it was
dried by gently blowing pressurized air into the bottom of the centri-
fugation flask where the solid had settled or directly onto the millipore
filter containing the caked solid. Drying took approximately 5 minutes.
The solid powder was then dessicated for at least a day to insure com-
plete dryness and saved for the diffraction analysis by freezing at
$-60^{\circ}C$.

3-3-8   Electron diffraction analysis

The electron diffraction analyses were performed on a Siemen
1A-100 KV" electron microscope.[2] A small amount of phosphate rock
sample was suspended in 3 drops of water, after which 1 drop of the
suspension was evaporated on a 200-mesh, 2.3-mm diameter copper
grid. The grid was carbon coated before and after the sample was
applied.

(1) International Equipment Co., Needham Hts., Mass.
(2) Siemens Corp.; Iselin, New Jersey. All electron microscope work
was performed by Mr. Henri Arnal and the author under the supervision
of Dr. Robert E. Villagrana, Calif. Institute of Technology.

The electron micrographs and electron diffraction patterns were recorded on film-coated glass plates. The glass plates were directly inserted on a "Spectroline scanner, Model 22.100" microphotometer[1] for nuclei size calculations.

3-4   Buffering methods

The initial batch experiments were performed in stoppered glass bottles that were completely filled with the reaction solution. With this system the pH fluctuated during a run by as much as 1.4 pH units. Since the rate of nucleation and crystal growth of HAP is dependent on the solution pH it became imperative to minimize the pH change during each run. Two methods for the batch runs were tried: a borax-HCl buffering method, and a $CO_2(g)$-bicarbonate buffering method. The borax-HCl method maintained a constant pH but seemed to interfere with the reaction process. The $CO_2(g)$-bicarbonate method was more representative of the buffering action of atmospheric carbon dioxide, but it produced a pH fluctuation of approximately 0.2 pH units. The $CO_2(g)$-bicarbonate method could only be used in batch systems that were vented. In the column runs the feed was buffered by the $CO_2(g)$-bicarbonate method.

3-4-1   Borax-HCl buffer

Reagent grade sodium tetra borate and reagent grade concentrated hydrochloric acid were dissolved in distilled water to establish the

---

(1) Applied Research Laboratories; Montrose, California.

pH desired, after which the various desired ion species were intro-
duced into the solution. The buffering action of borax-HCl can be
described by the following chemical reactions:

$$Na_2B_4O_7 \cdot 10H_2O = 2Na^+ + 2B(OH)_4^- + 2B(OH)_3 + 3H_2O \qquad (3-3)$$

$$B(OH)_3 + H_2O = B(OH)_4^- + H^+ \qquad (3-4)$$

$$B(OH)_4^- + H^+ + Cl^- = B(OH)_3 + H_2O + Cl^- \qquad (3-5)$$
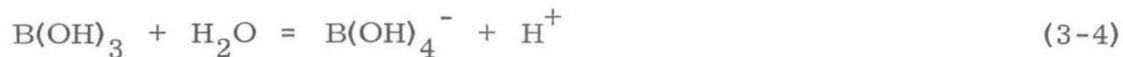
Although boron is not known to incorporate into the apatite crystal
structure it is found as a trace element in naturally occurring phos-
phate rocks (see Table 3-4). Apparently the $B(OH)_4^-$ form can adsorb
on the Ca^{+2} faces of the apatite crystal and thereby interfere in the
crystallization process. The approximate concentration of $B(OH)_4^-$
ions in the buffer solution used was 5 mM. This was at least 15 times
greater than the PO_{4T} concentration. Since the structures of the
$B(OH)_4^-$ and PO_4^{-3} ions are similar it was possible that the boron
form also physically interfered with the apatite crystallization by
locating in the apatite crystal lattice, especially since the excess of
the boron form over the total phosphate was so great. The primary
usefulness of the boron buffer system was in comparing surface area
effects at constant pH.

3-4-2 $CO_2(g)$ - bicarbonate buffer

All natural waters are buffered to some extent by atmospheric
$CO_2(g)$ and soluble bicarbonate concentrations. The reactions

describing this system are as follows:

$$CO_2(g) + H_2O = H_2CO_3^* \tag{3-6}$$

$$H_2CO_3^* = H^+ + HCO_3^- \tag{3-7}$$

$$HCO_3^- = H^+ + CO_3^{-2} \tag{3-8}$$

In these equations $H_2CO_3^* = CO_2(aq) + H_2CO_3$. The equilibrium conditions can be represented by:

$$(H^+)(OH^-) = K_w \tag{3-9}$$

$$(H_2CO_3^*) / P_{CO_2} = K_H \tag{3-10}$$

$$(HCO_3^-)(H^+) / (H_2CO_3^*) = K_1 \tag{3-11}$$

$$(CO_3^{-2})(H^+) / (HCO_3^-) = K_2 \tag{3-12}$$

If a pure solution of sodium bicarbonate is equilibrated with a O_2 - N_2 - CO_2 gaseous mixture, the pH can be calculated from the values of the sodium concentration and the partial pressure of CO_2. In such a system the charge balance equation is

$$(Na^+) + (H^+) = (OH^-) + (HCO_3^-) + 2(CO_3^{-2}) \tag{3-13}$$
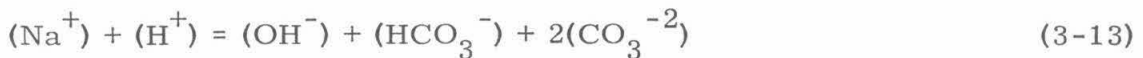
If the OH^- concentration[1] in Equation 3-13 is neglected and Equations 3-10 through 3-12 are substituted into Equation 3-13, it can readily

---

[1] In all the experiments in this research the pH range was from 5 to 8.3 and the concentration of sodium bicarbonate was approximately 1.0 mM, resulting in a $(HCO_3^-) / (OH^-)$ ratio always greater than 100.

be shown that

$$(Na^+) = P_{CO_2} K_H (K_1/(H^+) + 2K_1 K_2 / (H^+)^2) \tag{3-14}$$

If the pH is less than 8.3 the second term in Equation 3-14 can be neglected. By taking negative logarithms of all quantities and using the notation $pX = -\log_{10} X$, the general form of Equation 3-14 becomes

$$p(Na^+) = p(P_{CO_2}) - pH + Constant \tag{3-15}$$

Assuming an ionic strength of 0.01 M the constant in Equation 3-15 is calculated to be 7.77 (Stumm and Morgan, 1970). Equation 3-15 was reasonably well followed in an aqueous solution of $NaHCO_3$ and $CaCl_2$ equilibrated with a known partial pressure of CO_2.

When phosphate rock is introduced into a solution containing $NaHCO_3$ and $CaCl_2$ some of the impurities in the phosphate rock will dissolve, with the resultant pH in the system no longer being controlled only by bicarbonate and CO_2 gas equilibrium. However the major contribution to the buffering capacity of the new system is still from the carbon-dioxide equilibrium, and an empirical approach can be utilized to develop an equation similar to Equation 3-15 that can be used to predict pH under varying concentrations of Na^+ and P_{CO_2}. The experiments that were used to develop this empirical equation consisted of an aqueous solution of $NaHCO_3$, $CaCl_2$, powdered phosphate rock, and varying partial pressures of CO_2 gas. The equation predicted the pH values to within 0.2 pH units and is

$$pNa^+ = p(P_{CO_2}) - 1.033 \, pH + 8.00 \tag{3-16}$$

3-5   Experimental procedures and equipment

3-5-1   Closed vessel batch experiments

Early experiments were run in 300-ml stoppered bottles[1] with mixing by magnetic stirrers. The powdered phosphate rock was mixed with the buffer solution and introduced into each open bottle. At zero time the stock phosphate was added, the bottles were capped, and the reaction allowed to proceed. The 6-unit multi-stirrer[2] used for stirring was placed in a fume hood for temperature control. The room was air conditioned with a temperature of $23\pm2^{\circ}C$. Since the stirring magnets were belt driven by a vented motor no heat was transmitted to the bottles, and the reaction temperature fluctuated only as the room temperature. When the solution in each bottle was stirred for the desired time, the bottle was removed from the stirrer, the contents were centrifuged, and the supernatant was chemically analyzed. All borax-HCl buffered runs were executed in this manner.

3-5-2   Open vessel batch experiments

A sketch of the apparatus used in the open vessel batch experiment is shown in Figure 3-1. The phosphate rock, sodium bicarbonate, and calcium chloride were added to distilled water and allowed to come to equilibrium overnight with the CO_2 gas mixture. At zero time the stock K_2HPO_4 solution was added to the solution and aliquots were

---

(1) Commonly referred to as BOD bottles.
(2) "Lab Line Multi Magnister", Van Waters and Rogers, Los Angeles, California.
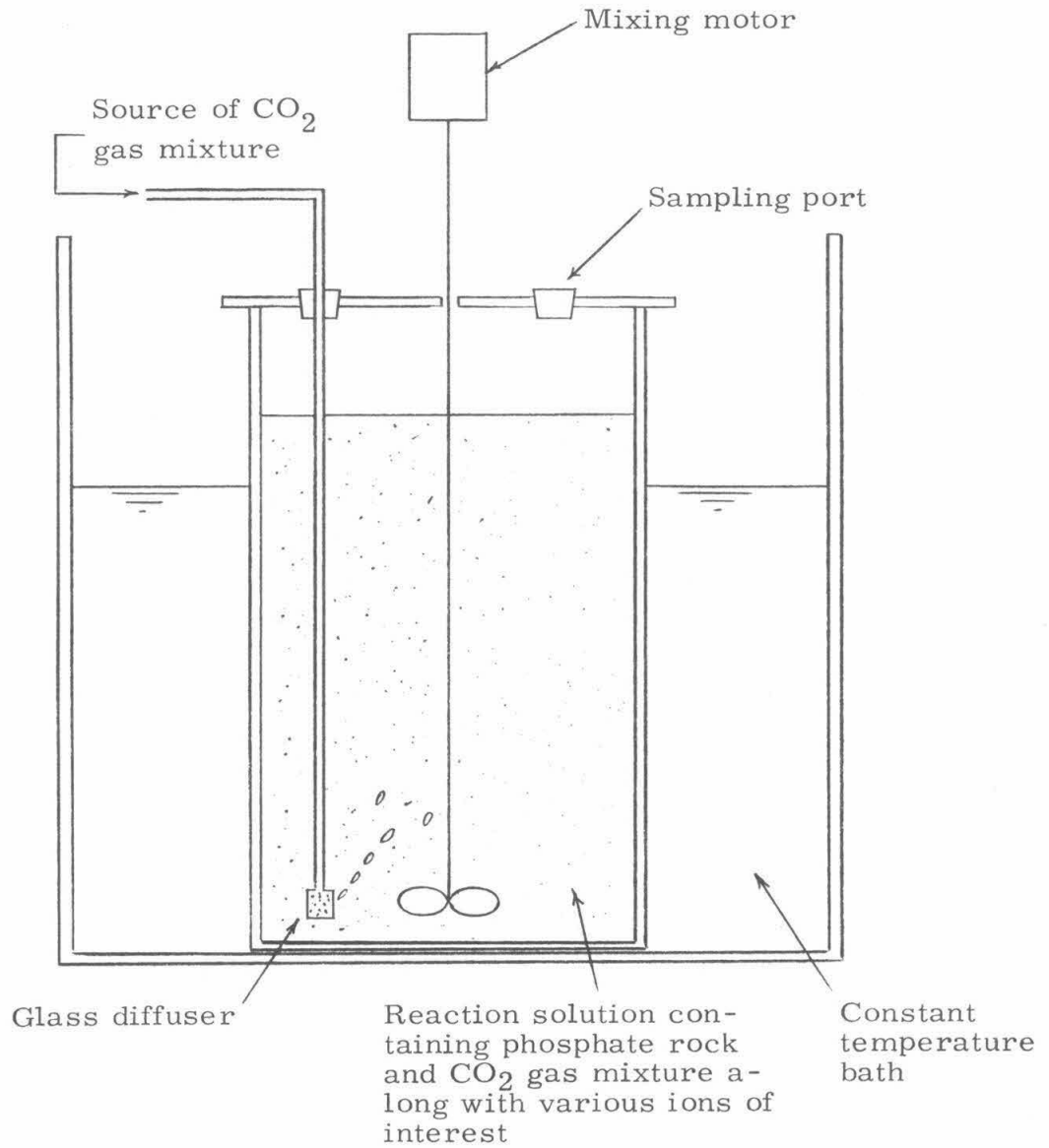
Figure 3-1. Schematic representation of the open vessel batch experiments.

removed at various times of the run for centrifugation or filtration and analysis. The temperature of the reaction solution was frequently checked and never varied by more than $0.1 C^O$. Since the internal pressure of the reaction mixture was slightly greater than atmospheric due to the bubbling in of the CO_2 gas mixture, a constant partial pressure of CO_2 was always maintained inside the system. It was found that vigorous stirring with a propellor-type stirrer was necessary in order to keep the slurry in suspension.

3-5-3   Column experiments

Column runs were made in 50-ml burettes[1] packed with various amounts and sizes of phosphate rock. The column feed was prepared beforehand and stored in glass or plastic carboys from which it was pumped into the column. Effluent samples were collected from the top of the column and were immediately analyzed for pH and alkalinity. The samples were then stored in a refrigerator, except when the remaining analyses were performed on the day of collection. A schematic of the apparatus is shown in Figure 3-2.

The water jacket was used in the $50^O C$ experiments, with all other runs made at room temperature. Feed pH was controlled by CO_2- bicarbonate equilibrium. Feed was pumped to the column by either a "Sigmamotor Model T8 driven by a Zero-MAX"[2] variable speed

(1) For a 6 minute retention time the column cross-sectional area was approximately 0.9 cm and the packed length was approximately 28 cm.
(2) Sigmamotor Inc., Middleport, N.Y. and Zero-max Co., Minneapolis, Minn.
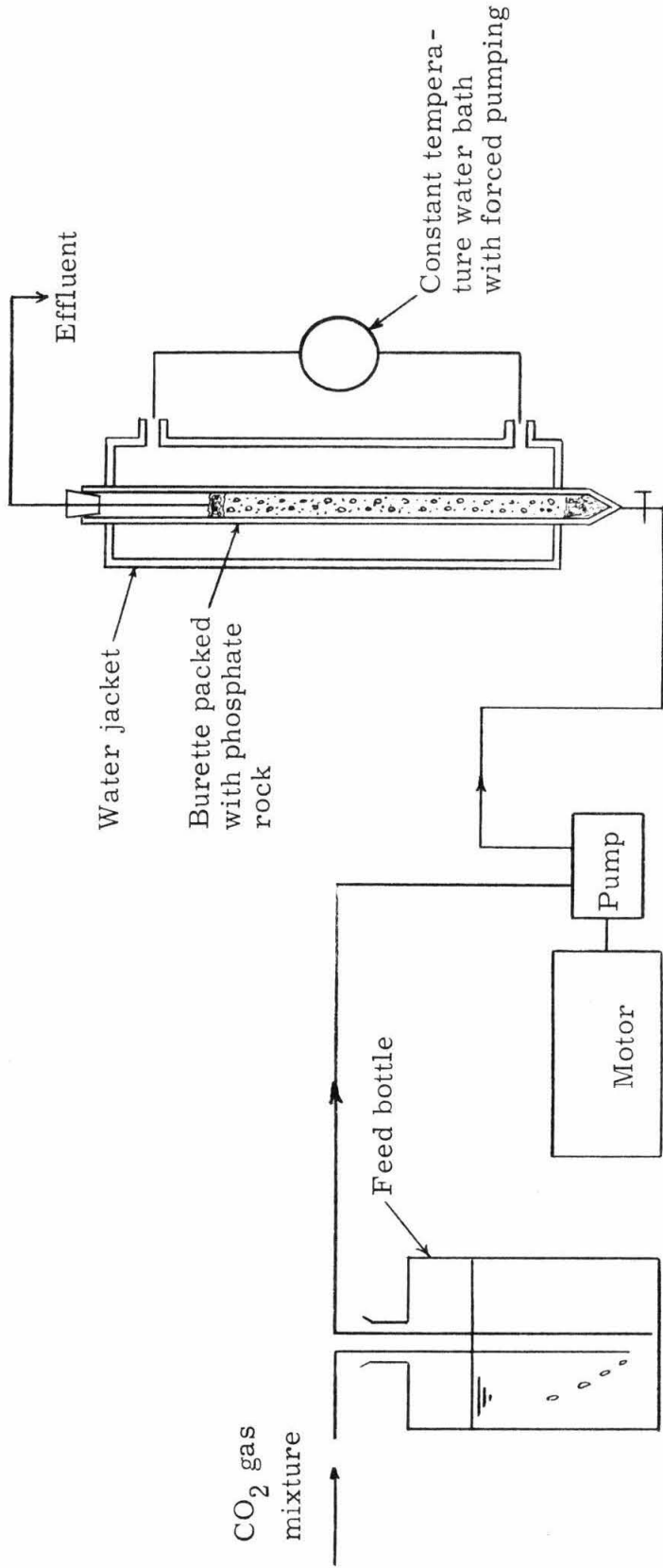
Figure 3-2. Schematic representation of the column experiment configuration.

motor, or by a "Holter Micro-Infusion Roller Pump Lab Model/ RL175"[1]. The constant temperature thermostat was a "Radio-meter-Type VTS13c"[2].

(1) Extracorporeal Medical Specialities, Inc., Mt. Laurel Township, N.Y.
(2) Labline Cat. #3052, Chicago, Ill.

-63-

Chapter 4

Models for the reaction of soluble orthophosphate

with phosphate rock

The inherent difference between a batch experiment and a column
experiment necessitated the formation of a separate model for each
system. The model for the batch system was developed from x-ray
diffraction analysis on separated solid samples in combination with
chemical data obtained during the batch runs. The model for the column
system was developed primarily from chemical data. The models are
presented in a separate chapter before the results and discussion
chapter in order to give the reader a frame of reference with which
to examine the results of this study.

4-1   Batch systems

In the batch system used in this study the soluble phosphate ion
is added at zero time to an equilibrated solution of phosphate rock,
calcium chloride, sodium bicarbonate and CO_2 gas. The reaction is
then observed to take place as time progresses. The soluble phosphate
concentration forming the micro-crystals follows a curve that is re-
presented by Figure 4-1. The soluble calcium concentration also de-
creased during micro-crystallization, but relatively not by as much as
the phosphate concentration. The (PO_{4T}) decreased from 0.4 mM to
approximately 0.02 mM (an order of magnitude drop), whereas the
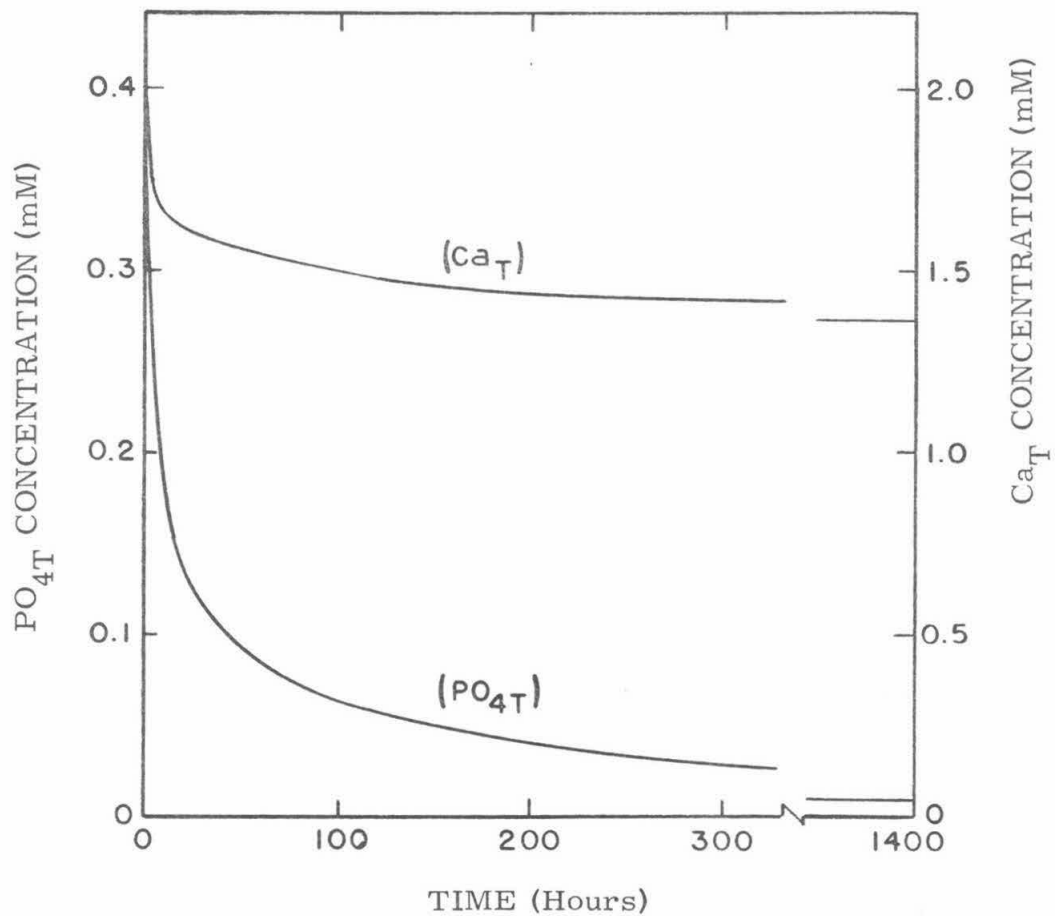
Figure 4-1. Time variation of typical soluble concentrations during a seeded batch experiment.

(Ca_T) decreased from 2.0 mM to 1.4 mM[1]. The pH remained relatively constant during each batch run, due to the $CO_2(g)$-bicarbonate buffering, but in one case a drop of approximately 0.2 pH units was noted.

The model for the batch system is presented in the following distinct steps:

1) The surface of the phosphate rock has sites of high attraction energy and at the start of the reaction the sites of highest energy are covered first. Figure 4-2 shows an active site being represented by 8 exposed unit cells partially covered by calcium phosphate nuclei. The size of 8 unit cells used to represent the active site has no special significance and was picked only for convenience in drawing. Since the phosphate rock is heterogeneous in composition the active sites will undoubtedly vary greatly in size. The solution is initially supersaturated with respect to TCP, OCP, and HAP, so it is probable that all of the foregoing solids will begin nucleating immediately on the surface to some extent. As used in this text a nucleus represents the initial few molecules that begin forming a unit cell. Water of hydration may still surround some of the molecules and thereby may initially create a somewhat large mass of nuclei. In Figure 4-2 this very rapid first step is shown in Frames a to b and occurs in a time period of minutes.

2) At c in Figure 4-2 the nuclei formed in steps a to b now have ripened into micro-crystals during a time period of approximately one

---

(1) In some batch runs an initial (Ca_T) of 1.0 mM was used, with a corresponding final (Ca_T) approximately equal to 0.5 mM.
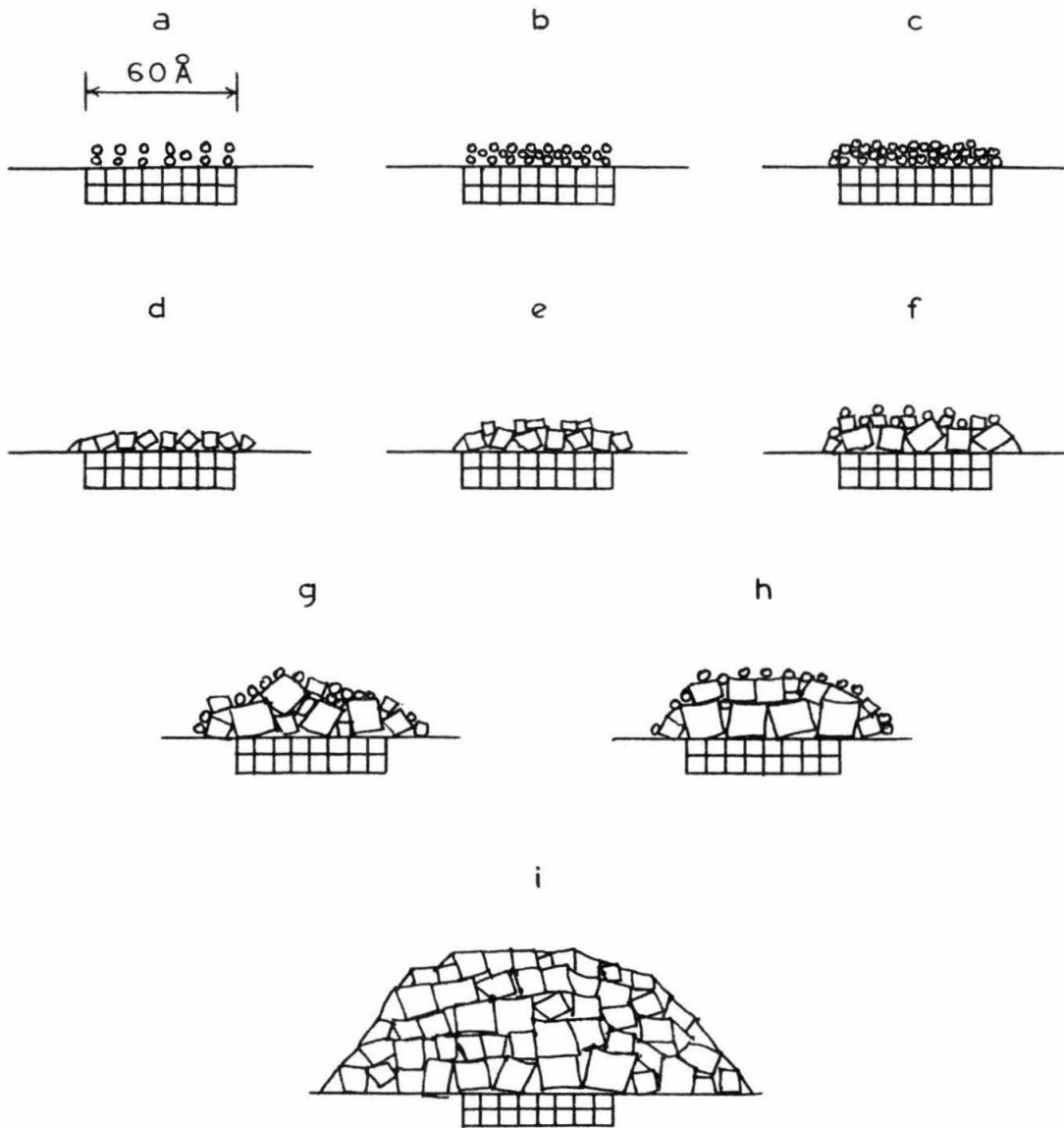
Figure 4-2. A cross-section schematic representation of the batch system model for calcium phosphate micro-crystallization on phosphate rock. The sketches represent the initial attraction of various calcium phosphate nuclei that eventually crystallize into an imperfect HAP crystal containing many defect structures.

hour. Frame d, another way of drawing Frame c, represents the mass of micro-crystals. Each of these is the approximate size of a unit cell of HAP,[1] with probably very little water of hydration present in these fractional unit cells. The imperfect heterogeneous micro-crystals are covering the active site on the surface of the phosphate rock and consequently reduce the attracting energy of the site. The micro-crystals themselves do not yet present a regular template at the solution-solid interface and thereby do not have the catalyzing effect of the original surface for inducing crystal growth. The micro-crystals continue to grow until a small cluster of crystallites is formed as shown in Frame f. Of course the small blocks representing these crystallites are not suspended on the surface as depicted in the sketch in Frame f, but are surrounded by various atoms and molecules existing in the heterogeneous suspension. At this point various molecules can bind to portions of the crystallites and can be incorporated into the emerging crystal as impurities. The crystallites continue to grow by ripening until their relative size is as shown in Frame g.

3) Frame g in Figure 4-2 represents the crystallite sizes after approximately 4 hours. Essentially a ripening process occurred where the micro-crystals grew into larger crystallites of approximately 18 Å in size. As this growth proceeded some new surfaces of high attraction energy were formed and consequently catalyzed the formation of a few new nuclei. At this time the concentration of soluble phosphate has

(1) The approximate dimensions of a unit cell of HAP_{10-6-2} are $a = 9.5$ Å, $c = 6.85$ Å, $V = 540$ Å^3 (Simpson 1965, Walters and Luth, 1969).

dropped to approximately three-quarters of its initial value. Con-comitantly the rate of new nuclei formation[1] has decreased consider-ably with a corresponding decrease in the rate of crystal growth. The primary phenomena occurring now are cell orientation along with crystal growth. It should be stressed that the cells "orienting" them-selves to states of lower energy are imperfect cells with many crystal defects, due primarily to the heterogeneous solution from which they were formed.

4) Beyond a reaction time of 4 hours the micro-crystal size can no longer be accurately discerned by x-ray diffraction analysis. The crystallites are beginning to agglomerate into a single mass as repre-sented in Frame h of Figure 4-2. The time period up to this point is approximately 1 day.

5) The final step can be thought of as a ripening process where the micro-crystallites continue to grow and form a more orderly large crystal that eventually appears to be part of the original apatite struc-ture. The final stage, represented in Frame i, now has properties similar to the original surface and can serve as a template for new crystal growth if the soluble concentration of crystal components is increased. The total elapsed time to reach the final stage varies, but

(1) From Figure 2-2 it can be seen that a small change in the super-saturation ratio produces a very large change for the nucleation rate in homogeneous nucleation systems. A similar effect between super-saturation and nucleation rate can be expected in heterogeneous nucleation as seen in Equation 2-15. Equation 2-15 can not presently be plotted because the critical free energy of nucleation depends on as yet unknown quantities such as lattice match and the interfacial energies between the crystal-solution, crystal-substrate, and sub-strate-solution.

is on the order of 10 days to a few months.

4-2   Column systems

At the initial startup of column operation the inlet end is subjected to a phosphate concentration equal to that in the feed solution while the outlet end of the phosphate concentration is relatively low. A sketch of the ratio of column outlet phosphorus to inlet phosphorus, C/C_o, plotted against time, is shown in Figure 4-3. Since the column flow rate in all cases was constant throughout each run, the abscissa could very well be represented by volume throughput, or a dimensionless value such as reduced time or empty bed column volumes.

T_1 in Figure 4-3 represents the time for breakthrough. It was found to be primarily a function of column residence time, feed phosphate concentration, and phosphate rock surface area. T_2 represents the time to reach steady-state conditions. Removal at this point was a function of residence time, phosphate rock surface area, temperature, pH, and concentration of ion species that can inhibit crystallization.

The primary difference between batch systems and column systems is that at a given time in a batch experiment all of the phosphate rock particles are subjected to the same ion concentrations, while in a column experiment the ion concentrations will vary with column longitudinal position. The respective concentrations throughout the lateral cross section area at each section of the column are assumed to be constant (i.e. there is no radial variation). The inlet end of the column always has a phosphate concentration equal to that in the column feed. As the feed progresses through the column, phosphate is removed
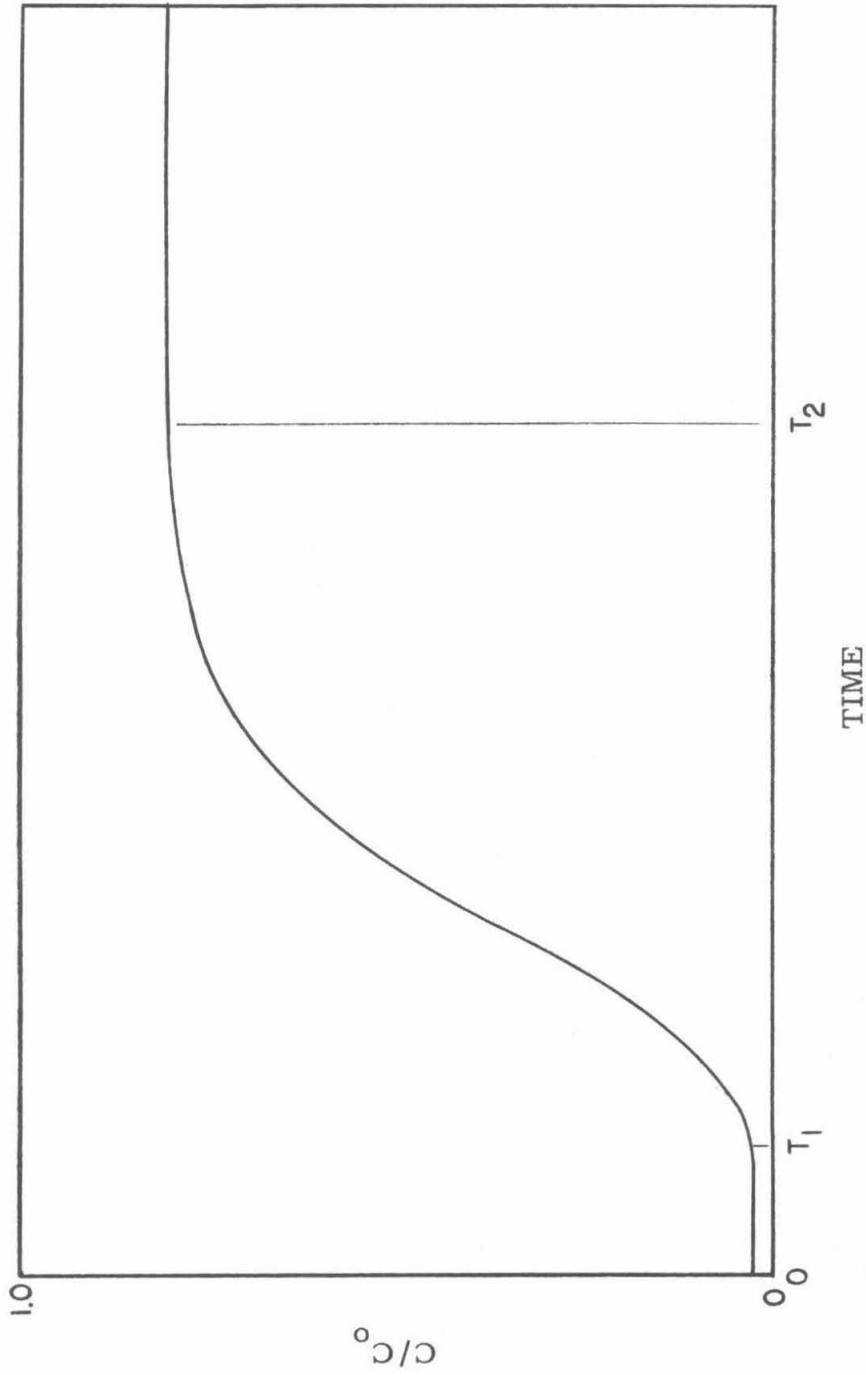
Figure 4-3. A schematic representation of column performance. C is the effluent concentration of phosphate, and C_0 is the feed concentration. T_1 is the time of breakthrough and T_2 is the time at which steady-state removal is achieved.

from solution and the soluble phosphate concentration decreases. This decrease must occur at all times, for the phosphate concentration in the column effluent is always less than that in the influent. The result is that for any instant of time each longitudinal section is subjected to a different concentration of ion species (not only (PO_{4T}), but also (Ca_T) and pH change with column position). Further complicating the situation is the fact that some chemical species are probably leaching out of the phosphate rock into the feed solution as the feed progresses through the column and probably affect the rate of nucleation and crystal growth.

As the column run progresses the phosphate concentration profile at any instant of time can be represented by the series of curves depicted in Figure 4-4. Curve 1 is the expected concentration profile at some time before breakthrough, and Curve 6 represents steady-state conditions in the column (time T_2 and beyond in Figure 4-3). The net result is that each section in the column is subjected to a changing phosphate concentration, and the way in which this change occurs is radically different between different sections.

The model developed for analyzing the column data is presented in Figure 4-5. It is separated into three sections: the period up to breakthrough; the period between breakthrough and steady-state; and the period after steady-state has been achieved.

1) The initial reaction that occurs up to the point of breakthrough is one of rapid nucleation and is depicted in steps a and b. This phenomenon is similar to the initial reaction that occurred in the batch experiments.
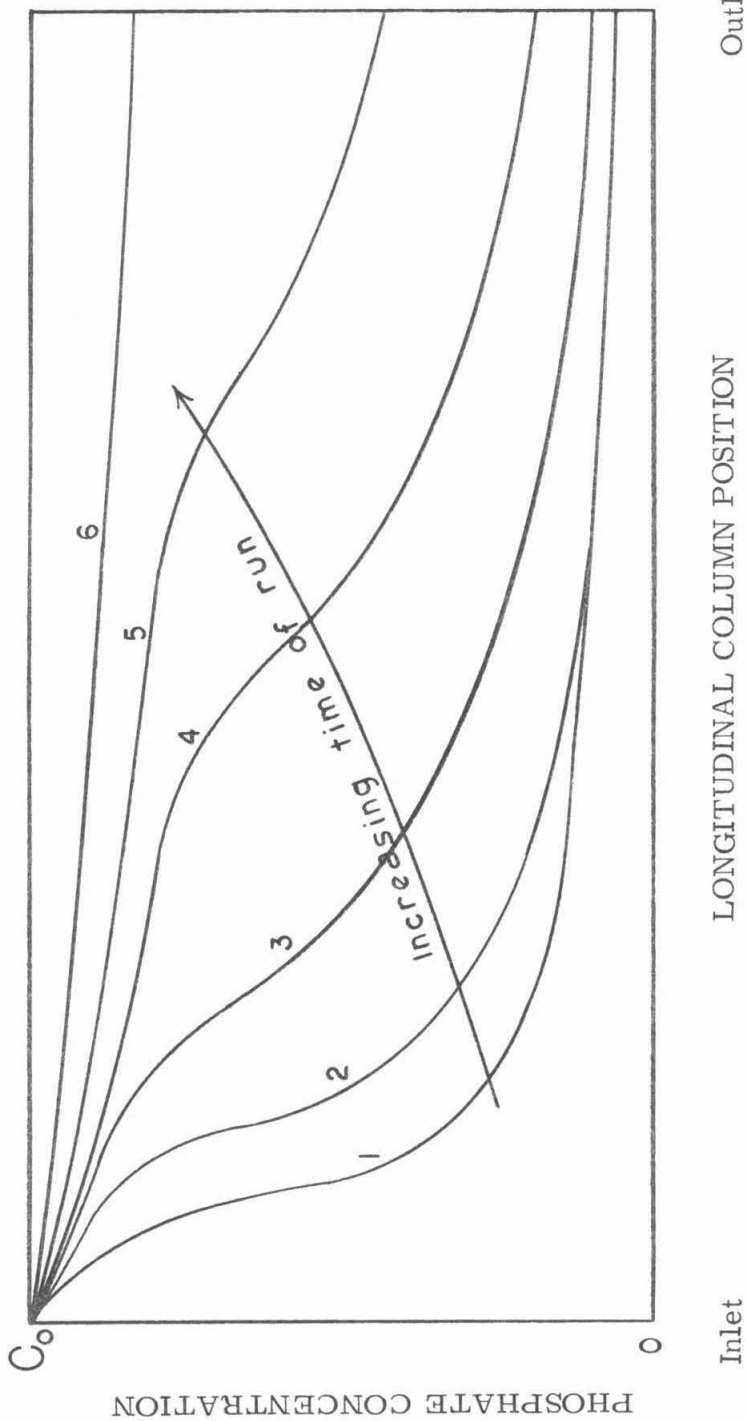
Figure 4-4. Variation of phosphate concentration with longitudinal location inside a column for various instants of time during a column run. Curve 1 represents a profile before breakthrough. Breakthrough occurs between Curves 2 and 3. Curve 6 represents steady-state conditions. This figure represents the phosphate concentration variation for a poorly operating column.
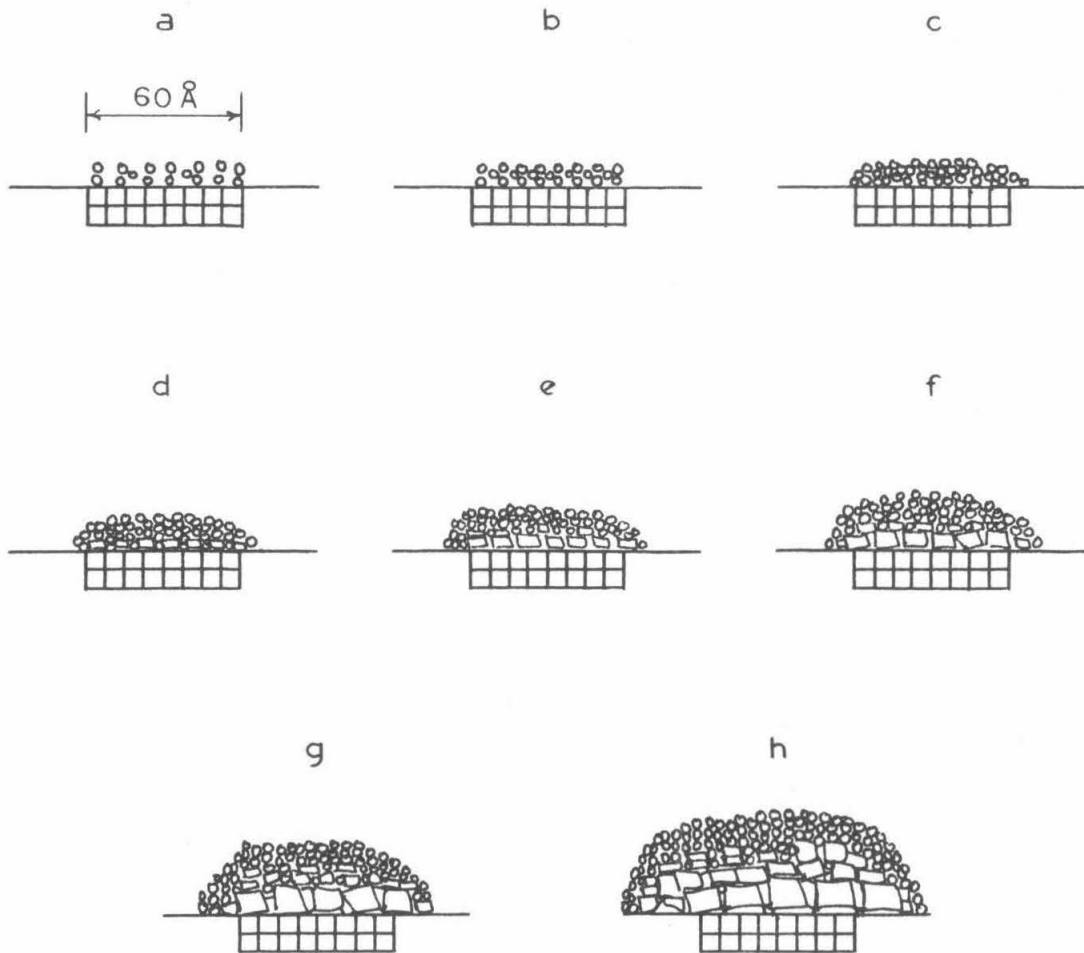
Figure 4-5. A cross-section schematic representation of the column system model for calcium phosphate micro-crystallization on phosphate rock. This model differs from that presented for the batch system due to the fact that the continuously high phosphate concentrations in the column result in the formation of a layer of nuclei that covers the emerging layer of growing crystal.

2) As the column run continues the phosphate concentration increases at each section of the column. The crystal ripening process occurs most rapidly at near equilibrium phosphate concentrations, with high phosphate concentrations having the effect of forming many small nuclei instead of the larger crystallites (Walton 1967, Nielson 1964). Consequently the tendency for nuclei to grow into larger and larger micro-crystals would be expected to be hampered in the column due to the ever-increasing phosphate concentration at each section of column.

Column operation between the states of breakthrough and steady-state is modeled in Steps c to h in Figure 4-5. Instead of forming discrete growing micro-crystals that eventually transform into an imperfect large crystal by ripening, as in the batch experiments, the nuclei in the column immediately adjacent to the active site surfaces begin crystallizing into a layer of HAP. The rate of formation of this HAP layer is retarded to a large extent by the mass of micro-nuclei that covers it.

3) At steady-state conditions, depicted in Frame h of Figure 4-5, the HAP layer continues to grow slowly and presents a moving front of crystal layer under the mass of nuclei. In column operation the micro-crystals can be thought of as growing from the "bottom-up" in heterogeneous and imperfect layers, rather than agglomerating from discrete micro-crystals.

Chapter 5

Experimental Results and Discussion

5-1   Batch studies

The powdered phosphate rock used for the batch systems could easily be examined in the electron microscope, and these analyses led to the development of the models presented in Chapter 4. Similarly since each particle of phosphate rock is subjected to equal solution conditions, the mathematical examination of the batch system is also substantially easier to analyze than is the column configuration, where solution conditions vary with position as well as time.

One of the major objectives of this research however was to develop engineering criteria for phosphate removal using phosphate rock in a column configuration. Unless an actual column system is used for analysis the application of batch data for design criteria is of questionable value. Therefore a substantial number of column runs were made under various chemical and physical conditions, with one run made on secondary treated wastewater collected at a local sewage treatment plant.

In all of the plots presented in this report the size of the plotting symbol approximately represents the 70% error limits of the data point.

5-1-1   Surface reactions

The chemical data for batch Run B-4, the one on which the electron

diffraction analyses were made, are depicted graphically in Figure 5-1. Not shown on the graph is the pH drop from 7.96 to 7.70 during the 1400 hours of the experiment. The (HCO_3^-) also dropped from 0.90 mM to 0.50 mM during the run.

Simultaneously with the collection of chemical component data the solid phase of each aliquot was saved[1] for electron diffraction analysis. Early in this study x-ray diffraction analysis was ruled out as a technique for observing the surface reaction occurring on the phosphate rock. In x-ray diffraction techniques the x-rays penetrate the entire mass of sample. The pattern obtained is very difficult to analyze unless the sample is uniform in composition and structure. In this study the weight ratio of the amount of HAP initially nucleated on the phosphate rock seed, divided by the amount of seed in solution, is approximately 0.5%. Consequently the nuclei and micro-crystals formed on the surface of the phosphate rock could not be differentiated from the bulk material with conventional x-ray analysis techniques.

However, since electrons do not have the penetrating power of x-rays, a judicious combination of particle size, film exposure time, and electron energy should give electron diffraction patterns indicative primarily of the surface of the sample. For the phosphate rock used in the study the 100 KV electrons in combination with particles approximately 0.3 microns in size produced diffraction patterns representative of the nuclei and micro-crystals on the surface of the phosphate

(1) As described in Section 3-3-7.
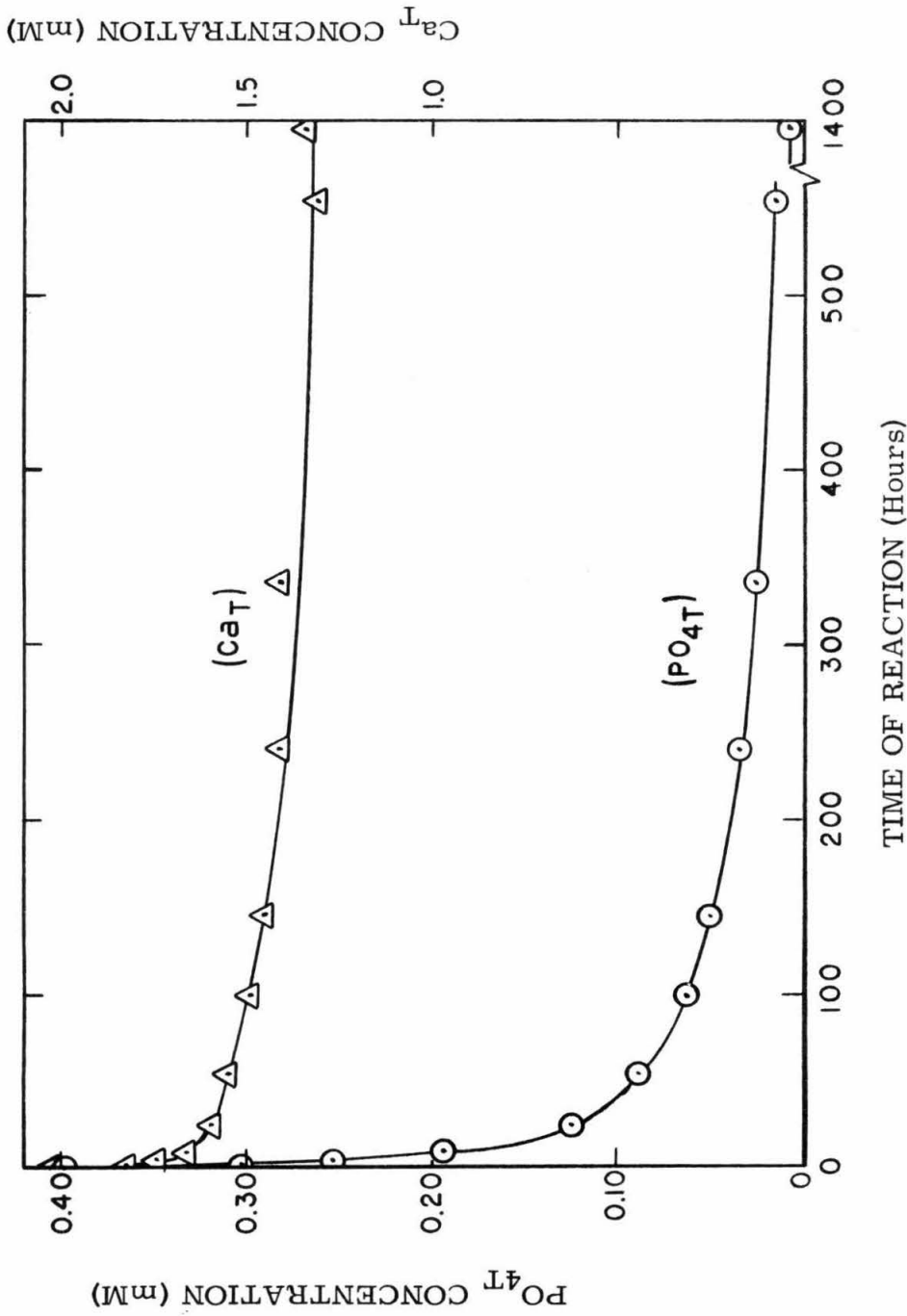
Figure 5-1. Variation of soluble (PO_{4T}) and (Ca_T) during the duration of Run B-4. Initial concentrations: $(Ca_T)_o = 2.0$ mM; $(Cl^-)_o = 4.0$ mM; $(Na^+) = 0.90$ mM; $(HCO_3^-)_o = 0.90$ mM; $(PO_{4T})_o = 0.40$ mM; $(K^+)_o = 0.80$ mM. Phosphate rock = 3.25 g/l, pH = 7.96, Temp. = 25.0 C, $P_{CO_2} = 3 \times 10^{-4}$.

rock particles. The Scherrer formula[1] was then used to approximate the micro-crystal size.

Sketches of the type of electron diffraction patterns that can be expected from different specimen structures are shown in Figure 5-2. In this figure each circle represents a unit cell of crystal. As the cells align themselves into larger and larger crystallites as shown in Frames a to c, the pattern changes from very diffuse rings into sharp dots whose geometric pattern is representative of the crystal being observed.

If a nucleation-crystal growth phenomena was taking place on the surface of the phosphate rock a pattern similar to Figure 5-2 should have been observed on electron diffraction analyses of the phosphate rock particles. The electron diffraction analyses of Run B-4 are shown in Figures 5-3 through Figures 5-11. Figure 5-3 is an electron micrograph of the particles of phosphate rock used in Run B-4. It was taken before the start of the run. Figure 5-4 is an electron diffraction pattern of the same particles shown in Figure 5-3. During Run B-4 the micrographs of all the phosphate rock particles on which the diffraction analyses were made were all very similar to Figure 5-3. The micrograph in Figure 5-3 shows that the phosphate rock particles vary greatly in size and the larger ones appear to be irregular masses possibly made up of the smaller units. The sharp dots in Figure 5-4 indicates that the raw phosphate rock is highly crystalline with the irregular pattern showing that it is very heterogeneous in composition.

---

(1) Heidenreich (1964) gives a derivation of the Scherrer formula for electron diffraction analysis (p 41).
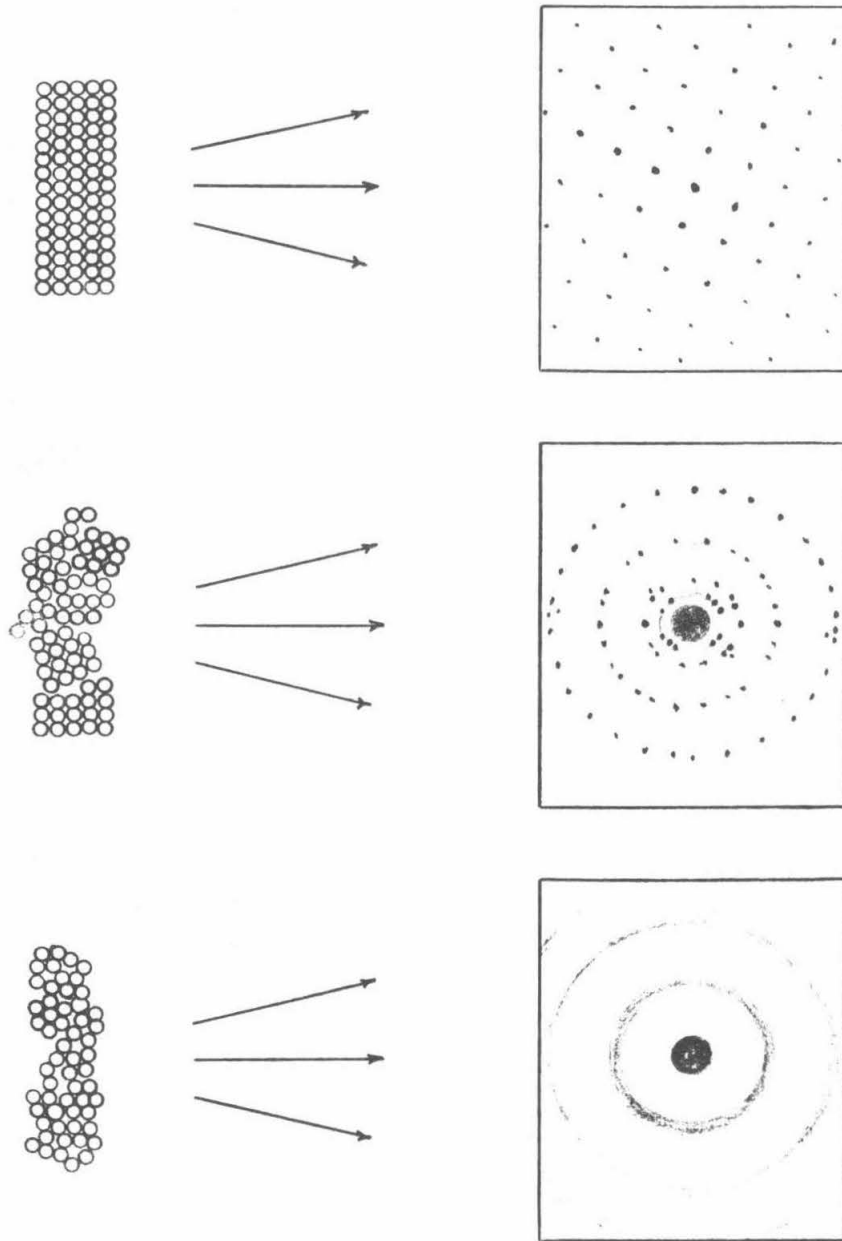
Figure 5-2. Sketches of the influence of specimen structure on the formation of electron diffraction patterns.

1.0 Micron

Figure 5-3. Electron micrograph of powdered phosphate rock.

Figure 5-4. Electron diffraction pattern of powdered phosphate rock.

Figure 5-5. Electron diffraction pattern for Run B-4, sample time = -0.0 hours. The sample was equilibrated with 1.0 mM $CaCl_2$, 0.65 mM $NaHCO_3$, and 3 x 10^{-4} atm $CO_2(g)$
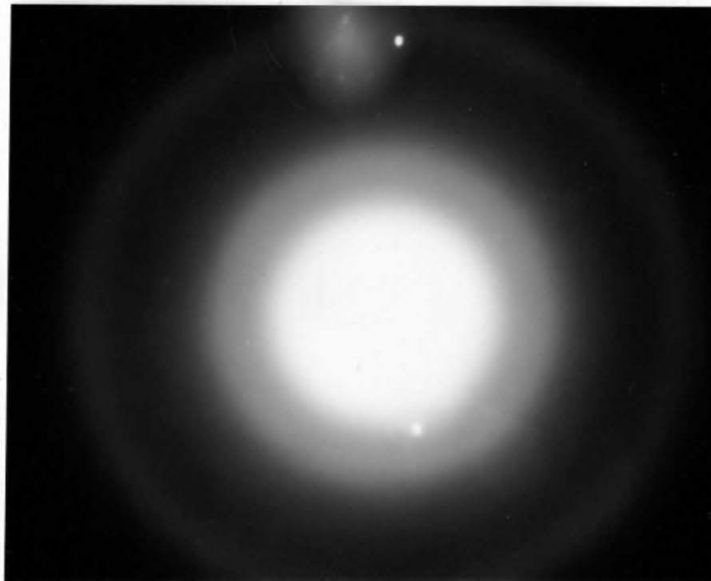
Figure 5-6. Electron diffraction pattern for Run B-4, sample time = 1.0 hour.
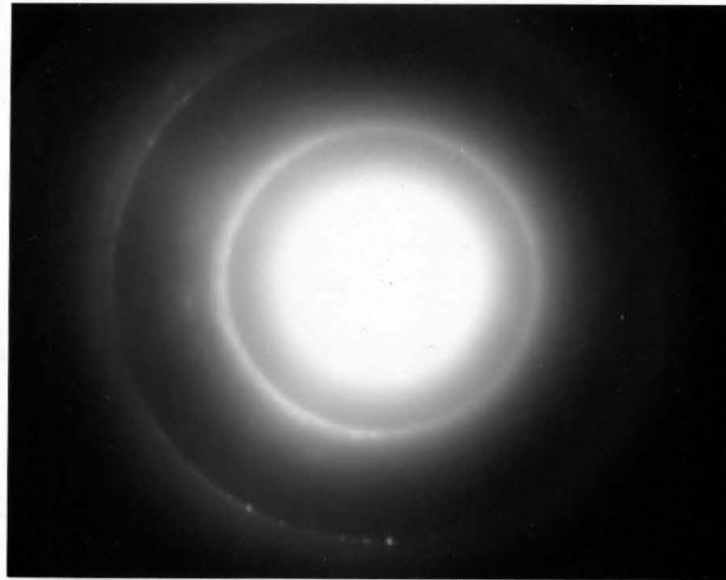
Figure 5-7. Electron diffraction pattern for Run B-4, sample time = 4.0 hours.
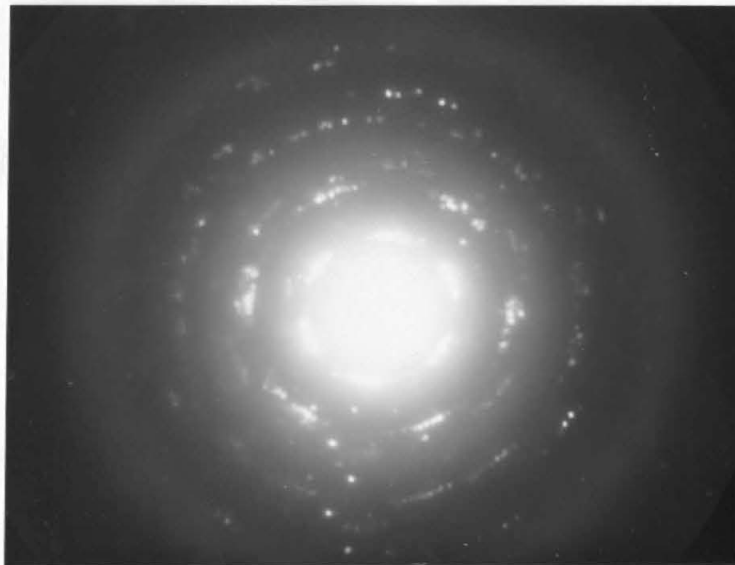
Figure 5-8. Electron diffraction pattern for Run B-4, sample time = 24.0 hours. Note the preferred orientation of the micro-crystals around the beam relative to each other that has taken place.

Figure 5-9. Electron diffraction pattern for Run B-4, sample time = 240.0 hours.

Figure 5-10. Electron diffraction pattern for Run B-4, sample time = 554.5 hours.
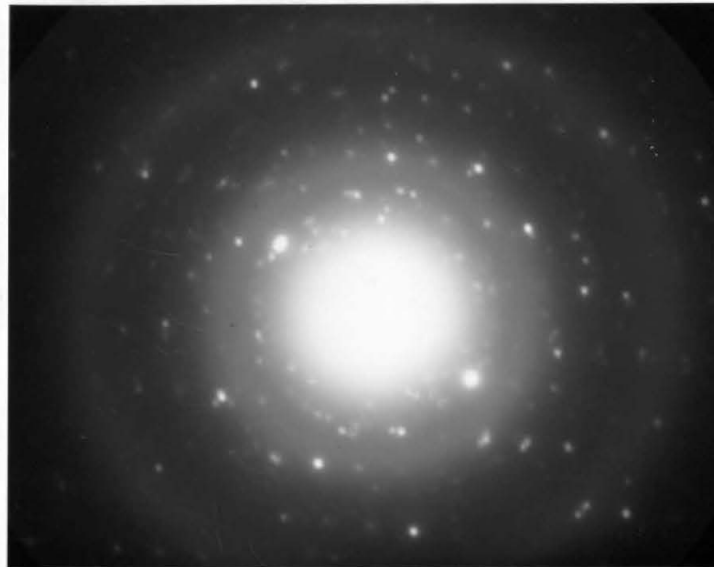
Figure 5-11. Electron diffraction pattern for Run B-4, sample time = 1393.5 hours.

Before the orthophosphate was added to Run B-4 the phosphate rock was equilibrated with the solution overnight. Figure 5-5, taken just before addition of the stock phosphate, shows that this equilibrated phosphate rock still has a crystalline surface composition. Some dissolution and micro-crystallization has occurred as indicated from the one dotted ring now seen which was not present in Figure 5-4. This period of equilibration did not seem to affect the catalytic properties of the phosphate rock. Figure 5-6, taken one hour after the addition of the phosphate stock, shows the surface of the phosphate rock to consist of large numbers of very small micro-crystals. The electrons striking the micro-crystals on the edge of the particle lose a smaller portion of their original energy then the electrons that are diffracted by the thicker portion of the particle. Consequently a short exposure time for the photographic plate results in a pattern governed primarily by the highest energy electrons, which are those diffracted only by the edge of the particle. The few sharp dots seen in Figure 5-6 are a result of a portion of the material that had few active sites, and consequently was not covered by micro-crystals. For each diffraction pattern it was attempted to use only a single particle of about 0.3 microns. Before the electron diffraction pattern was exposed to the film the grid containing the particles was scanned thoroughly until it was definitely established that all of the particles gave the same type of pattern. Figure 5-7 is an electron diffraction pattern taken 4.0 hours after the start of Run B-4. It is apparent that a significant change in crystallite size has taken place. Figure 5-8, the 24.0 hour sample, shows that a large amount of micro-crystal re-orientation has now

occurred. The diffuse rings have become sharp dot patterns and the crystallite size can no longer be determined accurately. Figure 5-8 also indicates that the micro-crystals are exhibiting some preferred orientation around the beam relative to each other. Figure 5-9 exhibits a pattern almost identical to Figure 5-5 (the equilibrated sample before any PO_4^{-3} is added) indicating the surfaces of both samples are in approximately equal states of crystallization. The surface crystals are still growing as seen by the continuing drop of phosphate concentration in Figure 5-1, but at a much slower rate with less tendency to form small micro-crystals due to the substantially lower phosphate concentration. It is significant to note that the only calcium phosphate solid whose solubility product is exceeded at this point is HAP, with the p^cQ of DCP, TCP, and OCP greater than their respective p^cK_{sp}, indicating that if any of the latter solids exist they are tending to go into solution. Examination of Figures 5-10 and 5-11 shows very little change in the electron diffraction characteristics of the surface after 240.0 hours. Apparently during this period ripening and crystal growth from solution are occurring simultaneously, because the calcium and orthophosphate concentrations continue to decrease. The electron diffraction Scherrer formula,

$$d = 0.9\lambda/(B/L) \cos \Theta \tag{5-1}$$

where   d = the crystallite size

         B/L = the half width in radians and

             $\cos \Theta$ is very nearly equal to 1

can be re-written as

$$d = 0.9 \, L\lambda/B \qquad\qquad\qquad (5-2)$$

The electron microscope constant, $L\lambda$, was 1.77 $\overset{o}{A}$ cm for this study. The computed crystallite sizes during Run B-4 were:

1 hr. = 7 $\overset{o}{A}$

4 hr. = 18 $\overset{o}{A}$

Since the cell parameters for the apatites are approximately a = 9.5 $\overset{o}{A}$ and c = 6.8 $\overset{o}{A}$, we see that in 1 hour the micro-crystals are computed to be approximately 1 unit cell in size. However the Scherrer formula is only accurate if the crystal has repeatability, and therefore this one-hour micro-crystal size determination can only be considered to be a gross approximation. In 4 hours the micro-crystals are about 3 unit cells across.

The effects observed in Figures 5-5 through 5-11 are thus in agreement with the model presented in Chapter 4, where nuclei form micro-crystals that slowly ripen into larger crystallites.

In order to identify the growing micro-crystals, the ring diameters observed with the sample must be compared to the ring diameters of a known substance. To simplify the comparison a sample of commercial HAP[1] was analyzed under conditions identical to those of the electron diffraction analyses of the samples in Run B-4. The ring diameters

---

(1) Certified Calcium Phosphate Tribasic #C-127, Lot 700011, Fisher Scientific Company, Fair Lawn, New Jersey.

were measured directly from the glass photographic plate by use of a "Diffraction Analyzer".[1]

Table 5-1 is a summary of the ring diameters observed in the commercial HAP sample and the 1.0, 4.0, and 24.0 hour samples of Run B-4. The other samples did not have identifiable rings.

The 1.0 hour sample of Run B-4 did not have any rings that matched the commercial HAP sample. This finding is understandable because at the small size of the micro-crystals (7 $\overset{\circ}{A}$) identification would be expected to be very difficult. At the start of the run DCP, TCP, OCP, and HAP were all in a state of supersaturation, and the initial nuclei probably consisted of a conglomeration of all of these calcium phosphate solids. Table 5-2 lists the various calcium phosphate supersaturation ratios for Run B-4. Only HAP remained in a state of supersaturation for the entire duration of the run.

The two analyses of the 4.0-hour sample had rings that matched with rings a, d, h and b, d of the HAP sample.

The two analyses of the 24.0-hour sample had rings that matched with rings c, f, and c, d of the HAP sample. The first ring of approximately 1.6 cm was never observed in any of the commercial HAP samples analyzed, nor in any of the samples of Run B-4. It is unique to the 24-hour sample and may be representative of the state of crystal transformation at that time.

From the data presented it appears that the initial mass of nuclei covering the active sites is a heterogeneous mixture of all of the

---

(1) Ernest F. Fullam, Inc.; Schenectady, New York.

Sample	Ring Diameters (cm)	Ring Code
Commercial HAP[1]	2.03	a
	2.35	b
	2.51	c
	3.12	d
	3.70	e
	4.02	f
	4.80	g
	5.57	h
Run B-4, 1.0 hr	3.37	
	6.32	
4.0 hr, #1	1.99	a
	3.28	d
	5.60	h
#2[1]	2.42	f
	3.10	d
24.0 hr, #1	1.61	
	2.88	c
	4.24	f
#2[1]	1.55	
	2.71	c
	3.14	d

Table 5-1. Ring diameters of commercial HAP and the samples of Run B-4. The values shown for the commercial HAP are averages of 3 samples of the same lot. The carbon film rings for all of the analyses are not listed.
(1) Photographs not included in the text.

Time of run (hours)	Supersaturation ratio, S			
	DCP	TCP	OCP	HAP
0.0	0.10	0.29	0.46	6.20
0.02	1.08	1.89	2.71	29.8
1.0	0.89	1.56	2.29	25.1
4.0	0.79	1.41	2.09	23.1
8.0	0.67	1.19	1.81	19.8
24.0	0.52	0.89	1.41	15.1
53.1	0.43	0.71	1.16	12.3
99.0	0.36	0.64	1.05	11.5
144.5	0.31	0.56	0.93	10.1
240.0	0.26	0.48	0.80	8.8
335.1	0.22	0.40	0.68	7.5
554.5	0.16	0.32	0.56	6.3
1393.5	0.13	0.25	0.44	5.0

Table 5-2. Supersaturation ratios of calcium phosphate solids calculated for Run B-4.

calcium phosphate solids in a state of supersaturation. Within hours these nuclei transform into identifiable HAP micro-crystals, which then continue to ripen into larger crystals until their properties can not be differentiated from those of the phosphate rock surface.

The surface reaction occurring in the batch systems can be mathematically described by plotting the soluble phosphate concentration as described by Equation 2-25. The equilibrium concentration of phosphate at pH 8.0 is less than 10^{-4} mM and can be neglected in the calculation. Equation 2-25 can then be re-written as

$$p(-d(PO_{4T})/dt) \ = \ p(kA/V) \ + \ np(PO_{4T}) \tag{5-3}$$

Figure 5-12 is a plot of the data for Run B-4. The first region is indicative of the initial rapid nucleation observed at the start of the run, with n approximately equal to 7. The next two regions have values of n approximately equal to 4 and 2.

When column runs were attempted utilizing the ion concentrations used in batch Run B-4 some difficulty was encountered with spontaneous nucleation and precipitation in the column feed solutions, even though earlier experiments with borax-buffer solutions indicated that a supersaturation ratio of 30 was necessary before precipitation occurred. Therefore another batch experiment (Run B-6) was performed at the same concentrations used in the column experiments and is summarized in Figures 5-13 and 5-14. Figure 5-13 is a plot of only the first 36 hours of the run and Figure 5-14 is a plot of the entire run. From these plots two lag periods are observed, one occurring at 1 hour and lasting approximately 1 hour, the other occurring at 150 hours into the run and lasting approximately 20 hours. When the
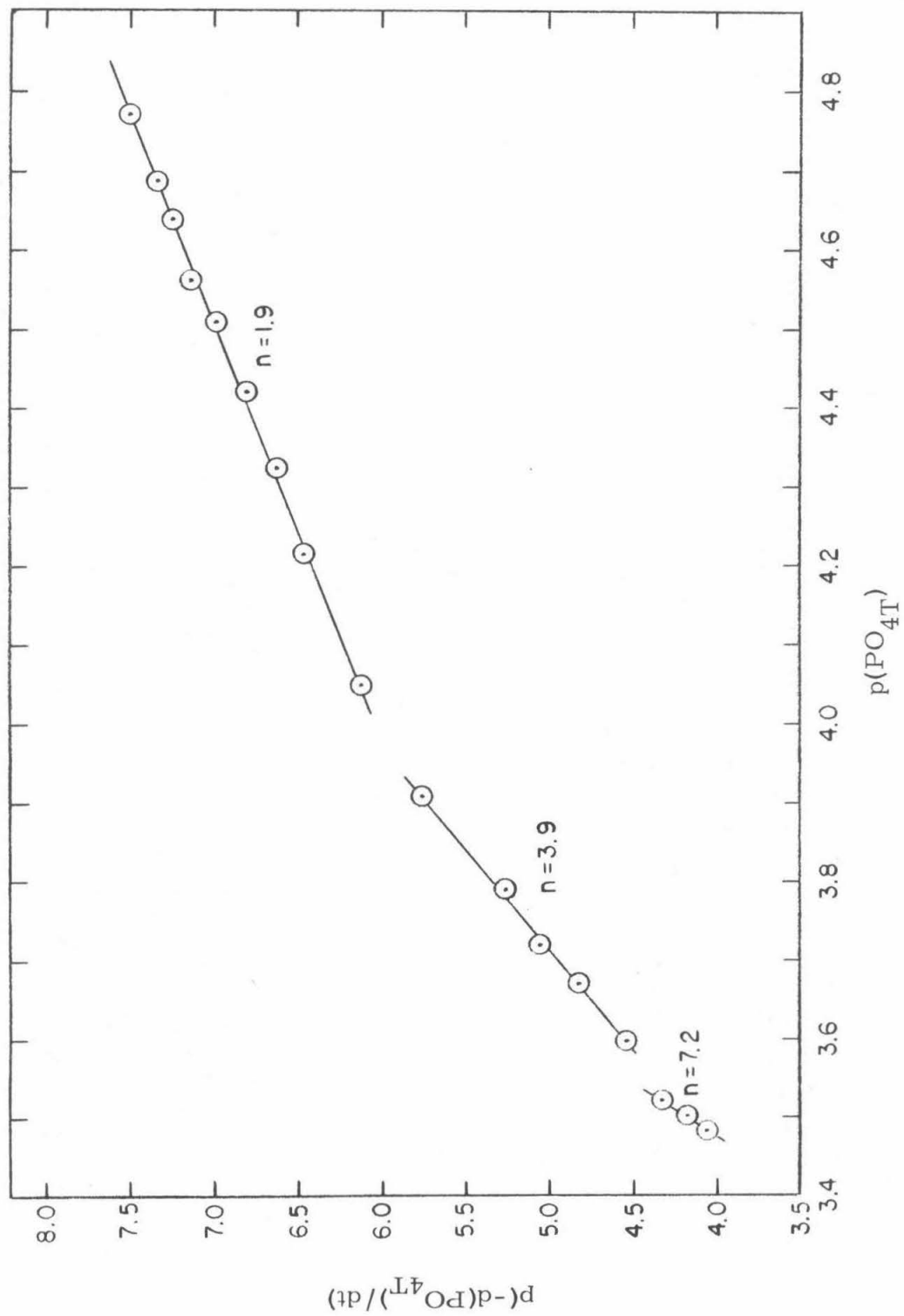
Figure 5-12. Logarithmic plot of the rate equation for Run B-4.
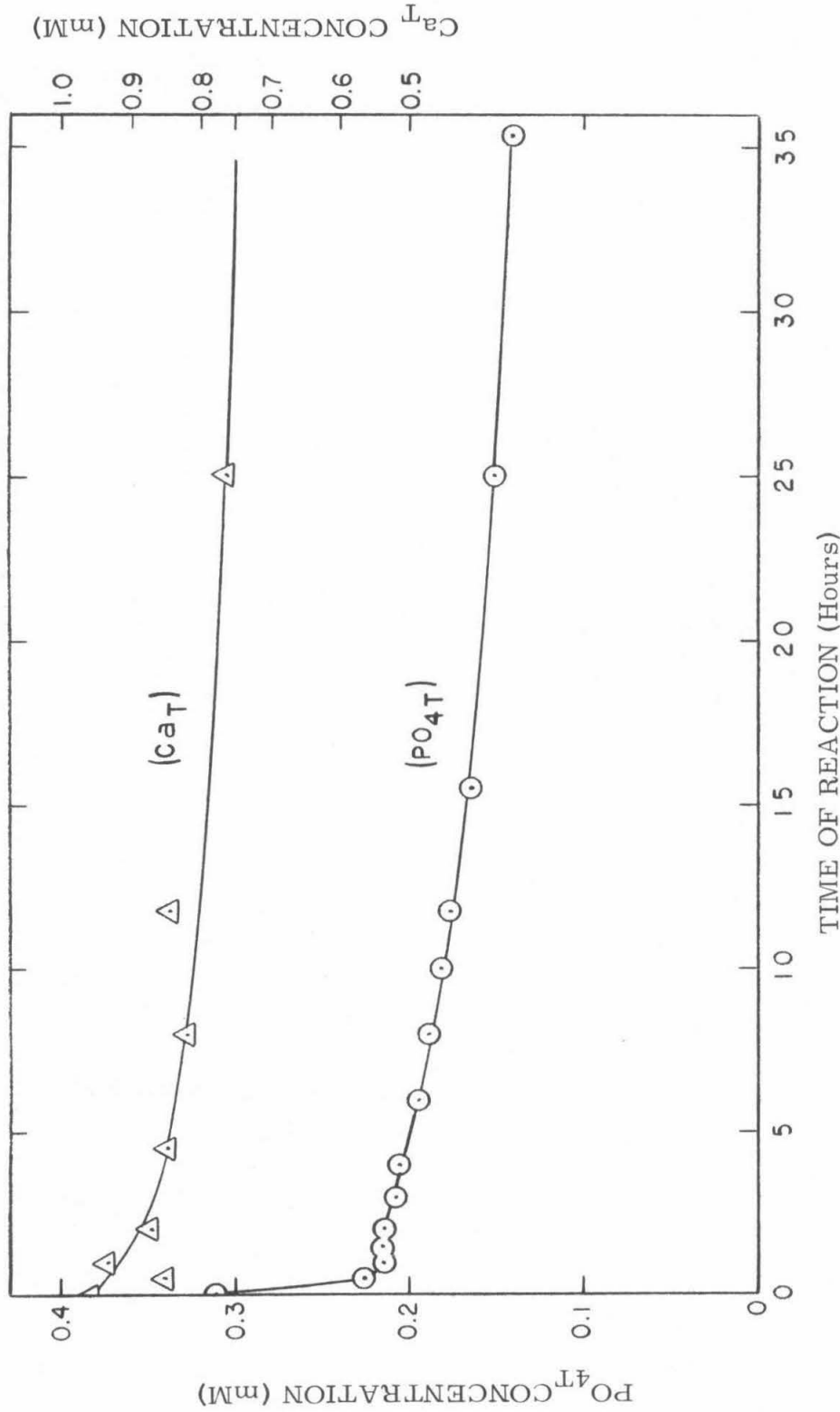
Figure 5-13. Variation of soluble (PO_{4T}) and (Ca_T) during the first 36 hours of Run B-6. Initial concentrations: $(Ca_T)_o = 0.96$ mM; $(Cl^-)_o = 2.0$ mM; $(Na^+)_o = 1.20$ mM; $(HCO_3^-)_o = 0.95$ mM; $(PO_{4T})_o = 0.310$ mM; $(K^+)_o = 0.60$ mM. Phosphate rock = 3.25 g/l, pH = 8.04, Temp. = 25.0 °C, $p_{CO_2} = 3 \times 10^{-4}$.
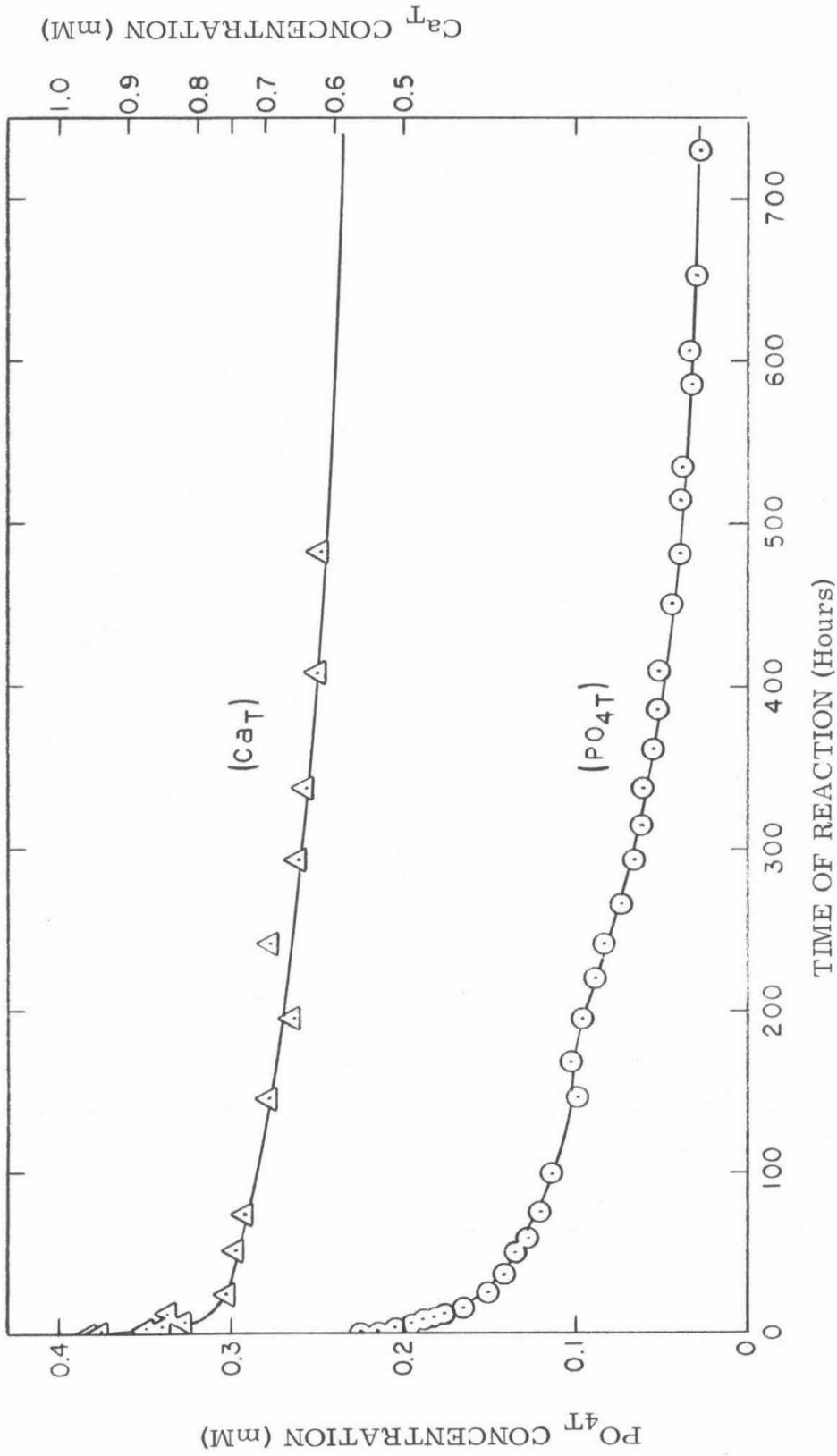
Figure 5-14. Variation of soluble (PO_{4T}) and (Ca_T) during the duration of Run B-6. Initial concentrations are the same as in Figure 5-13.

soluble phosphate data are plotted according to Equation 5-3, the lag periods show up as breaks in the slopes as shown in Figure 5-15. For Run B-6 the three regions depicted in Figure 5-15 had slopes approximately equal to 13, 4, and 2.

The form of the equation that is applicable to the batch systems therefore is

$$dC/dt = -(kA/V)C^n \qquad (5-4)$$

C is the concentration of total soluble orthophosphate and A/V is the surface area of the phosphate rock per unit reactor volume.

Table 5-3 summarizes the values of n and k for the 3 regions found in Runs B-4 and B-6. The values of k appear to be a function of the initial conditions at the start of nucleation. The difference between the n values of 13 and 7 for the initial rapid nucleation phase of each run is probably due to slope measurement error in Run B-4, where not enough initial sampling points were taken. However it is reasonable to conclude that phosphate rock catalyzes an immediate and rapid nucleation of orthophosphate from solution with the rate of removal described by Equation 5-4, and the order of the reaction approximately equal to 10. This rapid nucleation is then followed by two separate regions of micro-crystal growth and transformation whose rate reactions have approximate orders of 4 and 2. In all cases crystal growth was interface controlled.

5-1-2   Self-regeneration of the phosphate rock surface

If the model presented in Chapter 4 is valid a self-regeneration phenomenon of the active sites on the phosphate rock should be
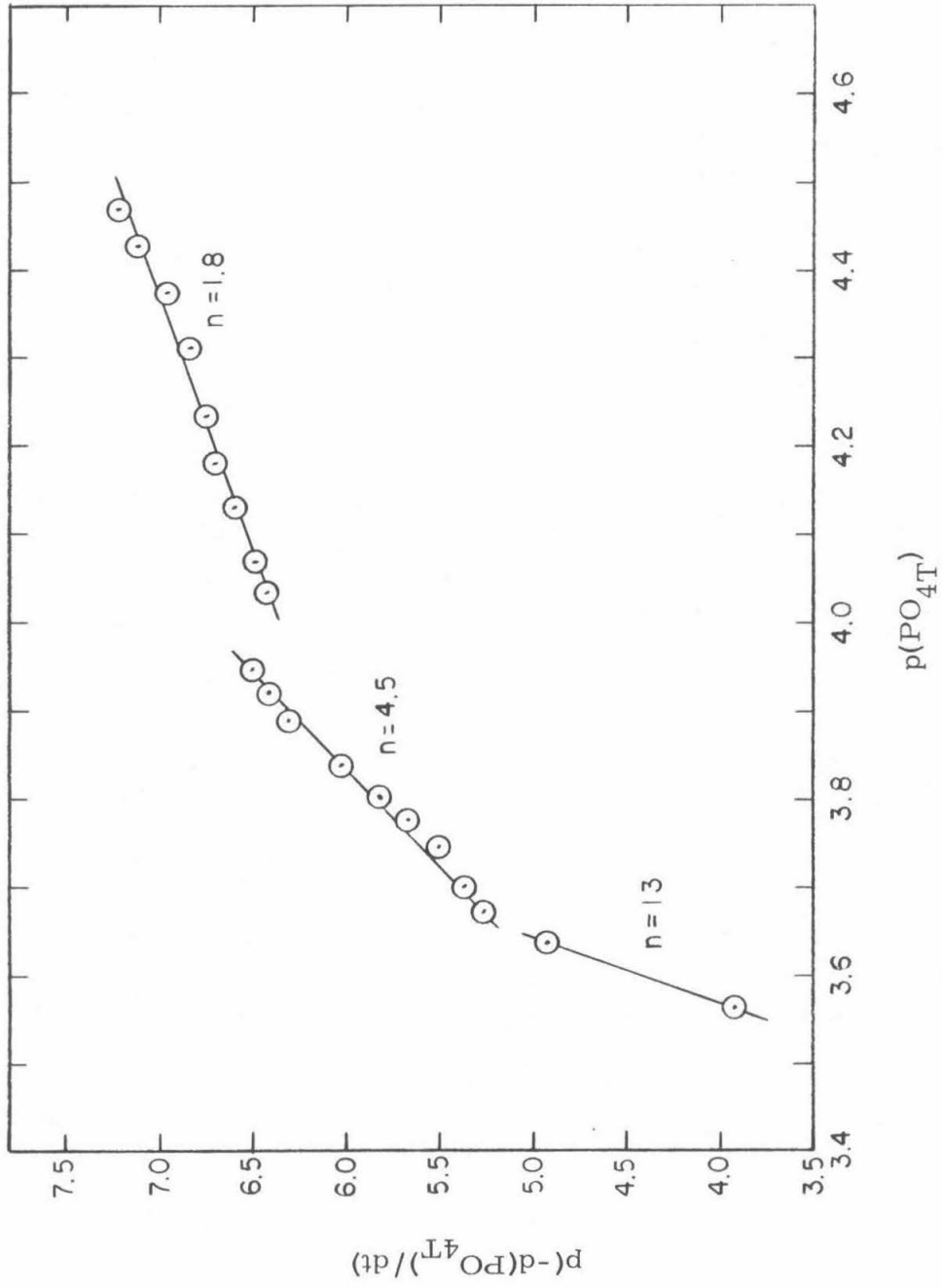
Figure 5-15. Logarithmic plot of the rate equation for Run B-6.

Run	Region	n	k $(\text{liter}^n \text{ mole}^{1-n} \text{ hr}^{-1} \text{ m}^{-2})$
B-4	1	7.2	10^{20}
	2	3.9	$10^{8.0}$
	3	1.9	0.68
B-6	1	13	10^{41}
	2	4.5	$10^{9.6}$
	3	1.8	0.10

Table 5-3. Values of n and k for Runs B-4 and B-6. n and k are the parameters of the rate equation $dc/dt = -(kA/V)C^n$, where C is the soluble phosphate molar concentration and A/V is the unit surface area of the reaction system in units of m^2/l.

observed. As the calcium phosphate nuclei and micro-crystals ripen into larger crystals of HAP new surfaces should form that can act as templates for inducing more crystal growth.

Run B-3, in which the CO_2-bicarbonate buffering system was used, is summarized in Figure 5-16. The phosphate rock was dosed three times with K_2HPO_4 at approximately 70 hour intervals. Some trouble was encountered in controlling the pH and 24 hours into the second reaction period sodium bicarbonate was added to the reaction resulting in a corresponding increase in the pH.

A substantial decrease in the soluble phosphate concentration was observed with each dosing. The pH change from 8.0 to 8.6 during the second reaction period resulted in a substantial drop in (PO_{4T}), indicating that the pH has a marked effect on the rate of crystallization. Unfortunately during this run no additional calcium was added at the start of each dosing, so the rate of phosphate removal was affected somewhat by the steadily decreasing initial calcium concentration. However phosphate rock does seem to be regenerating itself partially after the 70-hour reaction period.

From Runs B-3, B-4, and B-6 it was seen that phosphate removal from solution continued to occur during the entire duration of each run. The longer the phosphate rock reacts with the soluble phosphate the more crystalline the growing nuclei become, resulting in the phosphate rock being more capable of acting as a template for the nucleation of more HAP. An important function is whether or not the phosphate rock has some practical limit to the number of times it can regenerate itself. From Run B-3 it can be concluded that some self-
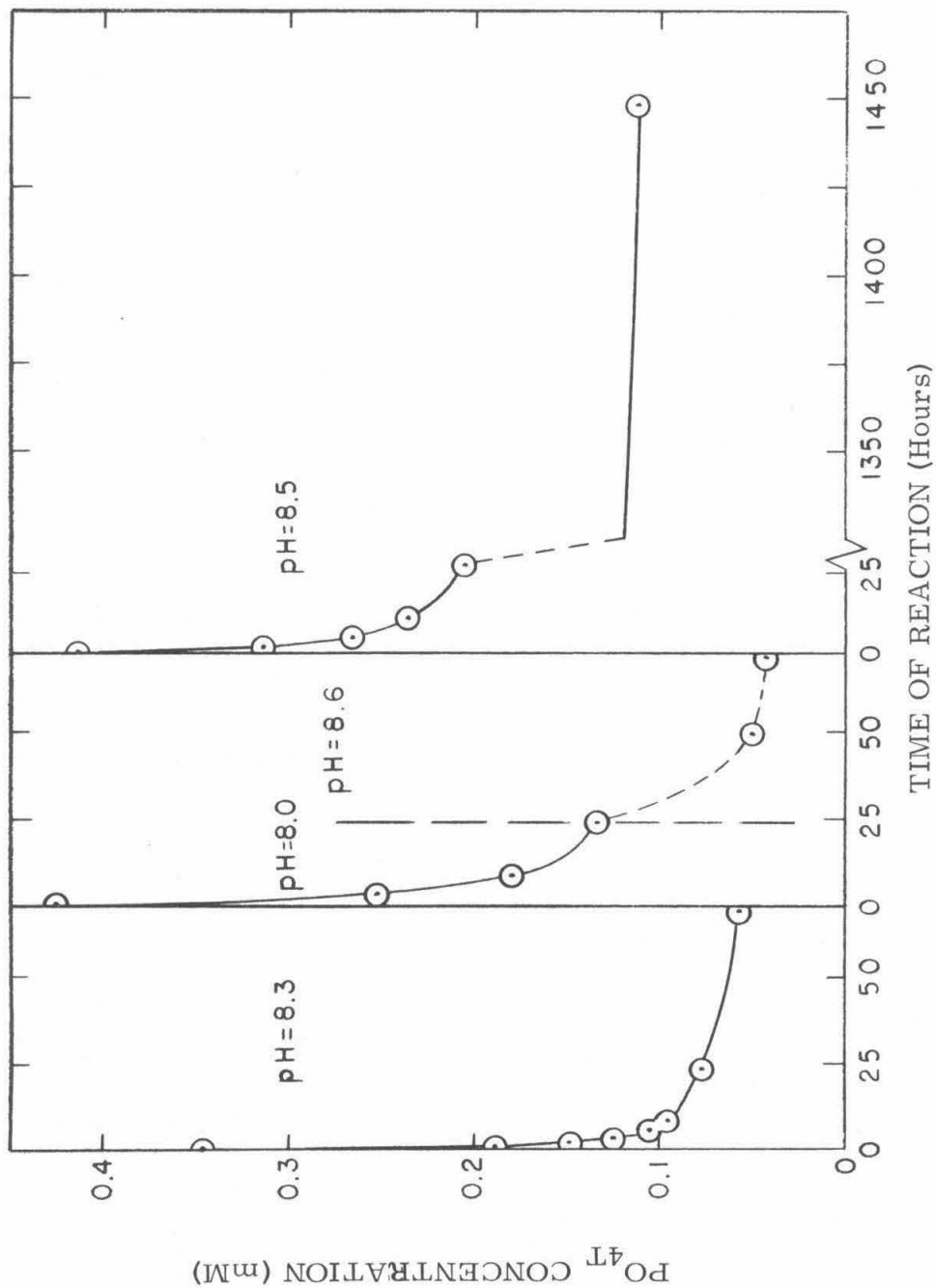
Figure 5-16. Repeated dosings of phosphate rock slurry - Run B-3. Initial concentrations: I = 0.01 mM; $(Ca_T)_o$ = 2.0 mM; $(Cl^-)_o$ = 4.0 mM; $(Na^+)_o$ = 2.5 mM; $(HCO_3^-)_o$ = 2.5 mM. At 24 hours into the second dosing period the (HCO_3^-) was increased to 6.8 mM. Temp. = $25 \pm 1°$C.

regeneration occurs at room temperature.

In order to determine some measure of self-regeneration a batch run was made at $50^{O}C$. Increasing the temperature should have a marked effect on the rate of phosphate removal if the nucleation-crystallization model is correct. If adsorption were the primary mechanism of phosphate removal very little change in the system would be observed. In studies of phosphate adsorption on α - Al_2O_3 Chen et al (1972) observed an increase of only 3.6% in the 10 day adsorption when the temperature was increased from $25^{O}C$ to $50^{O}C$.

The results of the $50^{O}C$ batch run (Run B-5) are summarized in Figure 5-17. At the end of each 48-hour dosing period, $CaCl_2$ and $NaHCO_3$ were added in order to increase their concentrations to the initial values. The drop in calcium concentration during each dosing was relatively equal in each case, and is represented by the dashed line in Figure 5-17. The solid line in Figure 5-17 is the curve of (PO_{4T}) for the first dosing. The (HCO_3^-) dropped during each dosing from 0.89 mM to approximately 0.54 mM. In raising the (Ca_T) and (HCO_3^-) after each dosing the ionic strength of the solution was concomitantly raised from approximately 5 mM during Dosing #1 to 13 mM during Dosing #5. This increase in I may have inhibited nucleation and crystal growth by decreasing the activities of the ions in solution.

In comparing Figures 5-13 and 5-17 it is obvious that a substantial increase in phosphate removal was achieved by the increase in temperature, which is in agreement with the model presented in Chapter 4. The first two dosings in Run B-5 followed the same (PO_{4T}) curve, after which the phosphate concentration rose slightly during each
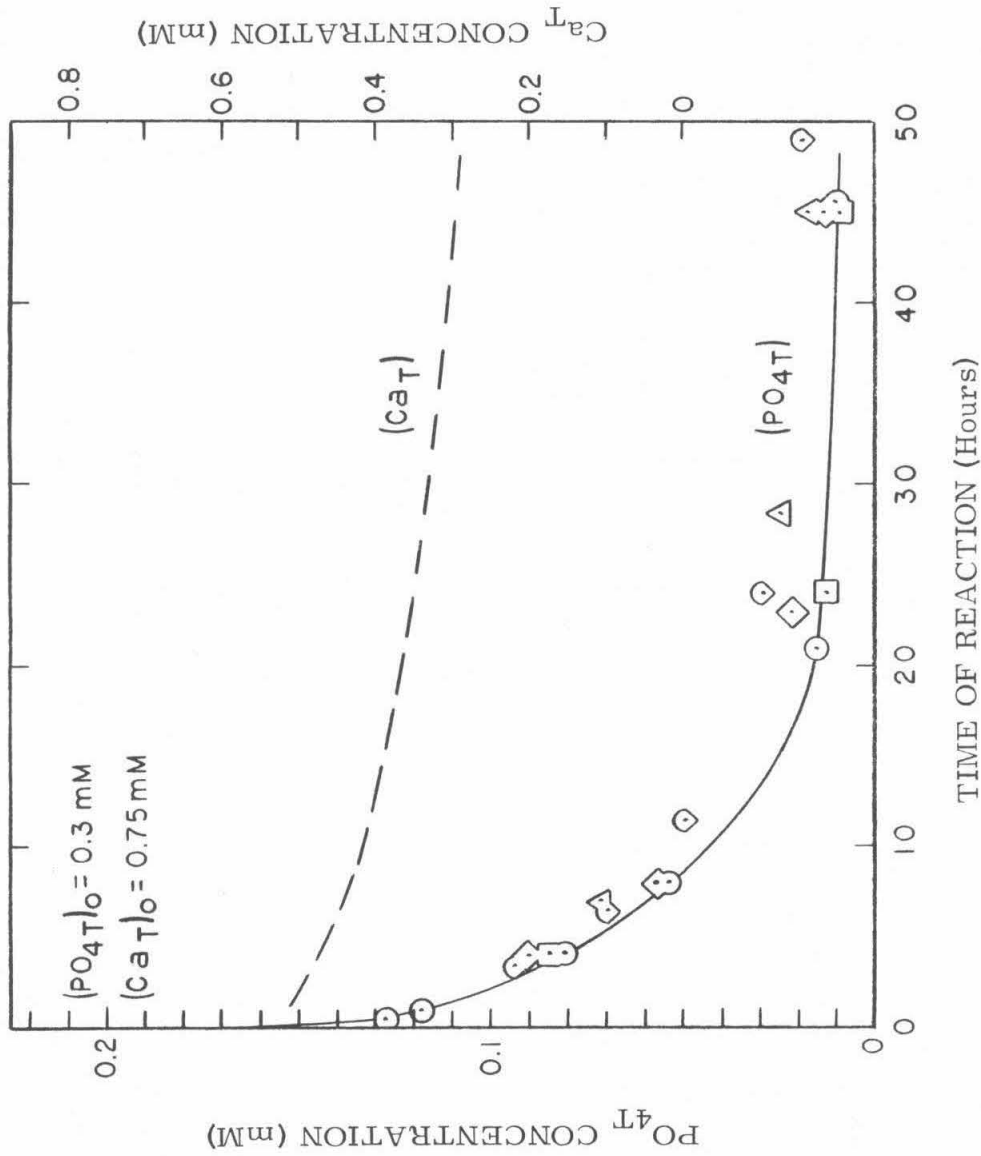
Figure 5-17. Variation of soluble (PO_{4T}) and (Ca_T) during the five dosings of Run B-5. Initial concentrations: $(Ca_T)_o = 0.72$ mM; $(HCO_3^-)_o = 0.90$ mM; $(PO_{4T})_o = 0.30$ mM; phosphate rock = 3.25 g/l; pH = 7.96; Temp. = 50°C; $p_{CO_2} = 3 \times 10^{-4}$. Dosings: 1 = ⊙ ; 2 = ☐ ; 3 = ◈ ; 4 = △ ; 5 = ⊙ .

dosing period. However even at the end of the fifth dosing period, the
(PO_{4T}) was only 0.018 mM, compared to the first dosing concentration
of 0.010 mM. This represents only a 2.8% decrease in the phosphate
removal ability of phosphate rock over five dosing periods.

Figure 5-18 is a logarithmic plot of the rate equation for the first
dosing of Run B-5. When comparing it to the plots of Runs B-4 and
B-6 which were run at $25^{O}C$ (Figures 5-12 and 5-15), it is seen that
the former "region 2" seems to have been suppressed when the temper-
ature was raised to $50^{O}C$. The initial rapid nucleation period is still
observed with the relatively high n value equal to approximately 13.
However the reaction then proceeds to a short period where n=2 and
then to a period where n=1. The points in triangles in Figure 5-18 are
the values for a curve drawn through the phosphate concentration values
of the fifth dosing period (this curve was omitted from Figure 5-17 for
clarity). The values for the fifth dosing period agree well with those
observed for the first period during the initial stage of the reaction,
but begin to differ somewhat at the end of the reaction. However the
last few points of dosing #5 do appear to follow a reaction of order 1.

In section 2-2-3 it was seen that a necessary (but not sufficient)
condition for diffusion controlled crystal growth was that n must equal
1 in the rate equation. In Run B-5 it was possible that interface re-
action became so rapid due to the increased temperature that crystal
growth was limited by the rate at which ions could migrate to the sur-
face. It may be of interest in future work to run experiments similar
to B-5 where the turbulence in the reaction vessel is varied between
runs in order to ascertain if the high temperature rate constant, and
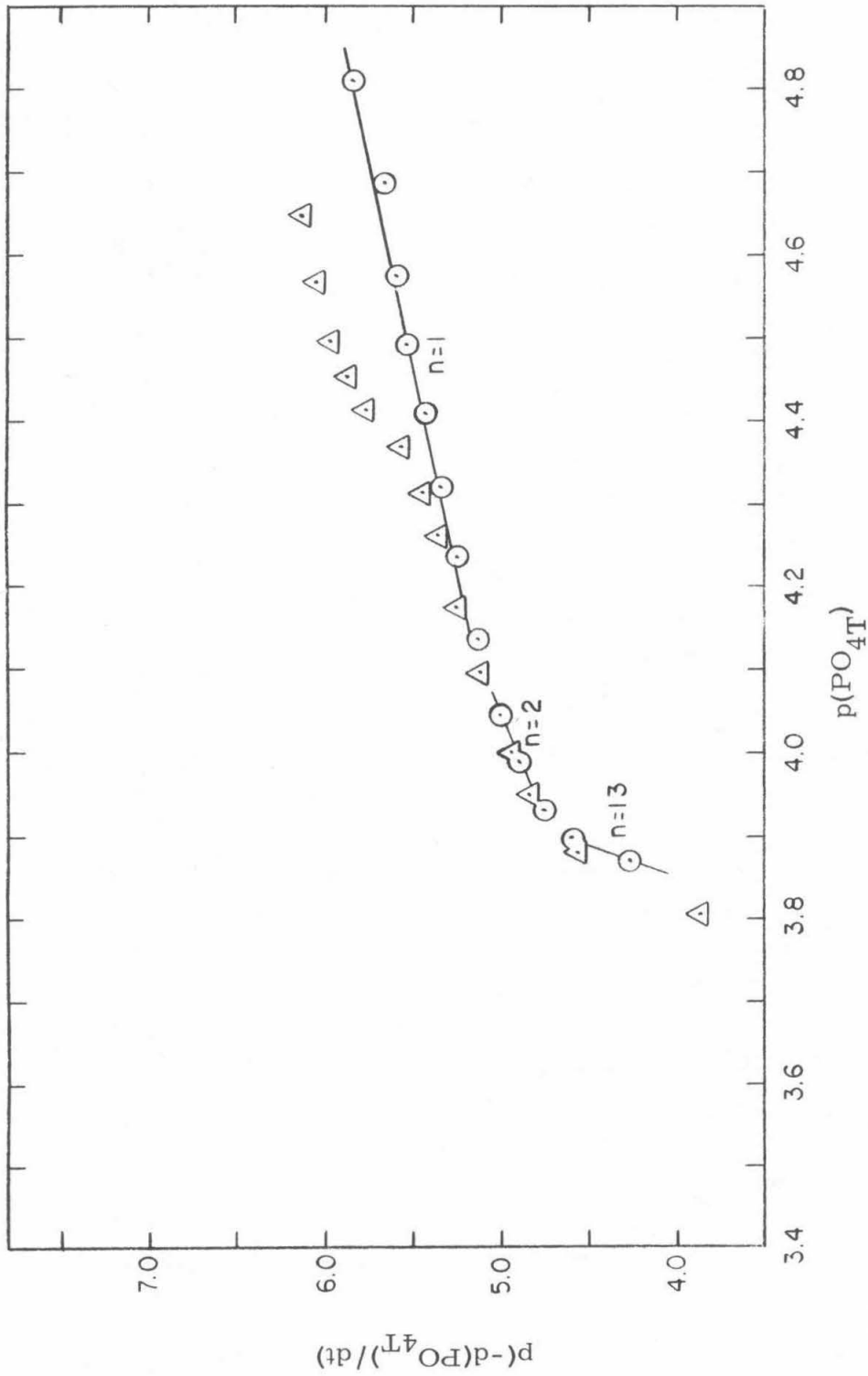
Figure 5-18. Logarithmic plot of the rate equation for Run B-5. Dosings: $1 = \odot$; $5 = \triangle$. Concentrations are the same as in Figure 5-16.

thereby the diffusion coefficient, is dependent on mixing.

For the three regions of Run B-5 where the values of n were 13, 2, and 1, the corresponding values of the rate constant k were 10^{44}, 32, and 0.002. These 50°C values of the rate constants are considerably higher than those observed at 25°C when comparing them at equal corresponding values of n. Increasing the temperature also markedly increased the rate constant for the column run and will be discussed later in the text.

5-1-3   Surface area effects

When removing phosphorus from solution by micro-crystallization on phosphate rock the surface area of the phosphate rock should be one of the important parameters in determining the amount of phosphorus removed during the initial period of rapid nucleation and micro-crystal growth. As the active sites are rapidly covered by nuclei and micro-crystals the attractive forces are reduced until the growth of surface crystallites are sufficient to develop large enough crystal surfaces that can act as templates for more nucleation and crystal growth.

To study the effects of varying the surface area a closed vessel batch experiment was made using borax-HCl as a buffer.[1] In this experiment the initial (PO_{4T}) was constant at .316 mM and the weight of the phosphate rock in suspension was varied. Samples were analyzed after 22 hours, with the results shown in Figure 5-19.

---

(1) Sections 3-4-1 and 3-5-1.
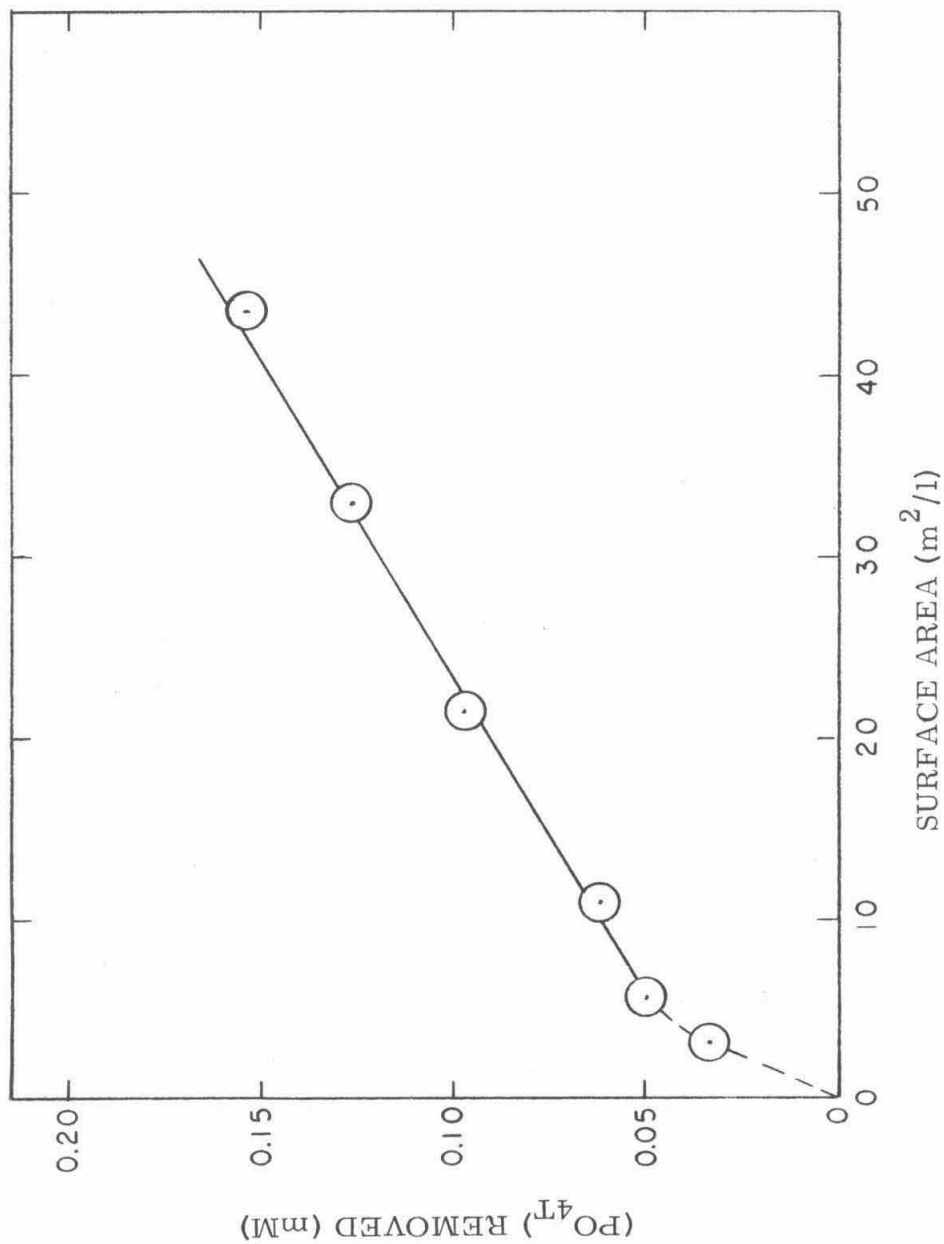
Figure 5-19. Plot of soluble phosphorus removed from solution in a 22 hour period against varying surface areas of phosphate rock in borax-HCl buffer. $(Ca_T)_o = 2.0$ mM; $(PO_{4T})_o = 0.316$ mM; pH = 8.30; Temp. = $24°$C.

In order to determine if the curve in Figure 5-19 should pass through the origin another similar run using the borax-HCl buffering method was performed where the (PO_{4T}) was varied without any phosphate rock in the reaction bottles. No spontaneous precipitation or decrease in phosphate concentration was observed over a 22-hour period until a (PO_{4T}) value of 0.56 mM was surpassed. Therefore no removal would have been observed in Figure 5-19 at a zero surface area value and the curve must therefore pass through the origin.

No simple interpretation seems to explain the observed break in the slope of the curve in Figure 5-19. In order to attain the low values of surface area in each reaction bottle it was necessary to use small amounts of phosphate rock. For example the first point in Figure 5-19 has only 7.5% of the weight of phosphate rock in it as does the last point. Apparently this low value of surface area induces rapid nucleation and micro-crystal growth that remove proportionally more phosphate from solution than do the higher values of surface area at an equal initial concentration. The slope of the solid line in Figure 5-19 gives an initial surface coverage value of 17 atoms $P/1000 \overset{o}{A}{}^2$, compared to a 22-hour coverage of 23 atoms $P/1000 \overset{o}{A}{}^2$ for the $CO_2(g)$-bicarbonate buffered Run B-6.

Although the initial uptake of phosphate from solution in the borax-HCl buffered system is not very different from that observed in the $CO_2(g)$-bicarbonate buffered system, the shape of the concentration versus time curves differed markedly. Figure 5-20, a plot of (PO_{4T}) versus time using the borax-HCl buffering method, shows that the buffer interferes substantially in the crystallization of HAP. It appears
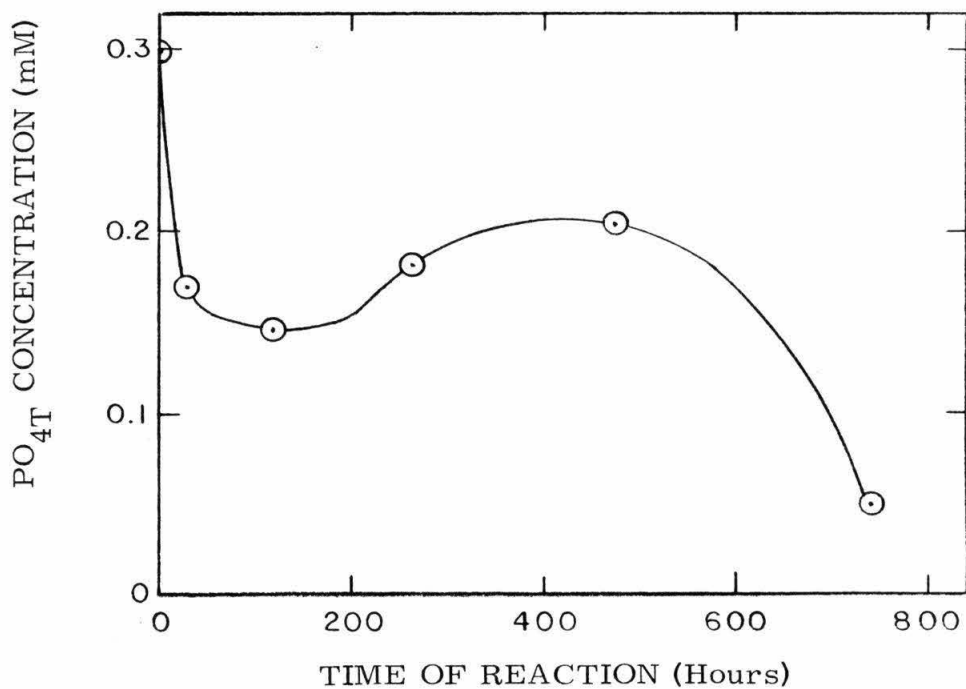
Figure 5-20. PO_{4T} concentration vs time using borax-HCl buffer: $(Ca_T)_o$ = 2.0 mM; $(PO_{4T})_o$ = 0.300 mM.

PHOSPHATE ROCK SLURRY CONCENTRATION (g/l)
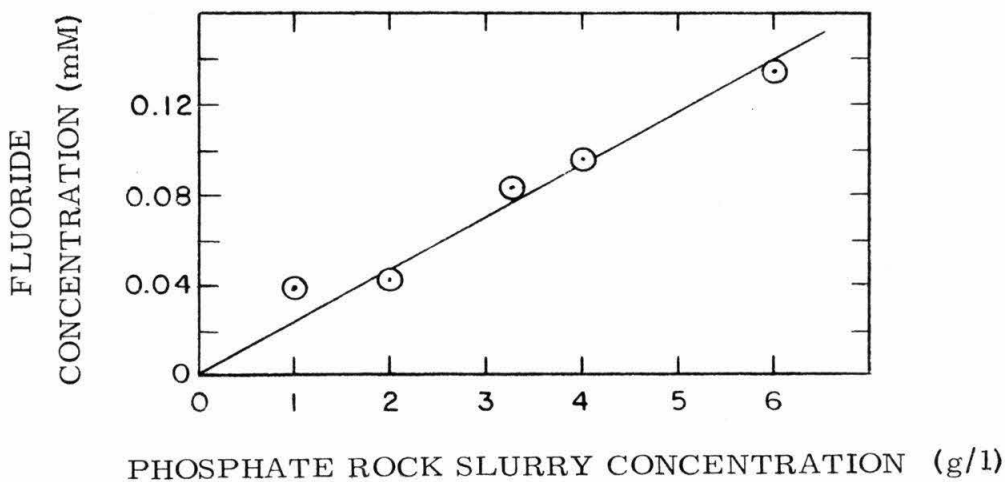
Figure 5-21. The leaching of solid CaF_2 out of a phosphate rock slurry. $(CaCl_2)$ = 1.0 mM; (Na^+) = 1.2 mM; (HCO_3^-) = 1.0 mM; p_{CO_2} = 3 x 10^{-4}; Temp. = $23 \pm 2°C$; pH = 8.0.

that a nucleation-dissolution reaction occurs during the first few hundred hours, after which HAP begins to crystallize producing a marked drop in (PO_{4T}). Apparently the non-HAP ions in solution do not affect the initial rapid nucleation step as much as they do the crystal-transformation step. Since the objective of the borax-HCl buffered system was to compare surface area effects in batch systems, further examination of the crystal-transformation step in borax-HCl buffer was not attempted.

5-1-4   The effect of fluoride in batch runs

During batch Runs B-5 and B-6 the fluoride concentration was measured throughout each run. In the 25°C run (B-6) the average fluoride concentration was 0.045 mM and ranged from 0.043 mM to 0.057 mM. The fluoride concentration did not follow any discernable pattern during the run. No fluoride was added to either of these runs, with the concentration measured being a result of what leached out of the phosphate rock. The supersaturation ratios for HAP and FAP for Run B-6 were S_{HAP} = 19 and S_{FAP} = 58 at the start of the run, and at the end of the run were S_{HAP} = 6.3 and S_{FAP} = 19. These results are surprising because FAP has been reported (Sillen and Martel, 1964; Leckie, 1969) to be substantially more insoluble than HAP, with a pK_{FAP} = 60.4 versus that of pK_{HAP} = 57.8 at zero ionic strength.

The $p^{c}Q$ of CaF_2 varied during Run B-6 from 11.67 to 11.93 with an average value of 11.77. The $p^{c}K_{sp}$ for CaF_2 was 10.14, indicating that the solubility of solid CaF_2 was not controlling the fluoride

concentration. No known solid form of fluoride explains the observed fluoride concentration. Apparently the phosphate rock contains some solid CaF_2 which dissolves into solution, accounting for the measured fluoride concentration, with not enough $CaF_2(s)$ in the phosphate rock so as to maintain solubility equilibrium. In order to test this hypothesis an experiment was performed where varying concentrations of solid phosphate rock were stirred for 22 hours in a solution of $NaHCO_3$ and $CaCl_2$ in contact with room air for buffering. If phosphate rock contains some $CaF_2(s)$, the measured fluoride concentration should vary directly with the concentration of solid phosphate rock.

The result of the experiment is plotted in Figure 5-21 and shows a relatively good direct relationship between the fluoride leached out of the phosphate rock and the concentration of phosphate rock. From the slope of the line it was calculated that the phosphate rock contains 0.09% of $CaF_2(s)$ by weight. The relatively constant fluoride concentration in Run B-6 indicates that no (or very little) FAP was formed during the reaction period.

During the $50^{\circ}C$ run (B-5) the fluoride concentration steadily decreased from 0.058 mM at zero time of the first dosing to 0.005 mM at the end of the fifth dosing. Each dosing decreased the (PO_{4T}) by approximately 0.29 mM, with a total uptake of (PO_{4T}) for all five dosings equal to 1.433 mM. This is 27 times the drop in fluoride concentration over the five dosings (no fluoride was added at any time), which differs considerably from the theoretical ratio of three if the phosphorus and fluoride were combining with calcium to form only FAP.

During the first dosing of Run B-5 the fluoride concentration

dropped from 0.058 mM to 0.035 mM. If all of this fluoride formed
FAP the ratio of FAP formed to HAP formed is approximately 1/4
during the first dosing period where the average fluoride concentration
was relatively high.

From the data presented it can be concluded that very little FAP
nucleates on phosphate rock at 25°C under the concentration conditions
of this study, which are approximately those found in secondary treated
wastewater. Even at 50°C the tendency is to form HAP over FAP in an
approximate 4 to 1 ratio. This leads to the interesting possibility that
natural formations of FAP may be representative of relatively high
temperature geological conditions, and perhaps a geological temper-
ature scale can be developed from the ratio of FAP/HAP in a natural
apatite deposit.

5-2   Column studies

In analyzing the column studies data, two regions of operation were
of major interest: the period up to breakthrough of phosphate, and the
period of steady-state operation. A completely different method of
analysis was used for each period, for the first is represented by up-
take due to initial rapid nucleation, whereas the steady-state condition
is representative of crystal growth. No satisfactory theoretical anal-
ysis was found for the region between breakthrough and steady-state.
In order to analyze this region fully, experiments utilizing much larger
columns would be necessary than were feasible under the conditions
of this research. Sampling from within the column would have to be
performed in order to characterize the type of rate equation that is

governing at any time and location. From the model presented in Chapter 4 it was seen that this region is characterized by the transition from rapid nucleation on one end to steady crystal growth on the other. The major problem in analyzing this transition period is that both the rate constant and order of reaction are constantly changing, both with time and position in the column.

Plots of the data are presented in the dimensionless values of $(PO_{4T})/(PO_{4T})_o$ and V'_c. The phosphate ratio is that of the measured phosphate concentration in the column effluent divided by the feed phosphate concentration. V'_c is the cumulative feed volume put through the column divided by the empty bed volume of the column. The use of dimensionless numbers is not intended to imply that the plots presented can be directly scaled up to prototype systems, but rather is intended to facilitate comparison of the results obtained during the various parameter changes that were made in this study.

The physical parameters that were varied between column runs were retention time, operating temperature, and unit surface area of the phosphate rock. The chemical parameters that were varied were pH, (HCO_3^-), (F_T), $(MgSO_4)$, and (NH_4Cl). A summary of the conditions under which each column run was performed is presented in Table 5-4.

The retention time is the true residence time that an average element of liquid spends inside the column. Its value is the void volume of the column divided by the column volumetric feed rate. In order to perform as many column runs as possible only retention times of 12 minutes or less were used in this study. In all cases the point

Run	Grade of ore in the column	Components added to the stock feed	Weight of ore in the column (g)	t_r (min)	Feed pH	Feed Temp. (°C)	V'_{cbt}	C/C_o at steady-state
C-1	PR-10	None	86.3	9.89	8.07	23	25	0.80
C-3	PR-10	None	44.6	2.60	8.08	23	5	0.92
C-4	PR-10	None	44.6	5.44	8.08	23	7.5	0.84
C-4-R	PR-10	None	44.6	4.64	7.99	23	(1)	0.76
C-5	PR14x32	None	74.1	12.4	7.89	23	8.9	0.84
C-6	PR14x32	None	38.9	6.02	7.89	23	4.6	0.91
C-6-R	PR14x32	None	38.9	6.31	7.84	23	⟨1⟩	0.74
C-7	PR14x32	None	38.9	5.85	7.86	50	17	0.54
C-7-R	PR14x32	None	38.4	6.05	7.98	50	(1)	0.34
C-8	PR14x32	(NaF) = 0.050 mM	38.4	5.86	7.86	23	5	0.79
C-9	PR14x32	(NaF) = 0.050 mM	38.8	6.26	7.88	50	16	0.35
C-10	PR14x32	(NaF) = 0.050 mM	75.8	11.6	7.88	50	30	0.28

Table 5-4. Continued on the following page.

Table 5-4 continued

Run	Grade of ore in the column	Components added to the stock feed	Weight of ore in the column (g)	t_r (min)	Feed pH	Feed Temp. (°C)	V'_{cbt}	C/C_o at steady-state
C-11	PR14x32	(NaF)=0.050 mM;(MgSO$_4$) = 1.0 mM	38.5	6.32	7.82	23	(1)	0.86
C-12	PR14x32	(NaF)=0.050 mM;(MgSO$_4$) = 1.0 mM;(NH$_4$Cl) = 0.70 mM	39.1	6.41	7.69	23	(1)	0.88
C-13	PR14x32	(NaF)=0.050 mM;P$_{CO_2}$ = 8.2 x 10^{-4} atm	39.1	6.50	7.50[2]	23	(1)	0.84
C-14	PR14x32	(NaF)=0.050 mM;P$_{CO_2}$ = 2.97 x 10^{-2} atm	39.1	6.25	6.60[2]	23	(1)	0.91
C-15	PR14x32	Secondary effluent, no stock used	37.8	6.20	7.68	23	(1)	0.95
C-16	PR14x32	(NaF)=0.050 mM;(HCO$_3^-$) = 1.46 mM[2];P$_{CO_2}$ = 8.2 x 10^{-4} atm	37.6	6.22	7.96	23	(1)	0.91

Table 5-4. A summary of the conditions under which each column run was performed. The concentrations in the stock feed are given in Table 3-1.
(1) Not observed due to the sampling time being larger than the time of breakthrough.
(2) Changed by varying the P_{CO_2}.

of breakthrough was achieved within 11 hours after the start of the run, but in some instances breakthrough occurred within the 45 minutes that was necessary to collect a sample for analysis. In these latter cases the value of V'_c at breakthrough (noted as V'_{cbt}) was not observed. Steady-state removal was achieved in approximately 1 week of operation.

5-2-1   Factors affecting column breakthrough

In the model presented in Chapter 4 it was seen that column operation up to breakthrough was representative of the period of initial rapid nucleation. If the model is correct then the factors that affect the rate and amount of initial nucleation should also affect the point of column breakthrough. Figures 5-22 and 5-23 are plots of the data for the column runs where the point of breakthrough was observed.

The total phosphate rock surface area in the column will determine the number of active sites available for nucleation and thereby affect the total mass of phosphate removed up to breakthrough. It was seen in Figure 5-19 that a straight line relationship existed between phosphate removal and available surface area.

The column retention time is the time period available for nucleation to occur and it should have a major effect on initial column removal. Increasing the temperature should also increase the initial removal by lowering the initial supersaturation (Equation 2-16) and by increasing the rate of formation of nuclei (Equation 2-9).

A method of interrelating the various parameters involved up to breakthrough is to examine the dependence of the phosphate surface
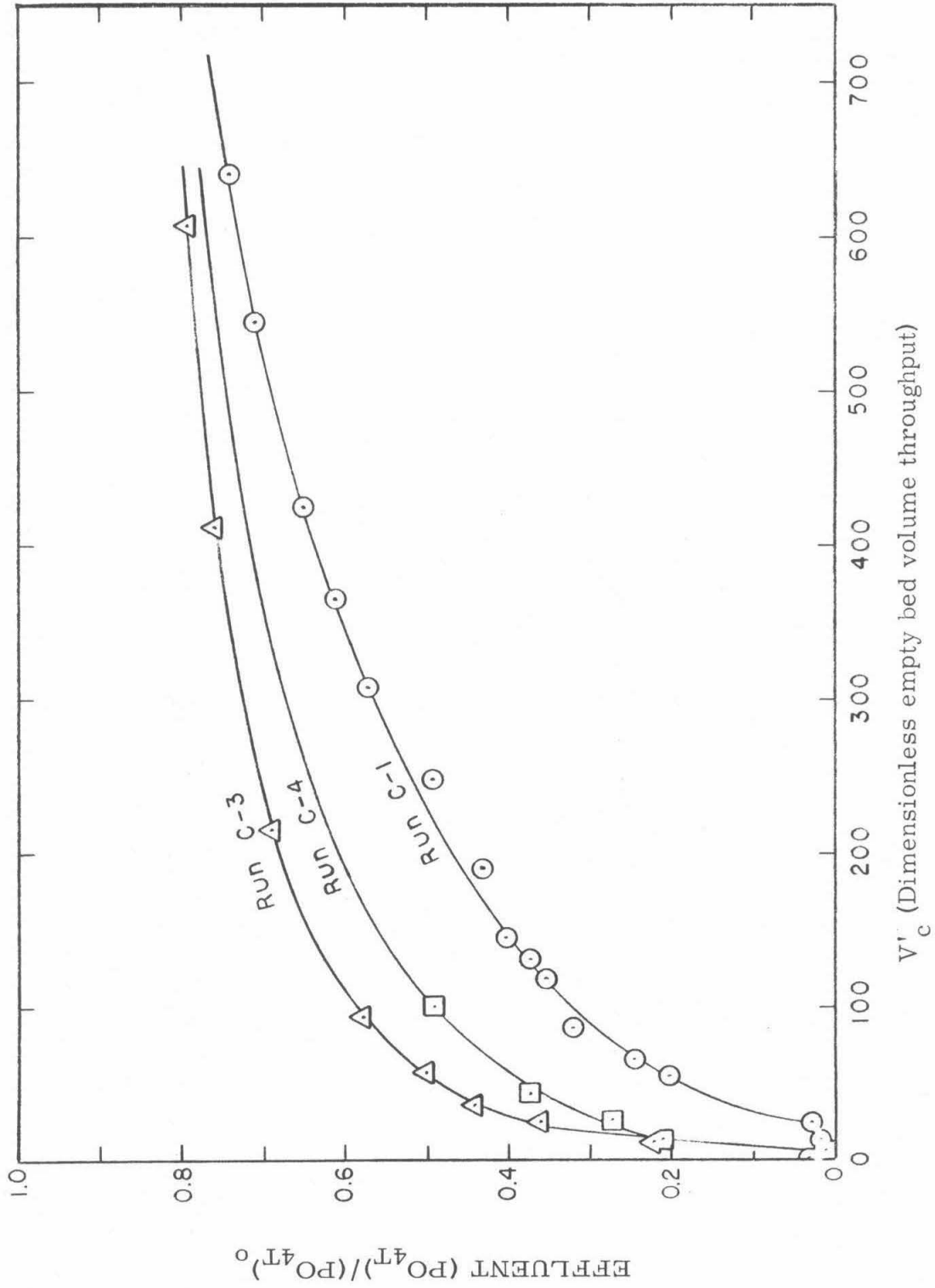
Figure 5-22. Column performance using the PR-10 phosphate rock and stock feed. The curves are not extended to steady-state conditions.
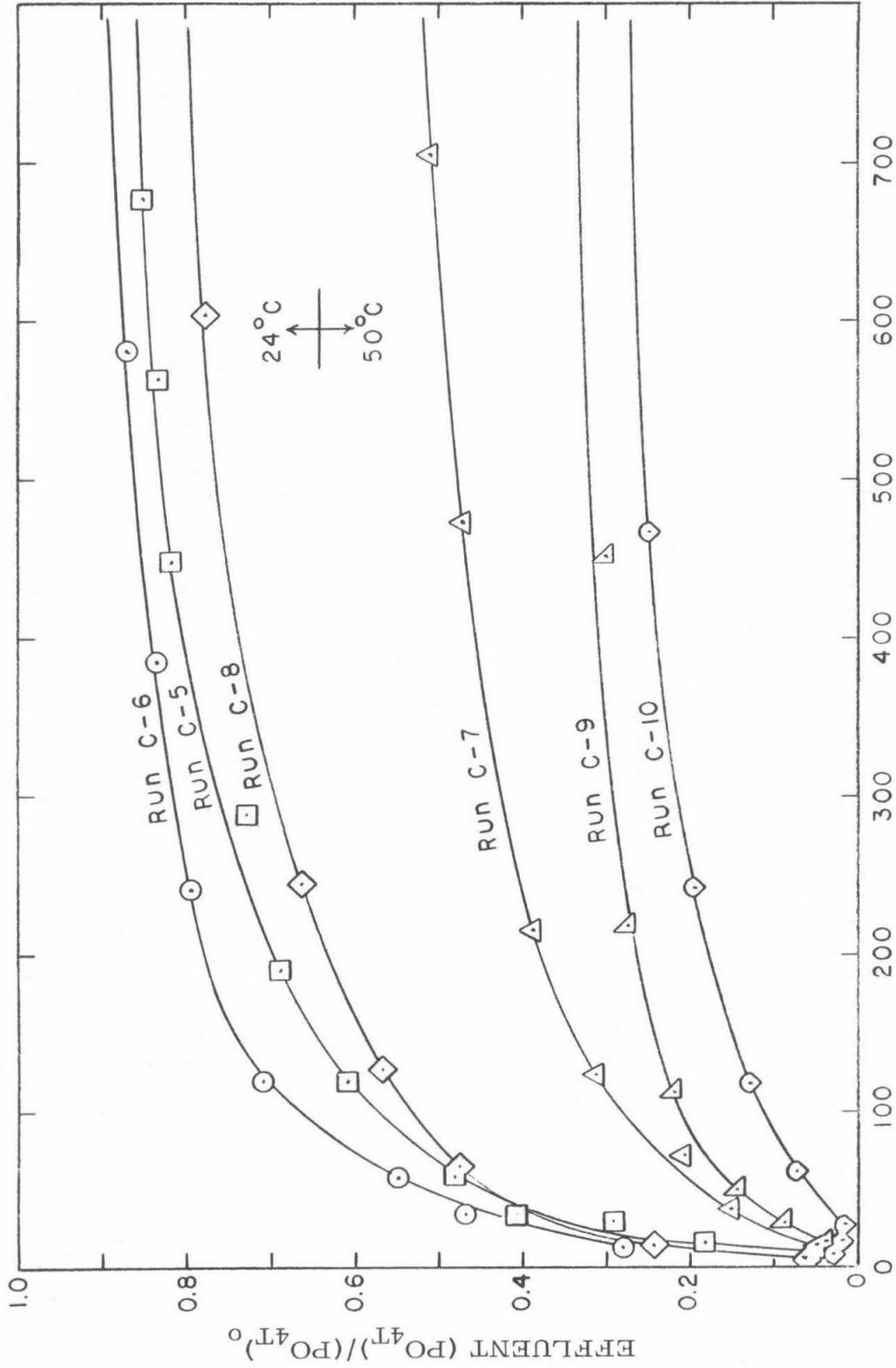
Figure 5-23. Column performance using the PR 14x32 phosphate rock at 24°C and 50°C.

coverage (in units of atoms of P removed from solution per unit phosphate rock surface area) on the column retention times. These plots are shown in Figure 5-24 for the temperatures and grades of ore used. It can be seen that increasing the temperature from 23°C to 50°C increased the initial surface coverage approximately 3.5 times when using the PR 14x32 phosphate rock. From the slope of the lines in Figure 5-24 a relationship between V'_c at breakthrough and retention time can be calculated. For the PR 14x32 sample at 23°C this relationship is

$$V'_{cbt} = (A/V_{eb}) \, 0.0526 \, t_r \tag{5-5}$$

where A/V_{eb} is the surface area per unit empty bed column volume in m^2/ml, and t_r is in minutes. For the PR 14x32 sample A/V_{eb} is equal to $13.3 \, m^2/ml$ and the bulk density is $1.50 \, g/ml$, which further reduces Equation 5-5 to

$$V'_{cbt} = 0.080 \, A_u t_r \tag{5-6}$$

where A_u is the unit surface area in m^2/g.

Equations 5-5 and 5-6 can be used to estimate column performance at longer retention times and will be further examined in the application chapter.

It was surprising to find that the PR-10 sample produced an initial removal approximately twice that of the PR 14x32 sample for equal retention times. According to the supplier the only difference between the samples was the particle size. This difference resulted in a larger unit surface area for the smaller sample, but since the surface coverage
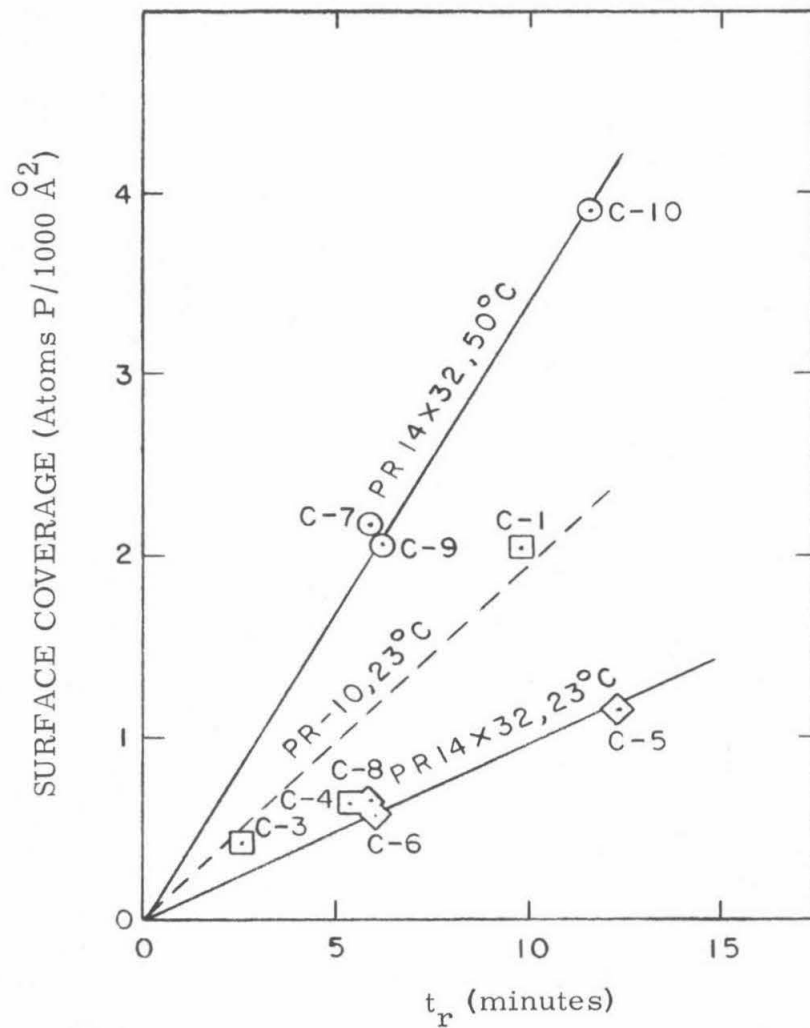
Figure 5-24. Plot of surface coverage up to break-through against column retention time. The numbers near each point denote the respective column run.

parameter puts the removal on a unit area basis, no difference should have been observed. The discrepency between the 23^OC lines in Figure 5-24 indicates that the PR-10 sample has approximately twice as many active sites as does the PR 14x32 sample. Apparently the grading techniques of the manufacturer in some way affect the activity of the phosphate rock.

Examining Figure 5-24 it can be seen that the data points for runs C-7 and C-9 fall relatively close together. These two points represent 50^OC runs with and without fluoride added to the stock feed. Similar results are obtained for the 23^OC Runs C-6 and C-8, indicating that the amount of initial rapid nucleation is not markedly affected by the feed fluoride concentration.

From Figure 5-21 it was seen that fluoride leaches out of the phosphate rock in direct proportion to the phosphate rock concentration in a suspension. Accordingly one would expect to observe high effluent fluoride concentrations during the start of a column run, for during this time the fluoride should be leaching out of the phosphate rock. Table 5-5 does show that at the start of each column run the effluent fluoride concentration is substantially higher than the 0.050 mM concentration in the feed and decreases as the run progresses. Therefore during the beginning of a column run fluoride is always available, a situation that tends to diminish the effect of whether or not fluoride is in the feed. The fact that the fluoride concentration has little effect on the amount of initial rapid nucleation also indicates that FAP probably is not being formed, a result in agreement with that found in the

COLUMN EFFLUENT FLUORIDE CONCENTRATION ($[F_T] \times 10^6$ M)

V'_c	C-9	C-10	C-8	C-11	C-12	C-13	C-14	C-15	C-16
5	12	108	50	70	70	69	61	157	126
10	87	108	60	65	65	59	52	113	42
	62	90	47	59	60	51	47	92	76
	48	76		54	55	44	44	74	60
50	31	50	35	49	47	37	42	60	46
100	23	35	36	47	44	35	40	56	38 / 42
	18	21		46	45	39	42	54	44
500	16	16 / 14	44	48	46	41	42	53	45 / 46

Table 5-5. Column effluent fluoride concentrations during Runs C-8 through C-16. In all runs $(F_T)_o = 51 \pm 2 \times 10^{-6}$ M.

batch runs.

5-2-2   Factors affecting column steady-state operation

Figures 5-25 through 5-27 are plots of the data for the column runs that were not shown in Figures 5-23 and 5-24. During column steady-state operation the rate of removal of phosphate from the feed solution must necessarily equal the rate at which a solid phosphate compound is forming on the phosphate rock surface. From the batch runs it was observed by electron diffraction analysis that the solid forming was HAP. If the solid growing on the phosphate rock during column operation was also an apatite, then the ratio of the drop in (Ca_T) divided by the drop in (PO_{4T}) should equal the theoretical HAP ratio of 1.67. This ratio was computed for each point in every column run with the overall average of all points for runs C-1 through C-16 being 1.61. Since the Ca/P ratio for OCP is 1.33 and for TCP is 1.50, it can be concluded that the growing phosphate compound was most probably a solid form of apatite.

In order to analyze any column operation mathematically, two factors must be taken into account: 1) the axial concentration inside the column at any position and time due to column dispersion; and 2) the concentration inside the column at any position and time due to material conversion by chemical reaction. Radial dispersion was assumed to be negligible for all cases. If the column were ideal and true plug flow existed (no element of fluid would overtake any other element) then only the concentration change due to chemical reaction need be considered.
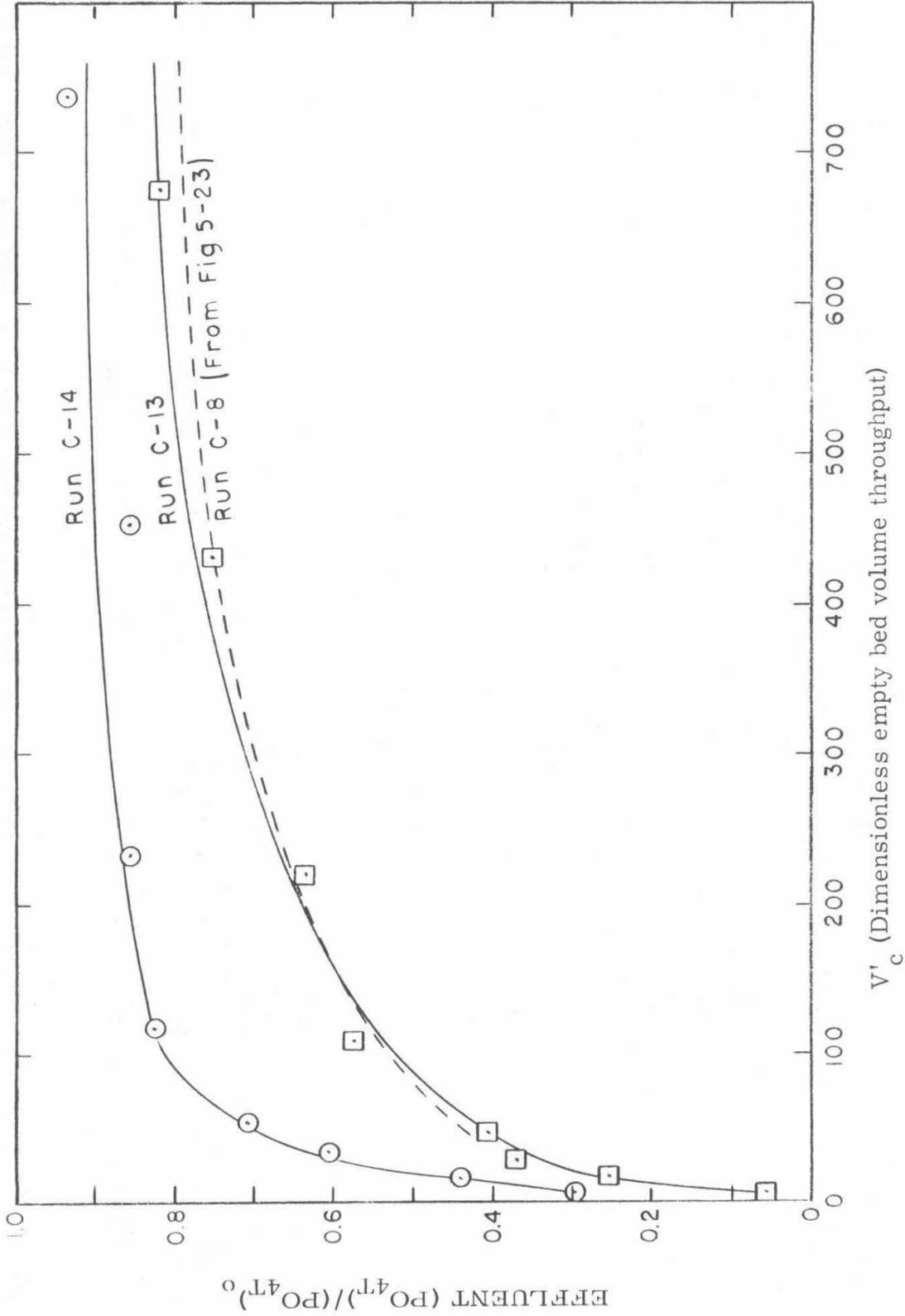
Figure 5-25. Effect of pH changes in the feed solution on the column performance. Run C-8 pH = 7.9, Run C-13 pH = 7.5, Run C-14 pH = 6.6. PR 14x32 and $t_r \cong 6$ minutes.
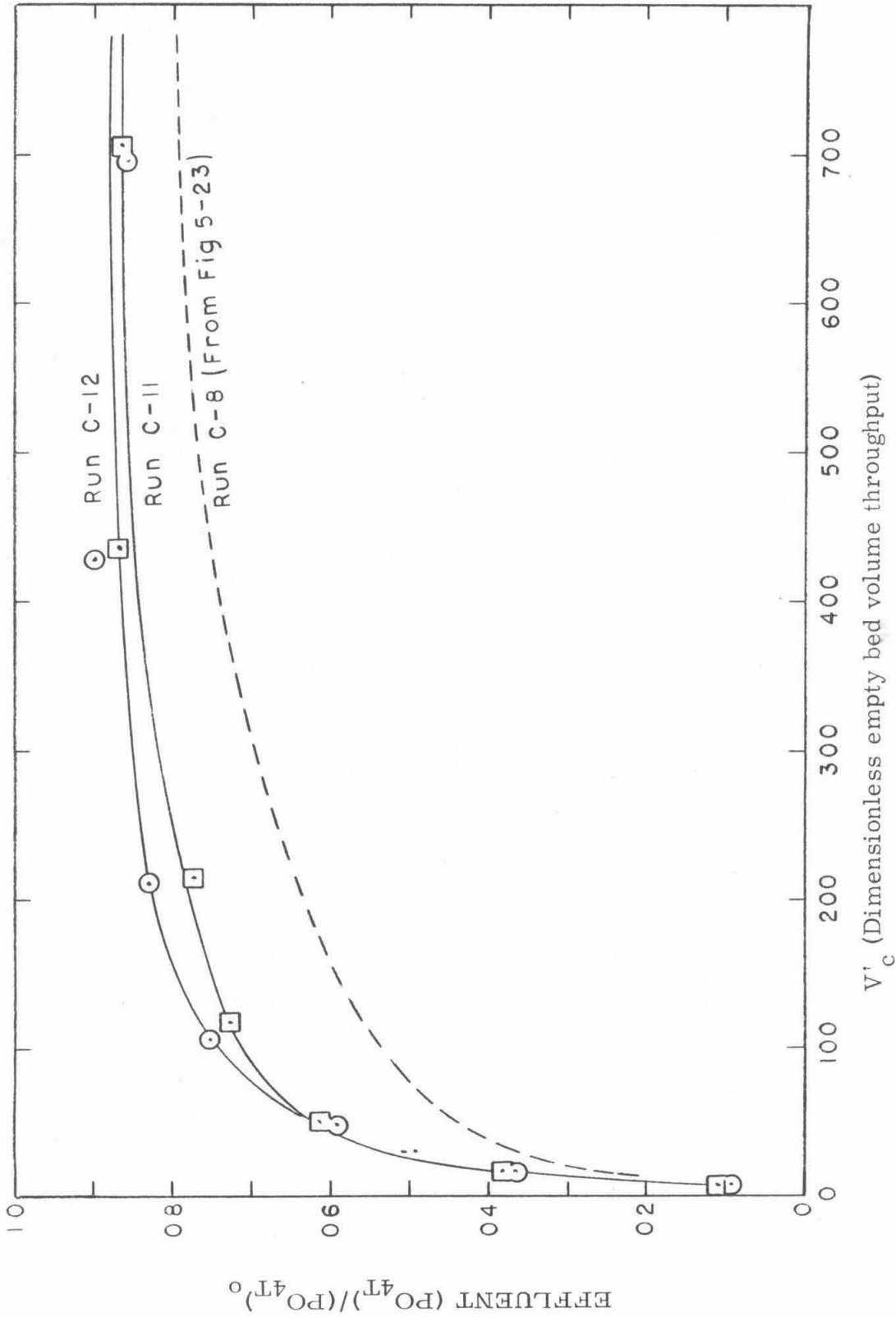
Figure 5-26. $MgSO_4$ and NH_4Cl effects on column performance. Run C-8 has no $MgSO_4$, Run C-11 has ($MgSO_4$) = 1.0 mM, and Run C-12 has ($MgSO_4$) = 1.0 mM and (NH_4Cl) = 0.7 mM. PR 14 x 32 and $t_r \cong 6$ minutes.
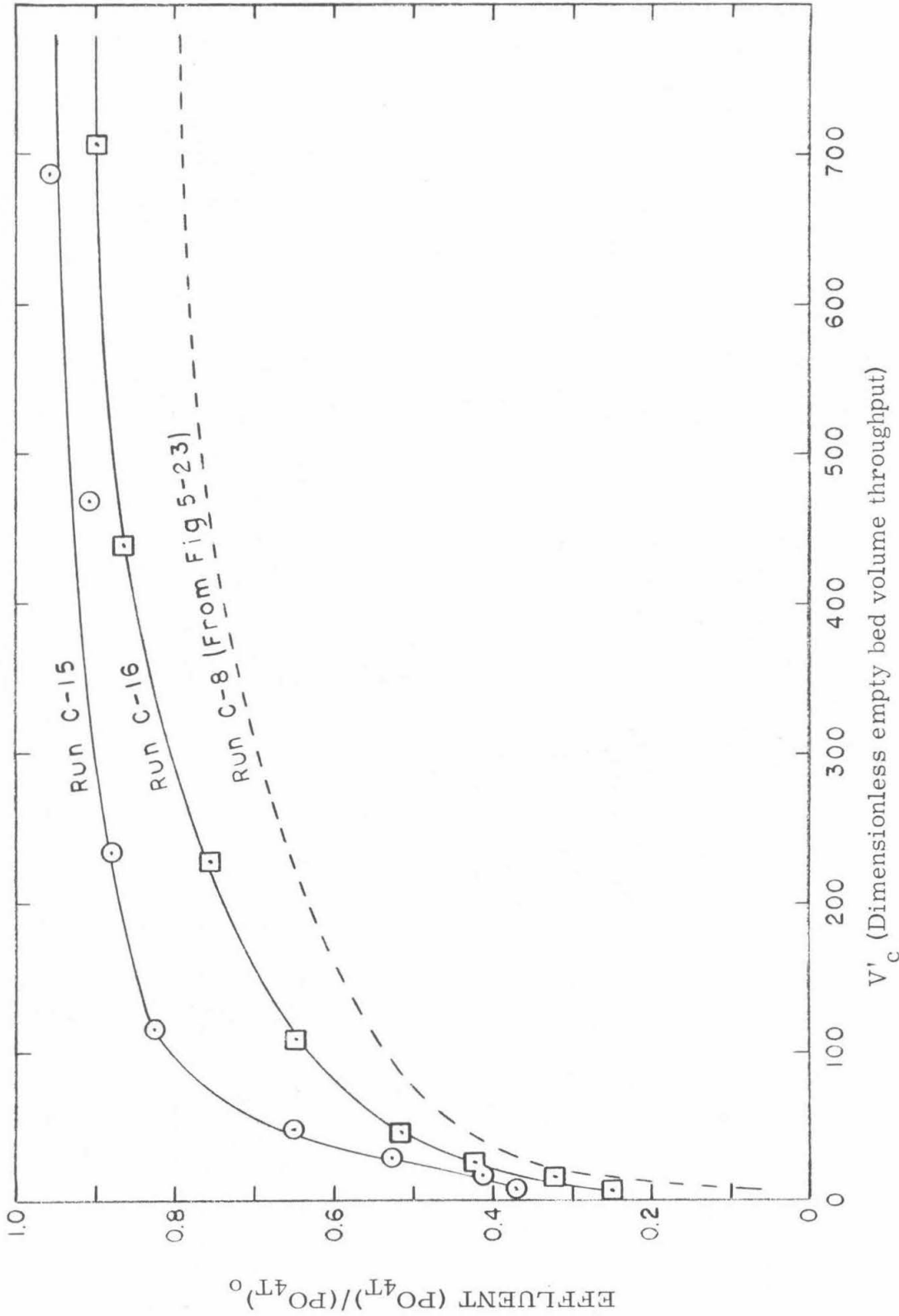
Figure 5-27. Effect of a (CO_{3T}) change in the feed solution on the column performance. PR 14x32 and $t_r = 6$ minutes. Run C-8 (CO_{3T}) = 0.68 mM, Run C-16 (CO_{3T}) = 1.51 mM, Run C-15 (CO_{3T}) = 5.40 mM.

A measure of the column diffusivity is the dispersion number, which is defined as D/uL, where D is the axial dispersion coefficient, u is the axial velocity, and L is the column length. D/uL uniquely characterizes the degree of backmixing during column flow and varies from zero at plug flow to infinity at complete backmixing.

The dispersion coefficient can be determined by injecting a slug of tracer into the feed solution during column operation and measuring the concentration of tracer in the effluent. Using the method of moments to determine the variance of the effluent concentration profile (a plot of effluent concentration vs. time), the dispersion number can be calculated from the equation given by Levenspiel (1962)

$$\sigma^2 = 2\,D/(uL) - 2\,(D/(uL))^2\,(1-e^{-uL/D}) \tag{5-7}$$

By using NaCl as a tracer and measuring the conductivity of the effluent solution the values of the dispersion coefficients were found to be 0.37 cm^2/sec for the PR 10 phosphate rock and 0.188 cm^2/sec for the PR 14x32 phosphate rock. From these values of dispersion coefficients the values of the dispersion numbers under the conditions of each column run can be determined. Using PR 14x32 the values of D/uL were 0.08 at 6 minutes retention time and 0.04 at 12 minutes retention time. At these low values of dispersion numbers the columns were very nearly operating under plug flow conditions. The error introduced by assuming plug flow varies with the total extent of chemical conversion that takes place inside the column. For (PO_{4T}) $(PO_{4T})_o$ values (at steady-state conditions) of 0.9 and 0.5, the errors are approximately 3% and 13% respectively for a dispersion number of

0.063 (Levenspiel 1962). For all column rate constant calculations plug flow was assumed to be occurring.

By assuming plug flow conditions inside the column the axial concentration of phosphate is determined solely by the rate of chemical transformation as the solution passes through the column. From the batch studies it was found that the mass rate of growth of HAP followed an equation of the type

$$dm/dt = k A C^n \tag{5-8}$$

Assuming this type of reaction occurs inside the column the general solution for steady-state conditions can be written as (see appendix 1)

$$t_r = (V/kA(PO_{4T})_o)(n-1)^{-1} (((PO_{4T})/(PO_{4T})_o)^{1-n}-1) \tag{5-9}$$

where t_r is the retention time in hours, V is the total void volume of the column in liters, A is the total surface area of the phosphate rock in m^2, and n is the order of the reaction.

If a value for n is assumed, k can be determined from Equation 5-9, because all of the other quantities can be measured. For the batch runs at $23^{\circ}C$, n varied among the three different regions observed, but in all cases was approximately equal to 2 after 150 hours into the run. Since steady-state conditions are not developed until approximately 200 hours of column operation, it can be assumed that the column crystal growth then occurring can be approximately represented by a second order rate equation. Tables 5-6 through 5-8 are listings for the computed second order rate constants that were calculated from the steady-state conditions of all of the column runs.

a) Effect of physical parameters on the steady-state rate constant

Table 5-6 lists the computed rate constants for the column runs where a comparison can be made on the effects of varying retention times, unit surface area, and temperature. The rate constant should theoretically be independent of the unit surface area or retention time, for these parameters are representative of the column configuration and not of the chemical reaction occurring inside the column. For the data using the stock feed it can be seen in Table 5-6 that varying the retention time or unit surface area[1] had little effect on the value of k, with the average k value for runs C-1 through C-6 being 0.115. This average value of the rate constant compares favorably with the rate constant of 0.10 and 0.68 observed for batch runs B-4 and B-6 (Table 5-3).

When the column temperature was increased from $23^{\circ}C$ to $50^{\circ}C$ using stock feed or stock feed + fluoride, the rate constant increased markedly. The k_{50}/k_{23} ratio was approximately equal to 9 for the stock feed and 5 for the stock + fluoride feed. Rootare et al (1962) and Clark (1955) found that the solubility of HAP increased with an increase in temperature. The result of this study that increasing the temperature produces lower phosphate concentrations in both batch and column systems indicates that the governing phenomenon in the uptake of phosphate by phosphate rock appears to be one of kinetics of nucleation and crystal growth.

---

(1) The unit surface area of the PR 10 phosphate rock is 40% greater than for the PR 14x32 phosphate rock.

Run	Feed	t_r (min)	Temp. °C	k liter^2 mole^{-1} hr^{-1} m^{-2}
C-3	Stock	2.60	23	0.120
C-4	Stock	5.44	23	0.136
C-1	Stock	9.84	23	0.094
C-6	Stock	6.02	23	0.114
C-5	Stock	12.4	23	0.112
C-8	Stock + 0.05 mM (F_T)	5.86	23	0.328
C-7	Stock	5.85	50	1.03
C-9	Stock + 0.05 mM (F_T)	6.26	50	2.01
C-10	Stock + 0.05 mM (F_T)	11.6	50	1.49

Table 5-6. Effect of physical parameters on the column reaction rate constant k.

b) Effect of chemical parameters on the steady-state rate constant

Table 5-7 lists the computed rate constants for the runs where a comparison can be made on the effect of varying chemical species concentrations. Perhaps the most interesting result is the large increase in k due to the presence of fluoride in the feed water. In the $23^{\circ}C$ batch runs it was found that very little FAP seemed to nucleate or crystallize on the phosphate rock, even though substantial fluoride was introduced into solution from the dissolving of $CaF_2(s)$. During initial column operation the high fluoride concentration resulting from the leaching out of $CaF_2(s)$ also diminished the effect that any feed fluoride might have had on rapid nucleation. However as column operation continued the effluent fluoride concentration levelled out to a value slightly lower than that in the feed (Table 5-5). Although regular fluoride analyses were made only on the runs that had fluoride in the feed, spot checks on Runs C-5 and C-7-R indicated that very little fluoride was present in the effluent at a throughput of approximately 1000 empty bed volumes. For these runs the measured respective (F_T) values of 0.004 mM and 0.003 mM are close to the lower limits of the fluoride analysis, indicating that the $CaF_2(s)$ completely leaches out of the phosphate rock. Fluoride in the feed at a concentration of 0.050 mM increased the value of k from 0.115 to 0.328 (Runs C-6 and C-8). From Tables 5-4 and 5-5 the value of $\Delta(PO_{4T})/\Delta(F_T)$ for steady-state operation in Run C-8 was calculated as 9.0. It appears that for the runs with fluoride in the feed solution approximately 1/3 of the

Run	Feed Stock + Component added	k $\text{liter}^2 \text{ mole}^{-1} \text{ hr}^{-1} \text{ m}^{-2}$
C-8	$(F_T) = 0.05$ mM, pH = 7.9	0.328
C-13	$(F_T) = 0.05$ mM, pH = 7.5	0.197
C-14	$(F_T) = 0.05$ mM, pH = 6.6	0.106
C-11	$(F_T) = 0.05$ mM; $(MgSO_4) = 1.0$ mM	0.178
C-12	$(F_T) = 0.05$ mM; $(MgSO_4)=1.0$ mM; $(NH_4Cl)=0.7$ mM	0.149
C-16	$(F_T) = 0.05$ mM; $(CO_{3T}) = 1.51$ mM	0.118
C-15	Whittier Narrows Secondary Effluent (See Tables 3-2 and 3-3)	0.083

Table 5-7. Effect of varying the concentration of soluble species on the column reaction rate constant k. All runs were made with PR 14x32 at 23°C and $t_r \cong 6$ minutes.

apatite forming during column steady-state conditions is in the form of FAP. In the $50^{\circ}C$ column runs the value of k increased from 1.03 to 2.01 with the addition of fluoride to the feed (Runs C-7 and C-9). For the $50^{\circ}C$ Run C-9 the $\Delta(PO_{4T})/\Delta(F_T)$ at steady-state is equal to 5.7, indicating that the formation of FAP is enhanced by increasing the temperature, a result that is in agreement with the batch runs.

From the rate data obtained at different pH values (Table 5-7) one can evaluate the influence of the pH on the rate constant. Figure 5-28 shows the logarithm of the observed reaction rate constant versus pH for the column runs where the only variable was pH. The line plotted through the points has a slope of 0.34, indicating that there is approximately a two-fold increase in the value of k for each unit increase in pH. The increase in the rate constant is a result of the increasing supersaturation ratio as the pH is increased. Both the PO_4^{-3} concentration and the OH^- concentration increase logarithmically with increasing pH. The theoretical value of $d(\log S)/dpH$ is calculated as 0.22 for the pH range in Figure 5-28. This is approximately equal to the observed value of 0.34 for $d(\log k)/dpH$, indicating that to a large extent the relationship between k and pH is a function of the supersaturation ratio S.

The effect of 1.0 mM $MgSO_4$ in the feed solution was to decrease the rate constant by a factor of 1/2 (Run C-11). Although no magnesium apatite is known to exist in nature some instances of its incorporation into the apatite structure have been reported (Eanes and Posner 1968, Simpson 1966). Ferguson et al (1971) found that magnesium in solution retarded the precipitation of calcium phosphate but could not find any
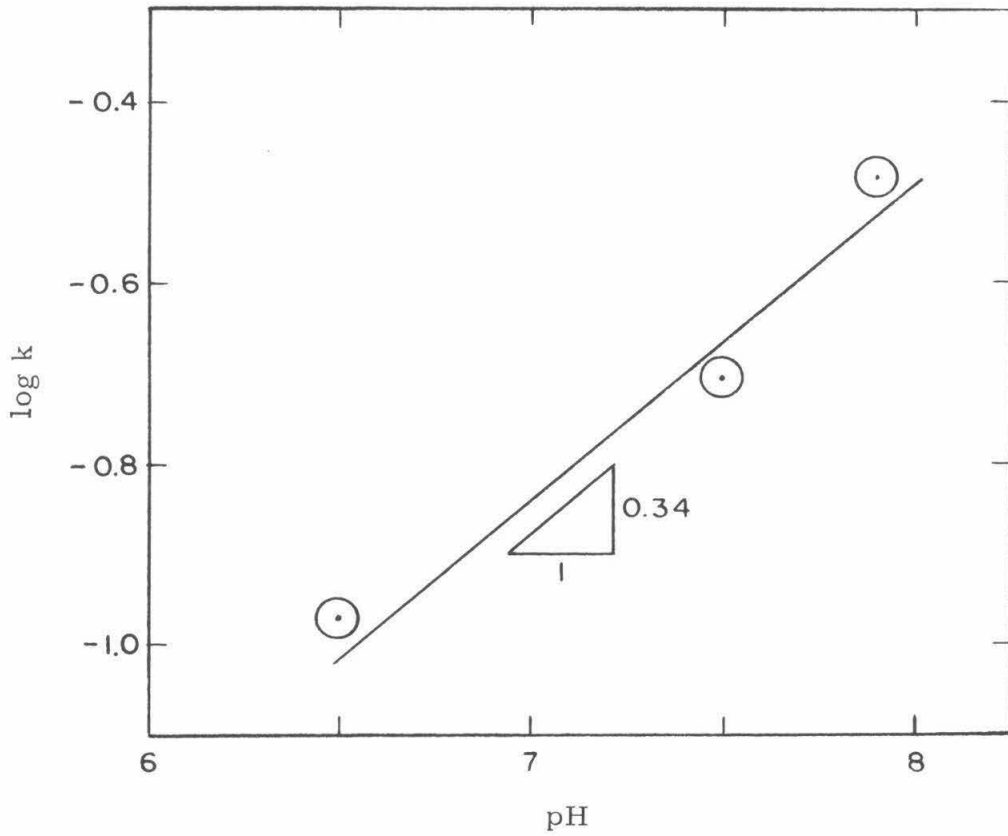
Figure 5-28. Dependence of the column rate constant on the feed pH. Runs C-8, C-13, and C-14.

relationship to describe the dependence. Apparently the incorporation of Mg^{+2} into the apatite crystal lattice in place of Ca^{+2} deforms the regular structure and acts to some degree as a crystal poison. In a similar manner SO_4^{-2} can replace the PO_4^{-3} group and will affect the overall charge balance. The unbalanced charge will result in crystal deformation and incorporation of other anions such as Cl^- in order to maintain a zero net charge.

The presence in the column feed of ammonium chloride at 0.7 mM in addition to 1.0 mM $MgSO_4$ was found to have little effect on steady-state column operation, lowering the rate constant from 0.18 to 0.15 (Table 5-7). Although this drop can be due to experimental error, examination of the plots of the column run in Figure 5-26 does show a slight decrease in column removal during the entire C-12 run. Therefore it can be concluded that the presence of NH_3 in solution does inhibit HAP crystallization to a slight degree.

The effect of the carbonate alkalinity is somewhat more pronounced on the rate constant. In other recent research on the formation of calcium phosphates from solution near pH 8, the dependence between the rate constant k and (CO_{3T}) has been reported to follow an equation of the form

$$k = K/(CO_{3T})^n \qquad (5\text{-}10)$$

where K is a proportionality constant dependent on solution conditions, and n is approximately equal to 1. This relationship is valid when the only variable is (CO_{3T}), with all other specie concentrations being held constant. In studying the precipitation of calcium phosphates

from a synthetic wastewater Ferguson et al (1971) reported n to be equal to 1. Leckie (1969) in his studies on the growth of HAP on calcite crystals in an aqueous slurry found n to be equal to 1.34. Using column Runs C-8 and C-16 (in these two runs only the (CO_{3T}) was varied) a value of 1.28 was found for n.

The plot for the column run using secondary effluent is shown in Figure 5-27 (Run C-15). The steady-state rate constant for this run was the lowest observed in this study. The primary factors responsible for this low value of k probably are the very high (CO_{3T}) of 5.4 mM, and the presence of approximately 1 mM $MgSO_4$ (Table 3-2).

5-2-3   Column regeneration

The methods that were tried for column regeneration consisted of a combination of resting the column by taking it out of service, and increasing the temperature and pH. The rate of crystal growth from solution is primarily affected by soluble component concentrations and temperature. Generally the higher the concentrations and temperature the more rapid the crystal growth. Therefore if a column operating at steady-state is removed from service and is fed with a higher pH solution at a higher temperature, the rate of micro-crystal transformation should be accelerated. The higher pH will have two effects: it will increase the concentration of PO_4^{-3} ions that otherwise are in a protonated form, and it will provide an increase in the OH^- concentration necessary for the formation of HAP crystals. Increasing the temperature will provide for more rapid molecule vibrations in the

nuclei formed at the active sites and consequently will increase the rate of transformation of these nuclei into the apatite crystal.

To raise the pH a distilled water solution containing 1 mM $NaHCO_3$ and enough NaOH to raise the pH to the desired value was used as feed. This feed was then pumped through the column until the effluent pH was a few tenths of a pH unit below the influent value. Approximately 15 empty bed volumes were pumped through each column during regeneration. The unsuccessful regeneration attempts are summarized below:

1. Eleven days at $23^{\circ}C$; no pH increase.

2. Eleven days at $50^{\circ}C$; no pH increase.

3. Eleven days at $50^{\circ}C$; pH raised to 9.7.

The columns were successfully regenerated when they rested for approximately 10 days at $50^{\circ}C$ and pH 11.9. The results of all of the regeneration attempts are shown in Figures 5-29 and 5-30. In each case of successful regeneration it was observed that steady-state column performance increased substantially. From Table 5-8 it can be seen that regeneration in each case increased the rate constant by a factor of about 2. Apparently the regeneration process used either creates more active sites on the phosphate rock or increases the capacity of the existing sites.

At the startup of each regenerated column run the effluent phosphate ratio was found to be between 0.2 and 0.5 in the first sample collected. It then dropped to a low point at about 30 empty bed volumes, after which it increased in a manner similar to the non-regenerated runs. In all cases the (Ca_T) was equal to zero during this poor initial
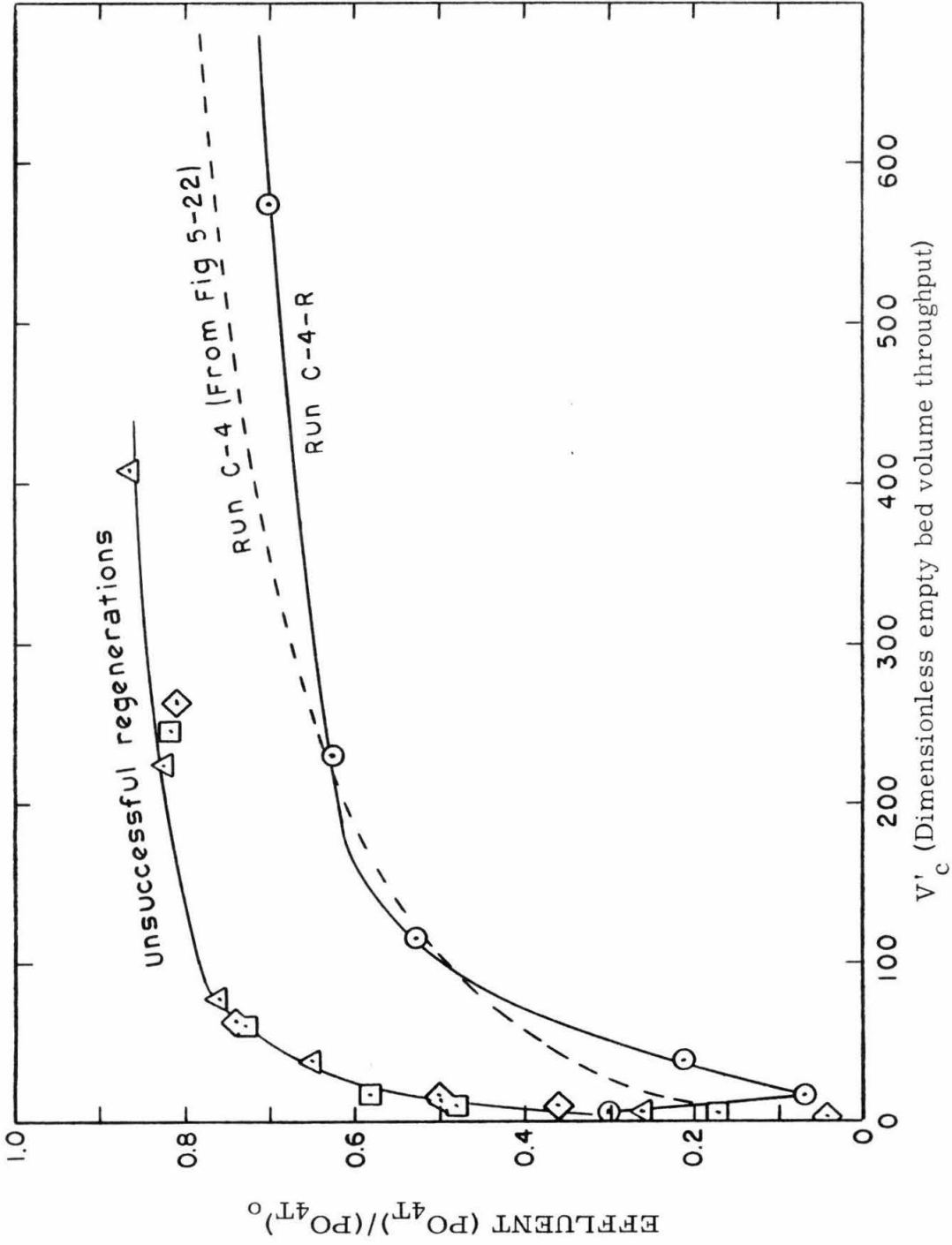
Figure 5-29. Regeneration of PR-10 columns. Steady-state effluent phosphate ratios for Run C-4 and the regenerated Run C-4-R were 0.84 and 0.76 respectively. Temperature = 23 °C.
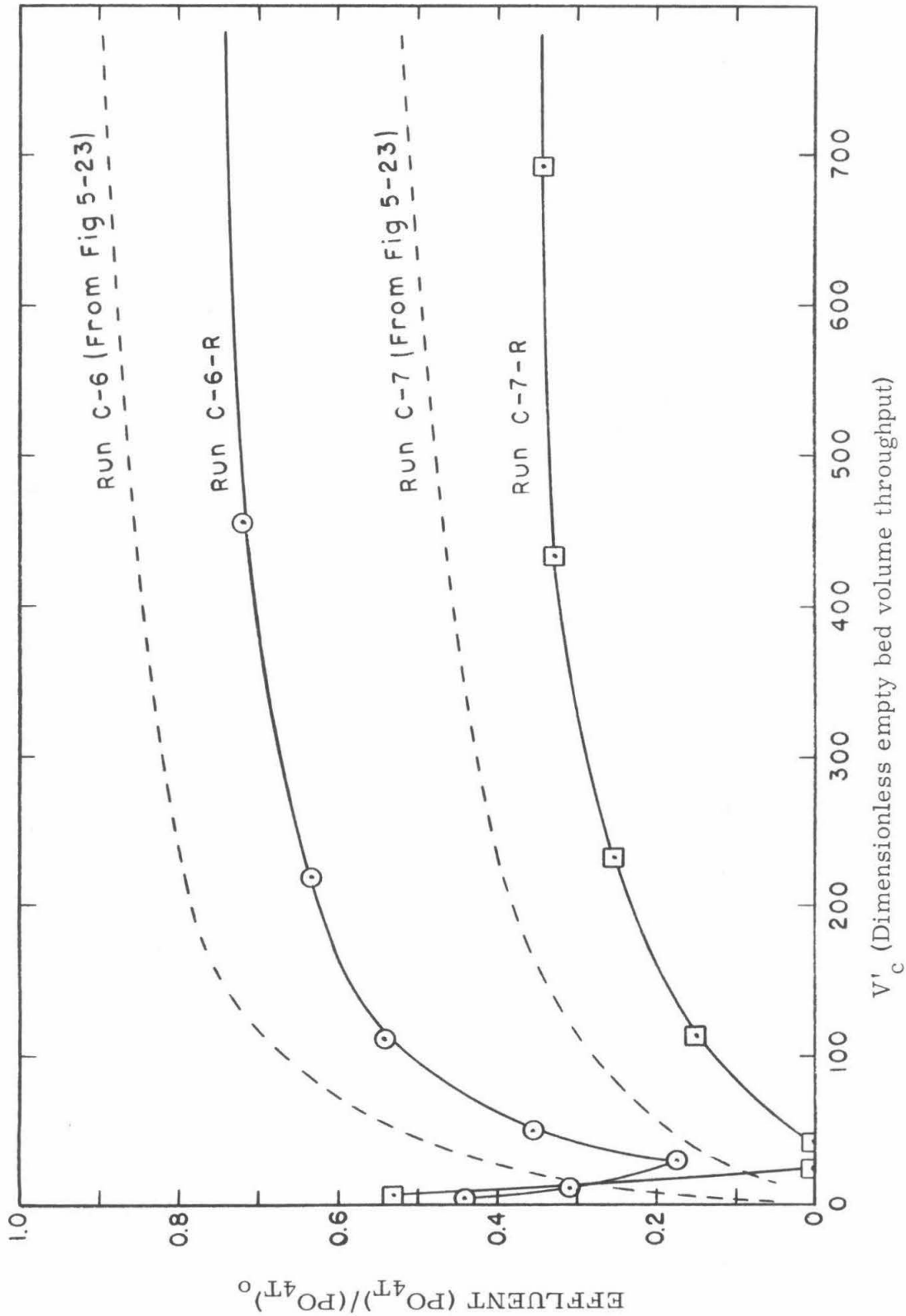
Figure 5-30. Regeneration of PR 14x32 columns. Runs C-6 and C-6-R were performed at 23°C, and Runs C-7 and C-7-R were performed at 50°C. The regenerated runs are denoted by -R.

Run	Temperature ^{o}C	k $\text{liter}^2\ \text{mole}^{-1}\ \text{hr}^{-1}\ \text{m}^{-2}$
C-4	23	0.136
C-4-R	23	0.233
C-6	23	0.114
C-6-R	23	0.372
C-7	50	1.03
C-7-R	50	1.93

Table 5-8. Summary of the reaction rate constants before and after successful column regeneration. Regeneration was accomplished by resting the column for about 10 days at 50°C and pH = 11.9. The regenerated runs are denoted by -R.

column performance. The calcium was probably disappearing from solution by an ion exchange phenomenon with the phosphate rock. The sodium in the NaOH used for regeneration adsorbed everywhere on the surface of the phosphate rock and later exchanged with the calcium in the synthetic feed solution. Van Wazer (1958) reports exchange capacities as high as 0.3 meq/g for some phosphate rocks. With very little Ca^{+2} in solution or adsorbed on the active sites, not enough calcium was available for the nucleation of HAP, thereby resulting in poorer column performance. This problem could be alleviated by using lime for regeneration instead of sodium hydroxide.

The objective of the regeneration experiments was to demonstrate that the phosphate rock could be regenerated while in a column configuration. Many of the parameters for regeneration such as concentration of Ca^{+2} ions and PO_4^{-3} ions, temperature, pH, and regeneration time, must be evaluated in order to determine optimum regeneration values. Since this will depend to a large extent on the type of wastewater treatment plant effluent used as feed, these types of studies are best performed in a pilot plant at the wastewater treatment site. The important finding in this study is that regeneration can be accomplished within reasonable operating and economic conditions.

Chapter 6

Engineering Applications

The engineering applications examined were: 1) very high removal of phosphate from wastewater, and 2) continual removal of phosphate with removal efficiencies in the region of 80%. The first application is represented by column operation up to breakthrough, and the second by steady-state operation.

6-1   High phosphate removal

6-1-1   High phosphate removal from secondary treated effluent

The treatment process system envisioned for high phosphate removal would be similar in design to the experiments performed in the laboratory columns. Granular phosphate rock of about 14x32 mesh size would be packed in a column configuration through which secondary treated effluent would be pumped for phosphate removal. Regeneration would take place inside the column by simultaneously increasing the feed temperature and pH. Recycling of the high pH and high temperature regenerating solution would be utilized in order to minimize the operating cost. Before detailing such a system it is advisable to examine the operating characteristics involved and roughly to determine a unit cost estimate for producing an effluent of comparable quality to that of other established treatment processes.

The first few readings of Figures 5-22 and 5-23 show that the phosphate removal efficiencies are approximately 97% before the

breakthrough point is reached. The corresponding phosphate effluent concentration of 0.01 mM (equal to approximately 0.3 mg/l P) is on the low side compared to the effluents obtained from standard phosphate removal processes using chemical coagulation (Weber et al 1970, Rohlich 1962). Cost estimates for phosphate removal by chemical coagulation are highly dependent on wastewater condition and removal desired, but generally average about $0.10/1000 gallons of water treated[1] (Nesbitt 1969, Spiegel and Forrest 1968) for treatment efficiency comparable to the phosphate rock nucleation proposed herein.

One method of making a rough cost estimate of any proposed and untested treatment process is to compare it with an established treatment system that is similar in design and operation. One such existing process for comparison with phosphate rock nucleation is activated carbon adsorption. In both systems packed columns of the reacting material are contacted with secondary treated wastewater for a similar retention time.

Typical criteria for the design of an activated-carbon adsorption plant as given by the U.S. Department of the Interior (1969) are:

1) Retention time = 25 minutes.

2) Superficial linear velocity = 7.0 gpm/ft^2.

3) Carbon particle sizes with resultant head losses:

    a) 8x30 mesh, 0.4 psi/ft at 7.0 gpm/ft^2.

    b) 12x40 mesh, 0.8 psi/ft at 7.0 gpm/ft^2.

---

(1) All cost estimates are for a 10 MGD plant size.

4) Ratio of bed depth to diameter should be greater than 1.0, with

    2.0 the recommended value.

Utilizing these criteria a typical 10 MGD activated carbon plant would

contain six carbon contactors, each being 30.0 feet long by 25.5 feet

in diameter.

An activated carbon column using a 25 minute retention time is

regenerated at about every 2000 empty bed volumes of throughput at

a total cost (operating and amortization) of approximately $0.10/1000

gallons (Parkhurst et al 1967). Regeneration is performed about once

per month. The initial and make-up cost of the activated carbon as

well as the elaborate regeneration technique[1] necessary accounts

for about 1/4 to 1/3 of the total cost of the treatment process. Since

the cost of the activated carbon is 35 times as great as the phosphate

rock ($700/ton vs $20/ton) and regeneration of the phosphate rock a

much simpler procedure, we can approximate the need for regeneration

of the phosphate rock system to occur at about 1500 empty bed volumes

of throughput for the equivalent cost of $0.10/1000 gallons. Basically

since the cost of materials is less for the phosphate rock system it

can tolerate more inefficiency while maintaining the same unit cost.

Therefore the column design parameters for high phosphate removal,

utilizing phosphate rock,are a retention time of 25 minutes with a

throughput capacity of 1500 empty bed volumes before regeneration

---

(1) In activated carbon regeneration the carbon is removed from the
contactor, burned to remove organics, quenched, stored, and then
returned to another contactor for re-use.

should become necessary. Utilizing Formula 5-6

$$V'_{cbt} = 0.080 \ A_u t_r \qquad\qquad (5\text{-}6)$$

with the unit area of 8.8 m^2/g for the PR 14x32 grade ore used, a throughput of 18 empty bed volumes is obtained before breakthrough occurs, the point at which the column must be regenerated. This is approximately 1/100 of the column capacity necessary for the process to be economical.

When comparing the time interval for regeneration the picture becomes even bleaker. The frequency of regeneration, F, can be related to the retention time by the formula

$$F \ (in \ hrs) = 2.78 \times 10^{-3} \ A_u t_r^2 \qquad\qquad (6\text{-}1)$$

At 25 minutes retention, F is calculated to be 15 hours. Since column regeneration requires approximately 10 days it would be necessary to have a total of 16 columns in a treatment system, with 15 in a state of regeneration at any one time. Considering throughput capacity alone it can be concluded that the cost of high phosphate removal utilizing raw grade phosphate rock is approximately 100 times too expensive

for consideration as a treatment process. The need for frequent re-generation would make the process far too demanding in operator labor force to be practical. Therefore high phosphate removal from secondary treated effluent by nucleation on the raw grade phosphate rock used in this study can not be recommended as a viable wastewater treatment process.

One of the properties of phosphate rock which has a major bearing on its nucleating capacity is the unit surface area of the material; hence increasing the unit surface area should have a direct effect on the economics of the proposed treatment system. The two different samples of granular phosphate rock used in this study varied in unit surface area by 40%, 8.8 m^2/g for the PR 14x32 sample and 12.3 m^2/g for the PR-10 sample. However the small mean diameter of 0.24 mm for the PR-10 sample virtually excludes its use in a prototype column system because of the resultant high head loss that would be incurred[1]. Furthermore the 40% increase in surface area realized by using smaller granules is relatively meaningless to the economics of the system, for in order to be economically competitive the treatment cost must be reduced by two or more orders of magnitude. Williams and Irvine (1954) and Loebenstein (1965) both report that the surface area of bone mineral was increased markedly by extraction with an aqueous solution of ethylene diamine, in one case from 13 m^2/g to 130 m^2/g. Olsen (1952) reports synthetic preparations of precipitated HAP with surface areas up to 60 m^2/g, and one sample of natural apatite with a surface area of 51 m^2/g. Although no reports of experiments have been found in the literature where the specific objective was to increase the surface area of HAP, it would appear that by partial chemical dissolution and extraction the surface area of phosphate rock could possibly be increased to about 100 m^2/g. As a comparison with other materials used in column wastewater treatment Neufeld and Thodos (1969) report

(1) The head loss for the PR-10 phosphate rock at 7.0 gpm/ft^2 is approximately equal to 20 psi/ft.

using activated alumina with a surface area of 210 m^2/g. Activated carbons generally have surface areas greater than 1000 m^2/g (Calgon Corporation, 1969).

Figure 6-1 graphically represents the relationship given in Formula 5-6 for different values of A_u. Assuming that the unit surface area of HAP could be increased to 100 m^2/g and a residence time of 30 minutes would be used, the column throughput capacity before breakthrough would still be only 250 empty bed volumes (Figure 6-1). From Formula 6-1 the corresponding regeneration frequency is calculated to be approximately every 10 days. On a basis of surface area alone it would appear that the phosphate rock unit surface area must be close to 1000 m^2/g before the economics of the system become favorable.

Other factors may be important in affecting the economics of the proposed treatment system. If the surface coverage is dependent primarily on the retention time, then as the feed concentration of phosphate is lowered the throughput capacity before breakthrough will increase directly as $0.3/(PO_{4T})_o$, where $(PO_{4T})_o$ is the milli-molar concentration of the feed in question. A lower feed concentration enables a greater volumetric throughput to be realized for an equal amount of surface coverage. For example a feed with 0.15 mM (PO_{4T}) would have a V'_{cbt} twice that of a 0.3 mM feed, all else remaining equal.

Pre-treatment of the phosphate rock may also have a bearing on its phosphate nucleating ability. As seen in Figure 5-24 the unit surface coverage at equal retention times was twice as great for the
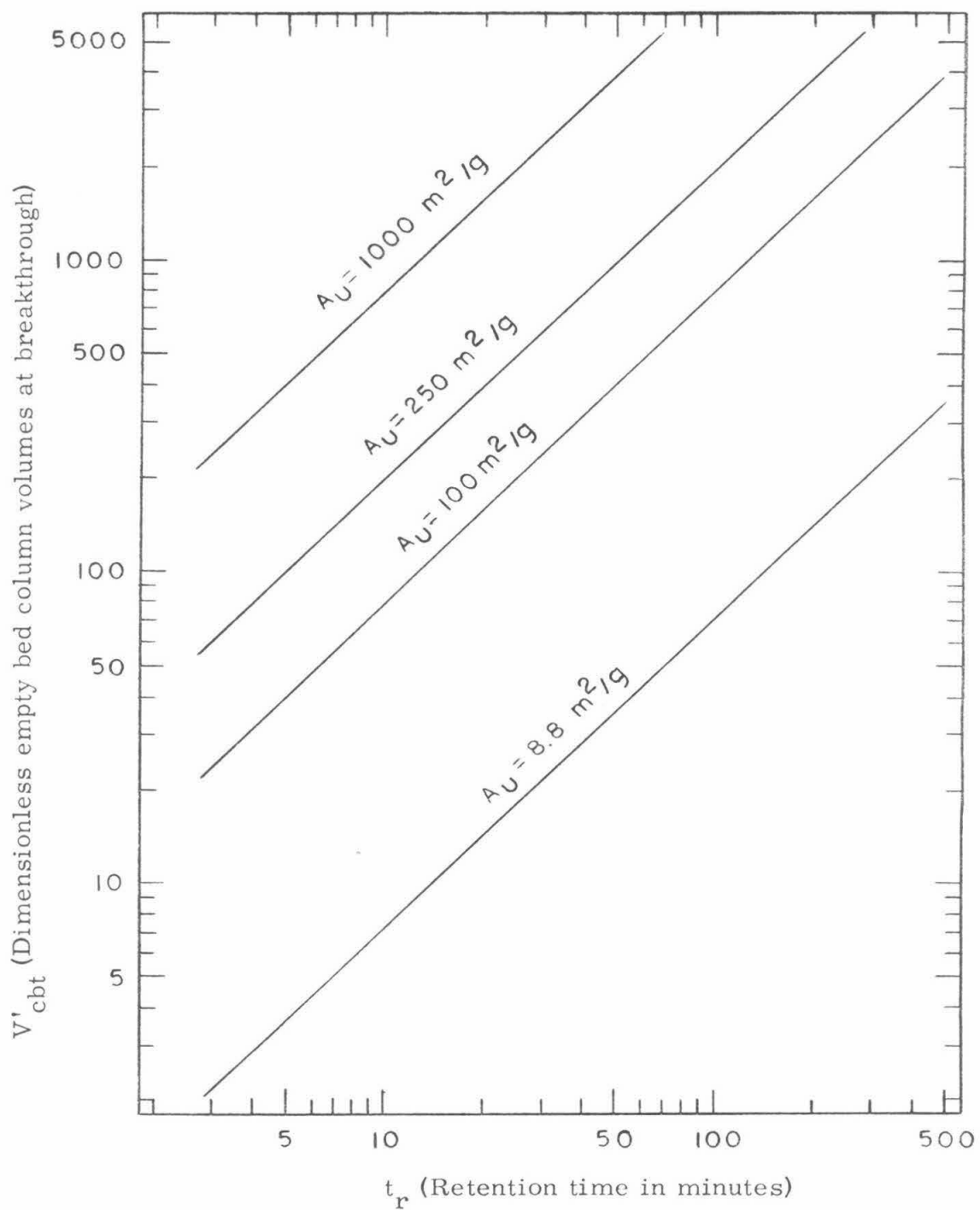
Figure 6-1. Dependence of column breakthrough on the unit surface area and retention time (Formula 5-6).

PR-10 as for the PR 14x32 ore. It was concluded that treatment in some way by the manufacturer increased the activity of the smaller grained sample.

Different grades of phosphate rock may have widely varying nucleating characteristics. Unfortunately only individual examination and testing can evaluate these presently non-definable characteristics.

6-1-2   High phosphate removal from lime-coagulation treated effluent

Another possible application of high phosphate removal by apatite nucleation on phosphate rock arises from the need for producing an effluent with a very low phosphate residual ($< 3 \times 10^{-4}$ mM, or 0.01 mg/l P) in order to minimize eutrophication in cases where treated wastewater effluents are discharged to lakes, estuaries, or slow-moving streams. In a chemical-coagulation treatment process the unit costs increase markedly when the desired effluent phosphate concentration is less than 0.01 mM. In a normally operated phosphate removal process involving lime-coagulation, the lime raises the pH to about 10, and the soluble orthophosphates precipitate as solid calcium phosphates, with the effluent (PO_{4T}) being approximately equal to 0.01 mM. From Figure 2-1 the equilibrium (PO_{4T}) at pH 10, taking complexation into account, is seen to be 10^{-6} mM. Therefore, by pumping the lime-coagulation treated effluent through a phosphate rock column and thereby providing a nucleating surface, a substantial drop in soluble phosphate can be expected to occur. During the column runs in this research the supersaturation ratio for HAP in the column effluent before the

point of breakthrough was equal to 2. Assuming that S_{HAP} = 2, pH 10, (Ca_T) = 1.0 mM, and complex formation, the concentration of soluble orthophosphate in the column effluent is then calculated to be equal to 10^{-5} mM. The capacity of the column, before regeneration becomes necessary, can be determined by use of Equation 5-6 with a multiplication factor of 0.30/0.01 = 30. The calculated breakthrough point is then 630 empty bed volumes when using raw-grade ore at a retention time of 30 minutes. Consequently the use of phosphate rock nucleation as a polishing process following lime coagulation appears to have some promise as a treatment system, even when utilizing raw-grade ore. A two-fold increase in the unit surface area of the phosphate rock would result in an approximate treatment cost of $0.10/1000 gallons. Substantial increases in the unit surface area would make the system highly attractive as a "polishing" process for producing a very low phosphate effluent when feed solutions have a high pH.

Finally there is one important benefit that stems from phosphate removal by nucleation on phosphate rock that no other present treatment process has: viz the recovery and reuse of the soluble phosphate in the wastewater. With phosphate rock nucleation the phosphate as well as some calcium (thereby softening the water to some extent) is removed from solution and deposited on the solid surface. When the phosphate rock is no longer capable of regeneration it can be sold for whatever use it may have had originally. Using it in the proposed treatment system would increase the phosphorus content of the material and thereby make it more valuable as a source of phosphorus.

6-2   Continual phosphate removal at steady-state

The treatment process envisioned for steady-state removal of phosphorus would be a continuous-flow contact chamber under hydraulic pressure with sufficient retention time to attain the desired removal. From a practical point of view the surface of the phosphate rock would eventually be so loaded with nucleated HAP that the effective surface area would be decreased to the point where replacement would become necessary. Therefore the contact chamber would have to be constructed in order to facilitate easy replacement of the phosphate rock.

In Chapter 5 steady-state column operation was mathematically described by Equation 5-9

$$t_r = (V/kA(PO_{4T})_o)(n-1)^{-1}(((PO_{4T})/(PO_{4T})_o)^{1-n}-1) \tag{5-9}$$

where t_r is the retention time in hours, V is the total void volume in liters, A is the total surface area of phosphate rock in m^2, and n is the order of the reaction. All other terms have been previously defined. The form of the equation can be simplified for the PR 14x32 phosphate rock by rearranging and noting that the void ratio equals 0.48, the bulk density equals 1.50 g/ml, and the reaction order equals 2. Equation 5-9 can then be re-written as

$$t_r = 0.0192 ((C_o/C) - 1)/kA_u C_o \tag{6-2}$$

where t_r is the retention time in minutes, C_o is the column influent molar phosphate concentration, C is the effluent phosphate concentration,

A_u is the unit surface area in m^2/g, and k is the rate constant in $liter^2 \, mole^{-1} \, hr^{-1} \, m^{-2}$. From Equation 6-2 the column retention time can be determined given a desired influent concentration, effluent ratio, unit surface area, and rate constant k. Figure 6-2 is a semi-logarithmic plot of Equation 6-2 for various A_u values and a rate constant of 0.083, the k value determined for the secondary effluent column run (C-15). The influent phosphate concentration was assumed to be 0.30 mM.

From Figure 6-2 the necessary retention time to affect 80% steady-state removal (corresponding to C/C_o = 0.2) at a unit surface area of 8.8 m^2/g is approximately 6 hours. The value of 80% was chosen because present chemical coagulation methods for removing phosphorus can easily achieve this removal at a relatively low cost of about $0.05/1000 gallons (Spiegel and Forrest 1969). In the proposed steady-state treatment process a retention time of 6 hours cannot be achieved at a unit treatment cost of $0.05/1000 gallons, and it must be concluded that raw-grade ore is unsatisfactory for use in such a system.

Figure 6-2 shows the inverse relationship between unit surface area and retention time for any effluent phosphate ratio. If the surface area of the phosphate rock could be increased to 100 m^2/g, then the retention time necessary for 80% removal would be 30 minutes. It was previously shown (page 142) that at a retention time of 25 minutes the unit cost of treatment would be about $0.10/1000 gallons, assuming column regeneration. Since a steady-state system does not require regeneration, the treatment costs would be slightly less at an equal retention time.
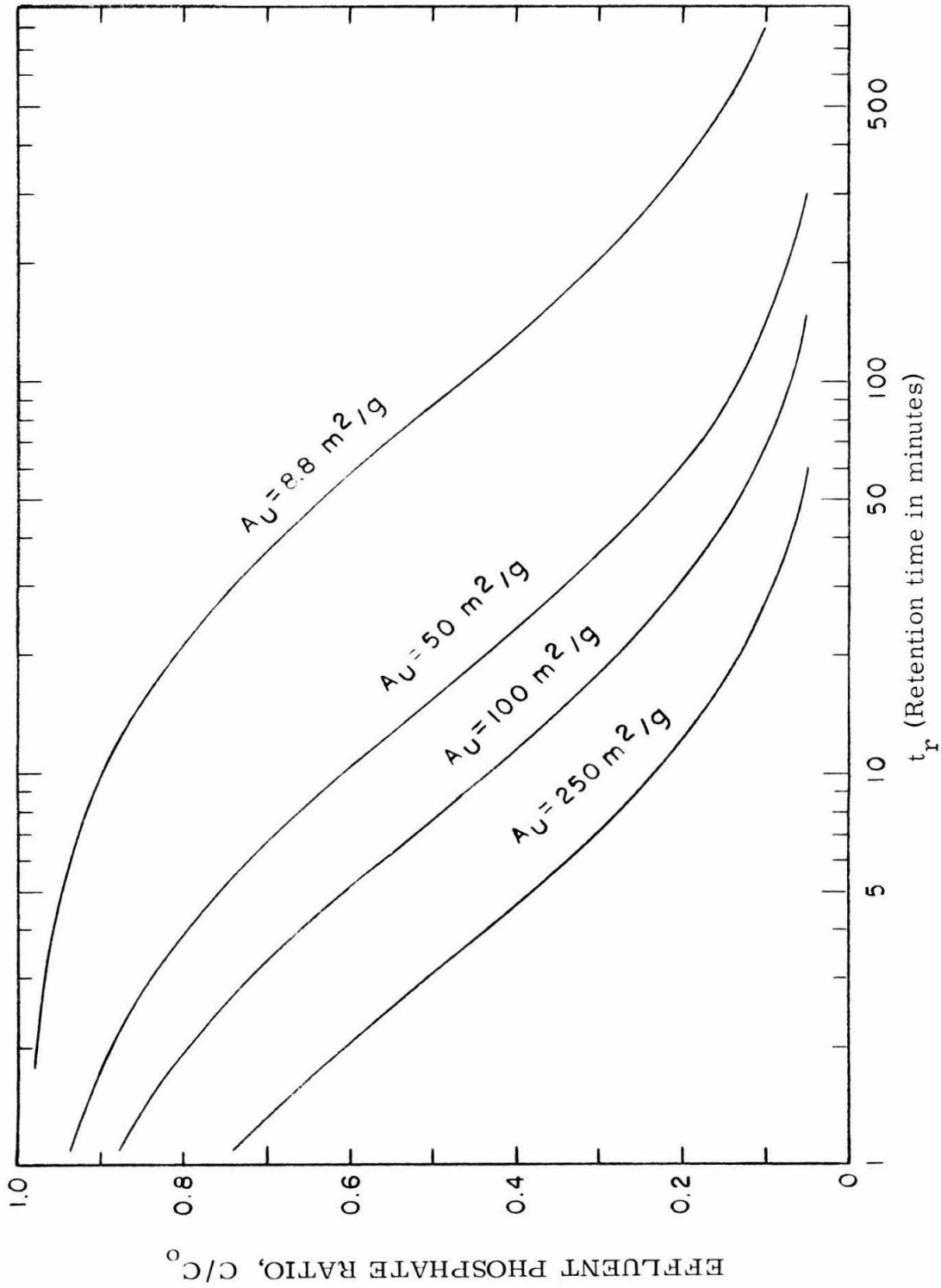
Figure 6-2. Dependence of column effluent phosphate ratio on the retention time and unit surface area for steady-state column operation (Formula 6-2). $C_o = 0.3$ mM, $k = 0.083$.

Therefore in order to be competitive with chemical-coagulation phosphate removal systems, the unit surface area of the phosphate rock would have to be increased to at least 100 m^2/g.

As in the analysis of the high phosphate removal system other factors can also be important in affecting the economics of the steady-state system. Pre-treatment of the phosphate rock may have a large effect on the surface properties. It was seen in Table 5-8 that regenerating the phosphate rock approximately doubled the rate constant. Different sources and grades of phosphate rock may have substantially better nucleating characteristics than observed in the two samples used in this study. The absence of a waste sludge can markedly affect the economics in certain circumstances. And although relatively minor in effect, the recovery and reuse of the otherwise wasted soluble phosphorus is a positive factor for general environmental improvement by reuse of our natural resources.

Chapter 7

Concluding Remarks

In this chapter the principal findings of this research are sum-
marized. Suggestions for further research projects are offered.

7-1   Principal theoretical findings

7-1-1   Rate equation

The rate of disappearance of soluble orthophosphate from an
aqueous suspension of phosphate rock and an initial phosphate concen-
tration range of 0.30 to 0.40 mM was found to follow an equation of
the form

$$dC/dt = k(A/V)C^n \qquad (7\text{-}1)$$

The value of n depended on the extent of the reaction. At $23^{\circ}C$ the
approximate values of n were 10, 4 and 2. The initially large value
of 10 represented rapid nucleation, the n value of 4 represented a
transition growth phase, and n equal to 2 represented crystal growth
after approximately 100 hours. The rate constant varied for each
region and also depended on the initial solution conditions in each case.
Apparently the conditions under which heterogeneous nucleation is
initiated governs to a large extent the rate at which crystal growth
proceeds in later stages.

At the concentrations used at $23^{\circ}C$ only very short lag periods
were found between the various regions of different n values. At $50^{\circ}C$

no lag periods were ever observed. Increasing the temperature from $23^{\circ}C$ to $50^{\circ}C$ increased the rate constant by approximately two orders of magnitude for equal values of n.

From the column studies the rate constant for the steady-state second order phase of crystal growth was found to:

a) Increase with pH over a pH range of 6.5 to 8.0. A two fold increase in k was observed for each unit pH increase.

b) Increase by a factor of three in the presence of 0.050 mM fluoride ion.

c) Decrease by a factor of 1/2 when 1.0 mM $MgSO_4$ was added to the feed solution.

d) Be reduced only slightly when 0.7 mM NH_4Cl was added to the feed solution.

e) Vary inversely with $(CO_{3T})^{1.3}$.

7-1-2   Micro-crystal size and composition during nucleation

By analyzing electron diffraction patterns the size and composition of the micro-crystals growing on the phosphate rock surface were determined for the first 24 hours of reaction. At the end of 1 hour of reaction the nuclei were approximately 7 $\overset{o}{A}$ in size but could not be identified due to their small size. At the start of the run DCP, TCP, OCP, and HAP were all in a state of supersaturation and the initial nuclei probably consisted of a conglomeration of all of these calcium phosphate solids. At the end of four hours the nuclei had ripened into HAP micro-crystals of approximately 18 $\overset{o}{A}$ size. At the end of 24 hours the micro-crystals had increased in size substantially but could still

be identified as HAP. Although at this time their size was impossible to determine with the Scherrer formula, the diffraction pattern obtained was representative of crystallites of about 50 Å size. At the end of 240 hours the diffraction pattern was almost identical to that of the raw grade phosphate rock before any reaction took place.

7-1-3   Regeneration of the phosphate rock surface

As the HAP crystallites grow on the phosphate rock they eventually develop the characteristics of the original nucleating surface. In so doing these larger crystallites can now act as templates for initiating more HAP nucleation and crystal growth. At $23^{O}C$ there was some self-regeneration of the active sites after 70 hours of reaction, but with repeated dosings of soluble phosphate the uptake capacity of the phosphate rock decreased markedly. At $50^{O}C$ the self-regeneration was more pronounced due to the increase in temperature, and five dosings of soluble phosphate with 48 hours between dosings decreased the uptake capacity of the phosphate rock by only 3%.

The columns of granular phosphate rock were successfully regenerated when they rested for approximately 10 days at $50^{O}C$ and pH 11.9. Lower temperatures or pH did not fully regenerate the phosphate rock.

7-2   Principal engineering findings

7-2-1   High phosphate removal

The large initial soluble phosphate nucleating ability of phosphate

rock was examined as a means of removing phosphate from waste-waters. Utilizing raw-grade ore with a unit surface area of 8.8 m^2/g in a column configuration resulted in a unit cost about 100 times too expensive for consideration. In order to be feasible for wastewater treatment the surface area would have to be increased to about 1000 m^2/g. It is unlikely that a unit surface area this high can be produced on the phosphate rock without increasing the material cost to the point where it is too expensive to use. It was concluded that high phosphate removal by nucleation on phosphate rock is not economically feasible as a wastewater treatment process when the feed phosphate concentration is equal to 0.3 mM.

When the column feed phosphate concentration equals 0.01 mM at pH 10 (e.g. after lime-coagulation treatment) nucleation on phosphate rock has promise as a "polishing" treatment system producing an effluent with less than 3×10^{-4} mM (PO_{4T}). This system should be investigated further in prototype field tests.

7-2-2   Steady-state phosphate removal

In the presence of soluble orthophosphate and calcium it was found that phosphate rock catalyzes the nucleation and crystal growth of HAP. By feeding wastewater to a column packed with granules of phosphate rock a steady-state condition will eventually develop where the continual growth of HAP crystals will result in a constant phosphate removal from solution. It was found that in order for the steady-state phosphate removal system to be competitive with present chemical-coagulation treatment processes producing 80% phosphate removal,

the unit surface area of the phosphate rock would have to be at least $100 \ m^2/g$.

7-3 Suggestions for further research

7-3-1 Theoretical considerations

The studies presented in this thesis can be extended to include a number of important theoretical aspects relating to the nucleation and growth of HAP crystals. The relationship between the micro-crystal size and its rate of growth should be further examined by the techniques utilized in this study. The short lag period of about one hour that immediately follows the initial rapid nucleation may be primarily a function of the micro-crystal size, and if this dependence can be defined it would certainly lead to a better understanding of some of the very long lag periods observed by other researchers.

Since fluoride is always present in wastewater the factors that govern the relative amount of growth of HAP and FAP should be examined. At $23^{o}C$ far more HAP then FAP nucleates and grows on the phosphate rock surface than would have been previously expected. A study on the effect of fluoride as a catalyst in the growth of HAP may help to explain some of the phenomena observed.

Since the rate constant for each growth region was found to be dependent on the initial conditions in solution, a study to explain this dependence would be of value in predicting the growth of HAP in situations where lab experiments are not feasible or possible.

7-3-2   Engineering considerations

The primary engineering consideration related to this study is that of lowering the unit cost of the proposed treatment systems. A study involving methods of increasing the unit surface area of the phosphate rock would be high on the list of different approaches. Varying the soluble specie concentrations in the column feed should be evaluated for its effect on performance and cost. The different factors relating to regeneration of the phosphate rock must be further examined to determine the optimum values of the various factors involved. Different grades of phosphate rock ores should be evaluated for both their unit surface areas as well as their nucleating characteristics.

Appendix

Figure A-1 represents the chemical reaction characteristics inside the test column once the steady state condition is reached. The rate of new crystal growth on the surface of the phosphate rock can be represented by an equation of the type

$$dm/dt = kAC_a^n \qquad (A-1)$$

C_a is the concentration of component a, in this case the soluble total orthophosphate concentration. All other terms have been previously defined. We can rearrange Equation A-1 to represent the change in bulk solution concentration by writing

$$dC_a/dt = -k(A/V)C_a^n = r_a \qquad (A-2)$$

V is the void volume inside the column and r_a is the rate change of the concentration. Assuming plug flow with no column dispersion and referring to Figure A-2, a material balance for a reaction component can be made for the differential element of volume dV. Thus for component a we obtain

Input = output + disappearance by crystal growth $\qquad (A-3)$

For the volume dV in Figure A-2 we see that

Input of a, moles/time = F_a

Output of a, moles/time = $F_a + dF_a$

a

b

c
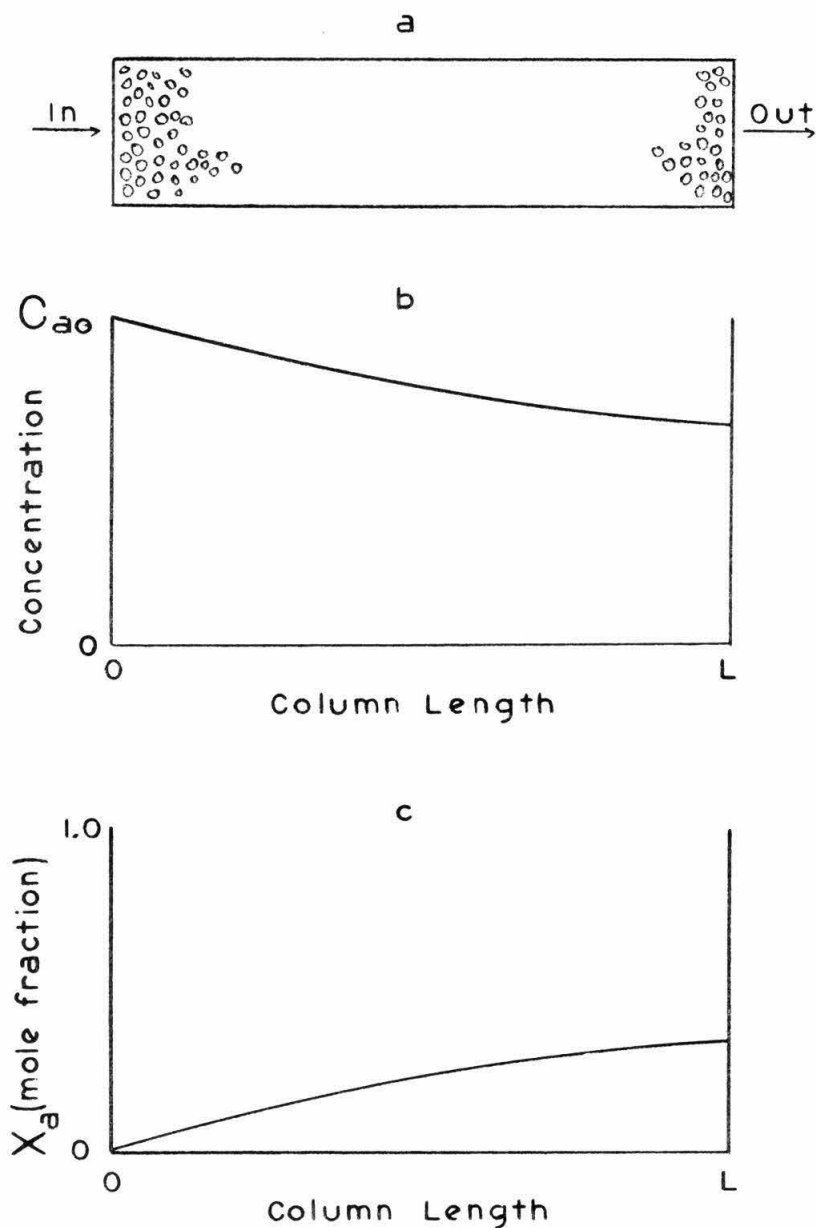
Figure A-1. Figure a represents the test column disre-
garding inlet and outlet conditions. Figure b represents
the drop in concentration of component a as bulk liquid
passes through the column. Figure c represents the growth
of component a on the packed phosphate rock. For liquids
it is equal to $1 - C_{af}/C_{ao}$.
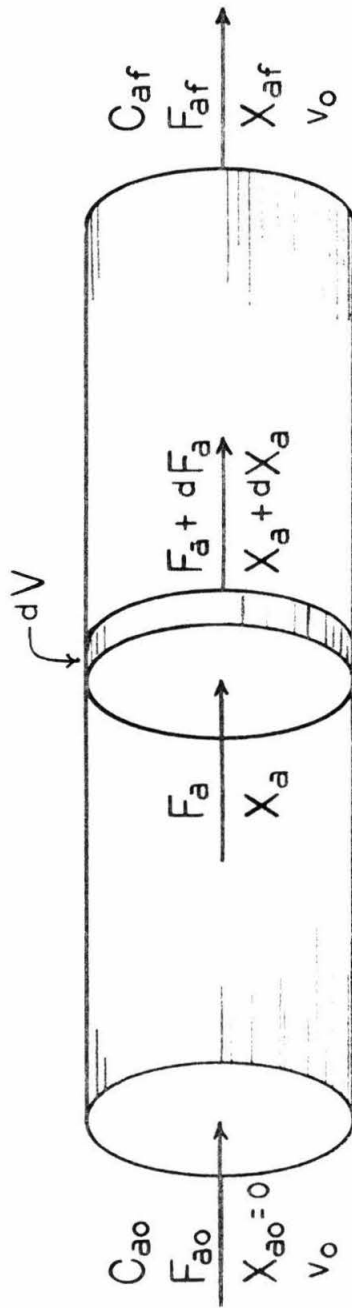
Figure A-2. Schematic representation of the test column packed with phosphate rock. The subscripts zero and f denote inlet and outlet values. The subscript a denotes values of component a. C is concentration, mole/liters; F is flow rate, moles/hr; X is mole fraction converted, unitless; and v_o is bulk fluid flow rate, liter/hr.

Disappearance of a, moles/time = $(-r_a)dV$

Substituting into Equation A-3, we obtain

$$F_a = (F_a + dF_a) + (-r_a)dV \qquad (A-4)$$

We can write

$$dF_a = d(F_{ao}(1-X_a)) = -F_{ao}dX_a \qquad (A-5)$$

where X_a is the mole fraction converted of component a, and F_{ao} is the column input of component a. Combining Equations A-4 and A-5 we obtain the differential equation describing the rate of removal of component a:

$$F_{ao}dX_a = (-r_a)dV \qquad (A-6)$$

Integrating over the entire column

$$\int_o^V dV/F_{ao} = \int_o^{X_{af}} dX_a/(-r_a) \qquad (A-7)$$

where X_{af} is the mole fraction of component a converted inside the entire column. F_{ao} can be written as

$$F_{ao} = v_o C_{ao} \qquad (A-8)$$

where v_o is the column volumetric flow rate and C_{ao} is the influent concentration of component a. Substituting Equation A-8 and A-2 into Equation A-7 and rearranging we obtain

$$t_r = V/v_o = (VC_{ao}/kA)\int_o^{X_{af}} dX_a/C_a^{\,n} \qquad (A-9)$$

C_a can be written in terms of X_a and C_{ao}

$$C_a = C_{ao}(1-X_a) \qquad (A-10)$$

Substituting Equation A-10 into A-9 we obtain the general integral equation for any reaction of order n

$$t_r = (V/kAC_{ao}^{n-1}) \int_o^{X_{af}} dX_a/(1-X_a)^n \qquad (A-11)$$

For any value of n greater than 1 the integral form of Equation A-11 is

$$t_r = (V/kAC_{ao}^{n-1})(n-1)^{-1}(1-X_{af})^{1-n}-1) \qquad (A-12)$$

Since X_{af} is equal to $1-(PO_{4T})/(PO_{4T})_o$, the final equation can be written as

$$t_r = (V/kA(PO_{4T})_o^{n-1})(n-1)^{-1}(((PO_{4T})/(PO_{4T})_o^{1-n}-1) \qquad (A-13)$$

Nomenclature

Symbols used in only one section are not included in this list

A	Total surface area
A_u	Unit surface area
C	Molar ion concentration
CFAP	Carbonate fluoroapatite, $Ca_{10}(PO_4, CO_3)_6 F_2$
CHAP	Carbonate hydroxyapatite, $Ca_{10}(PO_4, CO_3)_6 (OH)_2$
D	Diffusion coefficient
DCP	Dicalcium phosphate, $CaHPO_4$
DCPD	Dicalcium phosphate dihydrate, $CaHPO_4 \cdot 2H_2O$
FAP	Fluoroapatite, $Ca_{10}(PO_4)_6 F_2$
FHAP	Fluoride hydroxyapatite, $Ca_{10}(PO_4)_6 (OH)_x F_{2-x}$
HAP	Hydroxyapatite, $Ca_{10}(PO_4)_6 (OH)_2$
HAP_{5-3-1}	One half of a unit cell of HAP, $Ca_5(PO_4)_3 OH$
k	Reaction rate constant
K	Molar ion product at equilibrium
m	Mass
n	Reaction order
OCP	Octacalcium phosphate, $Ca_4H(PO_4)_3$
p^cQ	$-\log_{10}Q$ computed at the solution ionic strength
(PO_{4T})	Total orthophosphate concentration
$(PO_{4T})_o$	Initial or feed total orthophosphate concentration
Q	Molar concentration ion product

S   Supersaturation ratio

t   Time

TCP   Tricalcium phosphate, $Ca_3(PO_4)_2$

V   Total reactor void volume

V'_c Dimensionless empty bed volume column throughput

V'_{cbt} V'_c at column breakthrough

REFERENCES

1. Adamson, A.W., "Physical Chemistry of Surfaces", Interscience Publishers (1967).

2. AWWA Task Group Report, "Chemistry of Nitrogen and Phosphorus in Water", J. AWWA, 62, 127 (1970).

3. Bachra, B.N., Trautz, O.R., and Simon, S.L., "Precipitation of Calcium Carbonates and Phosphates", Arch. of Biochem. and Biophysics, 103, 124 (1963).

4. Bureau of Mines, "Mineral Facts and Problems", Bulletin 650 (1970).

5. Calgon Corporation, "Activated Carbon Product Bulletin", Bulletin 20-2a (1969).

6. Chen, Y.S.R., Butler, J.N., Stumm, W., "Adsorption of Phosphate on Alumina and Kaolinite from Dilute Aqueous Solution", Presented at the 163rd Nat. Meeting of ACS, Boston, Mass. (1972).

7. Clark, J.S., "Solubility Criteria for the Existence of Hydroxyapatite", Can. J. of Chem., 33, 1696 (1955).

8. Clark, J.S., and Turner, R.C., "Reactions between Solid Calcium Carbonate and Orthophosphate Solutions", Can. J. of Chem., 33, 665 (1955).

9. Cole, C.V., Sterling, R.O., and Scott, C.O., "The Nature of Phosphate Sorption by Calcium Carbonate", Soil Sci. Soc. of Amer. Proc., 17, 352 (1953).

10. Cullitz, B.D., "Elements of X-ray Diffraction", Addison-Wesley (1956).

11. Deitz, R.S., Emery, K.O., and Shepard, F.P., "Phosphate Deposits on the Sea Floor off Southern California", Geol. Soc. of Amer. Bull., 53, 815 (1942).

12. Deitz, V.R., Rootare, H.M., and Carpenter, F.G., "The Surface Composition of Hydroxylapatite Derived from Solution Behavior of Aqueous Suspension", J. of Coll. Sci., 19, 87 (1964).

13. Doremus, R.H., "Precipitation Kinetics of Ionic Salts from Solution", J. Phys. Chem., 62, 1068 (1958).

14. Duwez, P.E., Private communication to the Author (1972).

15. Eanes, E.D., "Thermochemical Studies on Amorphous Calcium Phosphate", Calcified Tissue Res., 5, 133 (1970).

16. Eanes, E.D., Gillesen, I.H., and Posner, A.S., "Intermediate States in the Precipitation of Hydroxyapatite", Nature, 208, 365 (1965).

17. Eanes, E.D., and Posner, A.S., "Intermediate Phases in the Basic Solution Preparation of Alkaline Earth Phosphates", Calcified Tissue Res., 2, 38 (1968).

18. Eliassen, R., and Tchobanoglous, G., " Removal of Nitrogen and Phosphorus from Wastewater", Environ. Sci. and Technol., 3, 536 (1969).

19. Ferguson, J.F., "The Precipitation of Calcium Phosphates from Fresh Waters and Wastewaters", Ph.D. Thesis, Stanford Univ., Calif. (1969).

20. Ferguson, J.F., Jenkens, D., and Eastman, J., "Calcium Phosphate Precipitation at Slightly Alkaline pH Values", Presented at the 44th Annual Conf. Of WPCF, San Francisco, Calif. (1971).

21. Fisher, D.J., and McConnel, D., "Aluminum Rich Apatite", Science, 164, 551 (1969).

22. "Handbook of Chemistry and Physics", 50th Edition, The Chemical Rubber Co., Cleveland, Ohio (1970).

23. Heidenreich, R.D., "Fundamentals of Transmission Electron Microscopy", Interscience Publishers (1964).

24. Heinke, G.W., and Norman, J.D., "Condensed Phosphates in Lake Water and Wastewater", 5th Intl. Water Poll. Res. Conf., Pergamon Press (1971).

25. Illig, G.J. Jr., "Use of Sodium Hexametaphosphate in Manganese Stabilization", J. AWWA, 52, 867 (1960).

26. Kessick, M., Private communication to the Author (1972).

27. Kramer, J.R., "Seawater: Saturation with Apatites and Carbonates", Science, 146, 637 (1964).

28. Leckie, J.O., "Interaction of Calcium and Phosphate at Calcite Surfaces", Ph.D. Thesis, Harvard University (1969).

29. Levenspiel, O., "Chemical Reaction Engineering", John Wiley and Sons (1962 - Fifth Printing, May 1967).

30. Loebenstein, W.V., "Surface Studies of Natural and Synthetic Bone Mineral and Teeth", Adhesive Restorative Dental Mat. II, p 213. Nat. Inst. of Dental Res., H.E.W. (1965).

31. McConnel, D., "A Structural Investigation of the Isomorphism of the Apatite Group", The Amer. Minerol., 23, 1 (1938).

32. Menar, A.B., Jenkins, D., "Fate of Phosphorus in Waste Treatment Process: Enhanced Removal of Phosphate by Activated Sludge", Environ. Sci. and Tech., 4, 1115 (1970).

33. Moreno, E.C., Brown, W.E., and Osborn, G., "Solubility of Dicalcium Phosphate Dihydrate in Aqueous Systems - Stability of Dicalcium Phosphate Dihydrate in Aqueous Solutions and Solubility of Octacalcium Phosphate", Soil Sci. Soc. of Amer. Proceed., 24, 94 (1960).

34. Murr, L.E., "Electron Optical Applications in Materials Science", McGraw-Hill (1970).

35. Nancollas, G.H., "Kinetics of Crystal Growth from Solution", J. of Crystal Growth, 34, 335 (1968).

36. Nesbitt, J.B., "Phosphorus Removal - The State of the Art", J. WPCF, 41, 701 (1969).

37. Neufeld, R.D., and Thodos, G., "Removal of Orthophosphates from Aqueous Solutions with Activated Alumina", Environ. Sci. and Technol., 3, 661 (1969).

38. Neuman, W.F., and Neuman, M.W., "The Nature of the Mineral Phase of Bone", Chem. Rev., 53, 1 (1953).

39. Nielson, A.E., "Kinetics of Precipitation", Macmillan Co. (1964).

40. Olsen, S.R., "Measurement of Surface Phosphate on Hydroxylapatite and Phosphate Rock with Radiophosphorus", J. of Phys. Chem., 56, 630 (1952).

41. Olsen, S.R., Watanbe, F.S., and Cole, C.V., "Soil Properities Affecting the Solubility of Calcium Phosphates", Soil Sci., 90, 44 (1960).

42. Palache, E., Berman, H., and Frondel, C. (Editors), "Dana's System of Minerology", John Wiley and Sons (1951).

43. Parkhurst, J.D., Dryden, F.D., McDermott, G.N., and English, J., "Pomona Activated Carbon Plant", J. WPCF, 39, R70 (1967).

44. Rohlich, G.A., "Methods for the Removal of Phosphorus and Nitrogen from Sewage Plant Effluents", Adv. in Water Poll. Res., Proceed. of the Intl. Water Poll. Res. Conf., London 1962.

45. Rootare, H.M., Deitz, V.R., and Carpenter, F.G., " Solubility Product Phenomena in Hydroxyapatite Water Systems", J. of Colloid Sci., 17, 179 (1962).

46. Scalf, M.R., Pfeffer, F.M., Lively, L.D., Whitherow, J.L., and Preising, C.P., "Phosphate Removal at Baltimore, Maryland", J. of the San. Eng. Div., Proceed. ASCE, 95, SA5, 817 (1969).

47. Sillén, L.G., and Martell, A.E., "Stability Constants", Special Publication No. 17, London, The Chemical Society, Metcalf and Cooper Ltd. (1964).

48. Simpson, D.R., "The Nature of Alkali Carbonate Apatites", Amer. Minerol., 49, 363 (1964).

49. Simpson, D.R., "Carbonate in Hydroxyapatite", Science, 147, 501 (1965).

50. Simpson, D.R., "Effects of Magnesium on the Formation of Apatite", Amer. Minerol., 51, 205 (1966a).

51. Simpson, D.R., "Apatite and Octacalcium Phosphate: Effects of Carbon Dioxide and Halogens on Formation", Science, 154, 1660 (1966b).

52. Simpson, D.R., "Effect of pH and Solution Concentration on the Composition of Carbonate Apatite", Amer. Minerol., 52, 896 (1967).

53. Simpson, D.R., "Substitution in Apatite: 1. Potassium Bearing Apatite", Amer. Minerol., 53, 432 (1968a).

54. Simpson, D.R., "Substitution in Apatite: 2. Low Temperature Fluoride-hydroxyl Apatite", Amer. Minerol., 53, 1953 (1968b).

55. Simpson, D.R., "Oxygen Rich Apatite", Amer. Minerol., 54, 560 (1969a).

56. Simpson, D.R., "Partitioning of Fluoride Between Solution and Apatite", Amer. Minerol., 54, 1711 (1969b).

57. Spiegel, M., and Forrest, T.H., "Phosphate Removal: Summary of Papers", J. of the San. Eng. Div., Proceed. of the ASCE, 95, SA5, 803 (1969).

58. Srivastava, S.C., and Agrawal, M.P., "Enhanced Solubility of Dicalcium Phosphate in the Presence of Magnesium and Sulfate Ions, and its Edaphic Significance in Calcerous Soils", Soil Sci., 104, 77 (1967).

59. "Standard Methods for the Examination of Water and Wastewater", Thirteenth Edition, Amer. Pub. Health Assoc., Inc., New York (1970).

60. Stumm, W., and Morgan, J.J., "Aquatic Chemistry", Interscience Publishers (1970).

61. Trautz, O.R., "Crystallographic Studies of Calcium Carbonate Phosphate", Annals N.Y. Acad. of Sci., 85, 145 (1960).

62. Turnbull, D., and Vonnegut, B., "Nucleation Catalysis", Ind. Eng. Chem., 44, 1291 (1952).

63. Upreti, M.C., and Walton, A.G., "Heterogeneous Nucleation of Alkali Halide Crystals in Solution", J. Chem. Phys., 44, 1936 (1966).

64. U.S. Dept. of the Interior, "Appraisal of Granular Carbon Contacting", Report No.TWRC-11 (1969).

65. Van Wazer, J.R., "Phosphorus and its Compounds", Interscience Publishers, Volume 1 (1958), Volume 2 (1961).

66. Walters, L.Y. Jr., and Luth, W.C., "Unit Cell Dimensions, Optical Properties, and Halogen Concentrations in Several Natural Apatites", Amer. Minerol., 54, 156 (1969).

67. Walton, A.G., "Theory of Surface Reaction Controlled Growth", J. Phys. Chem., 67, 1920 (1963).

68. Walton, A.G., "The Formation and Properties of Precipitates", Interscience Publishers (1967).

69. Walton, A.G., Bodin, W.J., Furedi, H., and Schwarz, A., "Nucleation of Calcium Phosphate from Solution", Can. J. of Chem., 45, 2695 (1967).

70. Weaver, P.J., "Phosphates in Surface Waters and Detergents", J. WPCF, 41, 1647 (1969).

71. Weber, W.J. Jr., Hopkins, C.B., and Bloom, R. Jr., "Physico-chemical Treatment of Wastewater", J. WPCF, 42, 83 (1970).

72. Wells, W.N., "Differences in Phosphate Uptake Rates Exhibited by Activated Sludges", J. WPCF, 41, 765 (1969).

73. Williams, J.B., and Irvine, J.W. Jr., "Preparation of the Inorganic Matrix of Bone", Science, 119, 771 (1954).